REPORT DOCUMENTATION PAGE

Form Approved OMB No. 0704-0188

Public reporting burden for this collection of information is estimated to average 1 hour per response, including the time for reviewing instructions, searching existing data sources, gathering and maintaining the data needed, and completing and reviewing the collection of information. Send comments regarding this burden estimate or any other aspect of this collection of information, including suggestions for reducing this burden to Washington Headquarters Services, Directorate for Information Operations and Reports, 1215 Jefferson Davis Highway, Suite 1204, Arlington, VA 22202-4302, and to the Office of Management and Budget, Paperwork Reduction Project (0704-0188), Washington, DC 20503.

1. AGENCY USE ONLY (Leave blank)	2. REPORT DATE	3. REPORT TYPE AND DATES COVERED
	August 1995	Final Report

4. TITLE AND SUBTITLE

Cryogenic Aluminum Armature Bar for High Power Generators

5. FUNDING NUMBERS

F6170894W0769

6. AUTHOR(S)

Dr Lidia Chubraeva

7. PERFORMING ORGANIZATION NAME(S) AND ADDRESS(ES)

Institute for Electrotechnical Problems (NIIElectromash)
Moskovsky av., 100
St Petersburg 196084
Russia

8. PERFORMING ORGANIZATION REPORT NUMBER

N/A

9. SPONSORING/MONITORING AGENCY NAME(S) AND ADDRESS(ES)

EOARD
PSC 802 BOX 14
FPO 09499-0200

10. SPONSORING/MONITORING AGENCY REPORT NUMBER

SPC 94-4095

11. SUPPLEMENTARY NOTES

12a. DISTRIBUTION/AVAILABILITY STATEMENT

Approved for public release; distribution is unlimited.

12b. DISTRIBUTION CODE

A

13. ABSTRACT (Maximum 200 words)

This report results from a contract tasking Institute for Electrotechnical Problems as follows: Generate designs or cryogenic armatures of the one to five megawatt class as described in the attached proposal dated 8 March 1994.

19980311 135

14. SUBJECT TERMS

Nil

15. NUMBER OF PAGES

98

16. PRICE CODE

N/A

17. SECURITY CLASSIFICATION OF REPORT	18. SECURITY CLASSIFICATION OF THIS PAGE	19. SECURITY CLASSIFICATION OF ABSTRACT	20. LIMITATION OF ABSTRACT
UNCLASSIFIED	UNCLASSIFIED	UNCLASSIFIED	UL

NSN 7540-01-280-5500

Standard Form 298 (Rev. 2-89)
Prescribed by ANSI Std. 239-18
298-102

DTIC QUALITY INSPECTED 3

Institute of Electrotechnical Problems
Department of Non-Conventional Electrical Machines
St.Petersburg, Russia

CRYOGENIC ALUMINUM ARMATURE BAR FOR HIGH POWER GENERATORS

Contract Number F6170894W0769 (SPC- 94- 4095)

Final Report

August 1995

By:

L.I.Chubraeva

V.A.Tutaev
I.S.Ganzhinov
V.E.Sigaev
D.V.Sirotko
S.M. Zrazhevsky
V.B.Berezhansky
V.A.Sapozhnikov
S.N.Pylinina
I.N.Popov
A.V.Kalmykov

DTIC QUALITY INSPECTED 5

Prepared for
Department of Air Force
USA

INTRODUCTION

To improve the design of light-weight cryogenic alternator it is necessary to pay extreme attention not only to the design of the rotor, but to the stator design as well. Main elements of the stator are: the three-phase armature winding and the outer screen, which protects the alternator exterior from the magnetic flux, induced inside, and the alternator interior from the outside stray magnetic fields. The outer screen may be ferromagnetic or electromagnetic. With the increase of the number of poles the role of magnetic screen decreases, so in multi-pole alternators it is possible to exclude the outer screen at all.

As for the armature winding there exist several problems which are to be solved. First of all it is desirable to introduce non-conventional geometries, which provide better weight characteristics and winding wire economy. Moreover it seems reasonable to substitute the heavy copper winding, operating at ambient temperatures, by light aluminum winding with cryogenic cooling. Application of high-purity aluminum at cryogenic temperatures will result in sufficient increase of armature winding current density. Application of cryogenic coolant not only for the rotor, but for the stator as well will simplify the total cooling scheme of the alternator. In case of liquid hydrogen or liquid nitrogen electrical insulation scheme will be more simple as well.

To decrease the amount of coolant for the armature it is necessary to pay attention to the problem of armature winding losses. They consist of the three components: the Ohmic losses, the eddy-current and circulating current ones. The eddy-current losses may be decreased by application of composite aluminum wire with small filament diameter. The circulating losses are suppressed by application of a multi-stage transposition scheme, accounting for three-dimensional magnetic fluxes acting in the armature winding area.

It is desirable to improve not only the size and weight parameters of the alternator, but the manufacturing processes as well. Introduction of new helical armature winding geometry helps to apply new technologies, making the manufacturing process less complicated and time consuming.

The design developments and parametrical studies are to be based on experimental investigations. In case of helical armature winding development it means experimental studies of the armature bars in a special test fixture, simulating the cooling system, insulation scheme and support structure of a real armature.

1. PRELIMINARY CRYOGENIC ARMATURE DESIGN

1.1. Parametrical armature study for 1-5 MW class generator

To develop preliminary design of the cryogenic armature and to carry out paramertical studies od the cryogenic generator it is necessary to settle the prime cooling scheme and the total alternator layout. The lowest size and weight parameters may be obtained in case both the excitation and the armature windings are positioned in a single cryostat. There may appear problems with the sealing unit for the cold air-gap, separating the rotor and the stator, but successful tests of the seal model in the beginning of the year proves that the design may be developed. Below is presented the description of the principal scheme of the alternator with a single cryostat, shown in Fig.1.1.

The coolant is supplied into the rotor *1* via the central vacuum tube *2* in the hollow shaft. From the central tube the cooling agent flows to the rotor radial channels *3* and then is pumped through the axial channels of the excitation winding *4* taking away the heat losses.

At the exit from the channels of the rotor winding the coolant enters chamber *5* with radial channel *6*, which plays the role of centrifugal pump. Radial channel ends with a nozzle *7*, via it the coolant flows from the rotor to the stator and cools the armature winding *8*. The stator frame *9* is made of fibre-glass. The air-gap between the rotor and the stator is sealed *10*. The armature outer screen *11* may be electromagnetic in case of superconducting machine or ferromagnetic in case of a hyperconducting one. It may be situated either in cryogenic zone directly or at intermediate temperature.

Rotor surface losses are withdrawn by means of thermal conductivity to the coolant inside the rotor. The coolant flow-rate is determined by the value of losses in the excitation winding (if any), on the rotor surface and in the armature.

In case the liquid coolant is being thrown into the air-gap the pressure in the air gap is increased thus preventing development of the process. The gaseous coolant from the air-gap is exhausted via the stator together with the main coolant flow.

Parametrical studies, carried out for a number of variants of the armatures are based on an assumption that the excitation winding is manufactured either of high-purity aluminum or of HTSC and is capable to produce the radial magnetic flux on the average diameter of the armature winding in the range of 0.3 - 0.35 T. The excitation winding is a 4-pole one, which is optimal for the 1-5 MW class synchronous generators. It is supposed that the rotor frequency will be a certain value within the range of 12000 - 16000 rpm with the armature current frequency

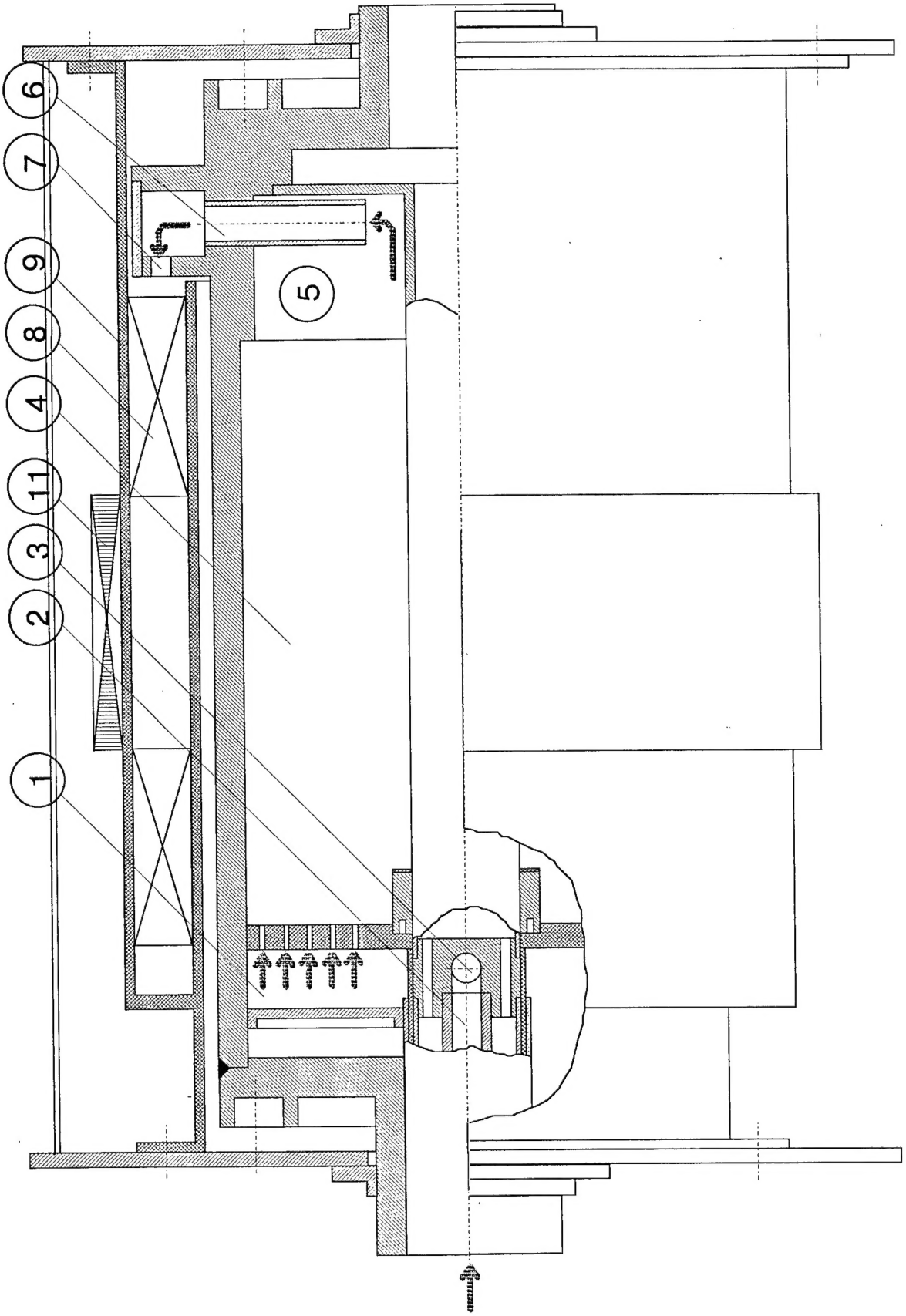

Fig.1.1. Principal scheme of cryogenerator with a single cryostat.

in the range of 400 - 533.3 Hz. The generator voltage may be in the range 1.0 - 10.0 kV. Some evaluations of the armatures are presented in Tables 1.1 and 1.2.

As there exists a relatively large variation of the armature bar sizes in cross-section and length, for experimental investigations there was chosen an intermediate version of the armature winding bar, mostly typical for the generators of 1-5 MW class. The design developments presented below refer to an intermediate case as well. The experimental investigations cover all the ultimate cases which may happen when the full-sized alternator armature will be manufactured.

1.2. Hyperconducting armature with iron screen

Relatively small thickness of the iron core in a four pole alternator makes it reasonable to manufacture the outer armature screen of amorphous steel ribbon. The screen will be characterized by relatively low specific losses (Fig.1.2) and it may be positioned inside the cryogenic zone and cooled by the main armature coolant. Decreased distance between the field winding and the outer screen (as compared to the one out of cryostat at ambient temperature) makes it more efficient for the main radial flux in the armature winding region.

The thickness of the iron core is determined as

$$h = \frac{\Phi}{l_a B_a}, \tag{1.1}$$

where Φ - resultant magnetic flux penetrating into the iron screen, l_a - length of the screen, B_s - saturation magnetic flux density.

The screen mass equals

$$P = H_{o\,max}^2 \pi R_s l_a \sqrt{\frac{\omega \mu_0 \rho}{2}}, \tag{1.2}$$

where g - specific mass of the screen material, R_s - average screen radius.

Application of amorphous steel for the armature screen opens way for significant decrease of the iron screen weight. It may be achieved by subdividing a single outer screen shell into a system of multiple shells with an air-gap distances in between them. The screening system of multiple shells is mostly efficient in case of high values of magnetic permeability μ and with an increase of a number of shells n [1.2]. Fig.1.3 illustrates the ultimate cases. The screening coefficient k_{scr} characterizes the effectiveness of the screening system.

Table 1.1

INITIAL PARAMETERS FOR THE DESIGN DEVELOPMENT OF THE HELICAL ARMATURE WINDING OF THE 5 MW CLASS GENERATOR

PARAMETERS	L-V	H-V
Rated data		
- rating, MW	5.0	5.0
- frequency of rotation, rpm	12-16 000	12-16 000
- voltage (phase), kV	1.0	10.0
- current, kA	1.7	0.17
- number of poles	4	4
- number of phases	3	3
- cos φ	0.98	0.98
- frequency, Hz	400-533.3	400-533.3
Loadings		
- armature winding current density, A/mm^2	170	170
- magnetic induction in AW region, T	0.30-0.35	0.3-0.35
Geometric sizes, mm		
- rotor diameter	250	250
- armature winding ID	300	300
- armature winding OD	340	340
- armature iron screen ID	350	350
- armature screen OD	380	380
- active length	500	500
- armature bar cross-section, mm^2	40.0	4.0

Table 1.2.

INITIAL PARAMETERS FOR THE DESIGN DEVELOPMENT OF THE HELICAL ARMATURE WINDING OF THE 1 MW CLASS GENERATOR

PARAMETERS	L-V	H-V
Rated data		
- rating, MW	1.0	1.0
- frequency of rotation, rpm	12-16 000	12-16 000
- voltage (phase), kV	1.0	10.0
- current, kA	0.330	0.033
- number of poles	4	4
- number of phases	3	3
- cos φ	0.98	0.98
- frequency, Hz	400-533.3	400-533.3
Loadings		
- armature winding current density, A/mm^2	170	170
- magnetic induction in AW region, T	0.30-0.35	0.3-0.35
Geometric sizes, mm		
- rotor diameter	220	220
- armature winding ID	270	270
- armature winding OD	285	290
- armature iron screen ID	295	300
- armature screen OD	320	325
- active length	250	250
- armature bar cross-section, mm^2	8.0	1.0

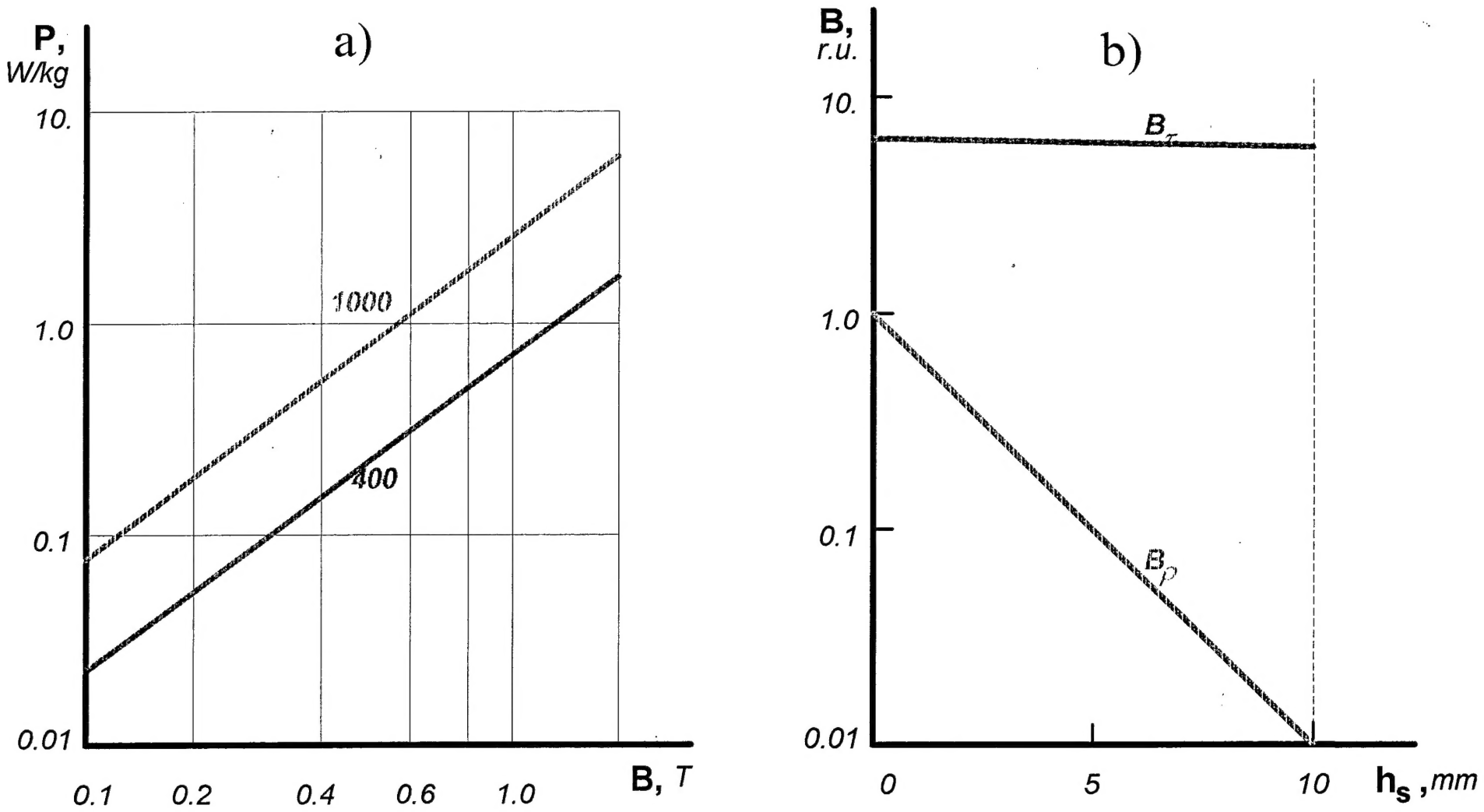

Fig.1.2. Specific losses in the amorphous steel 0.03 mm thick (a) and flux density components in the iron screen (b)

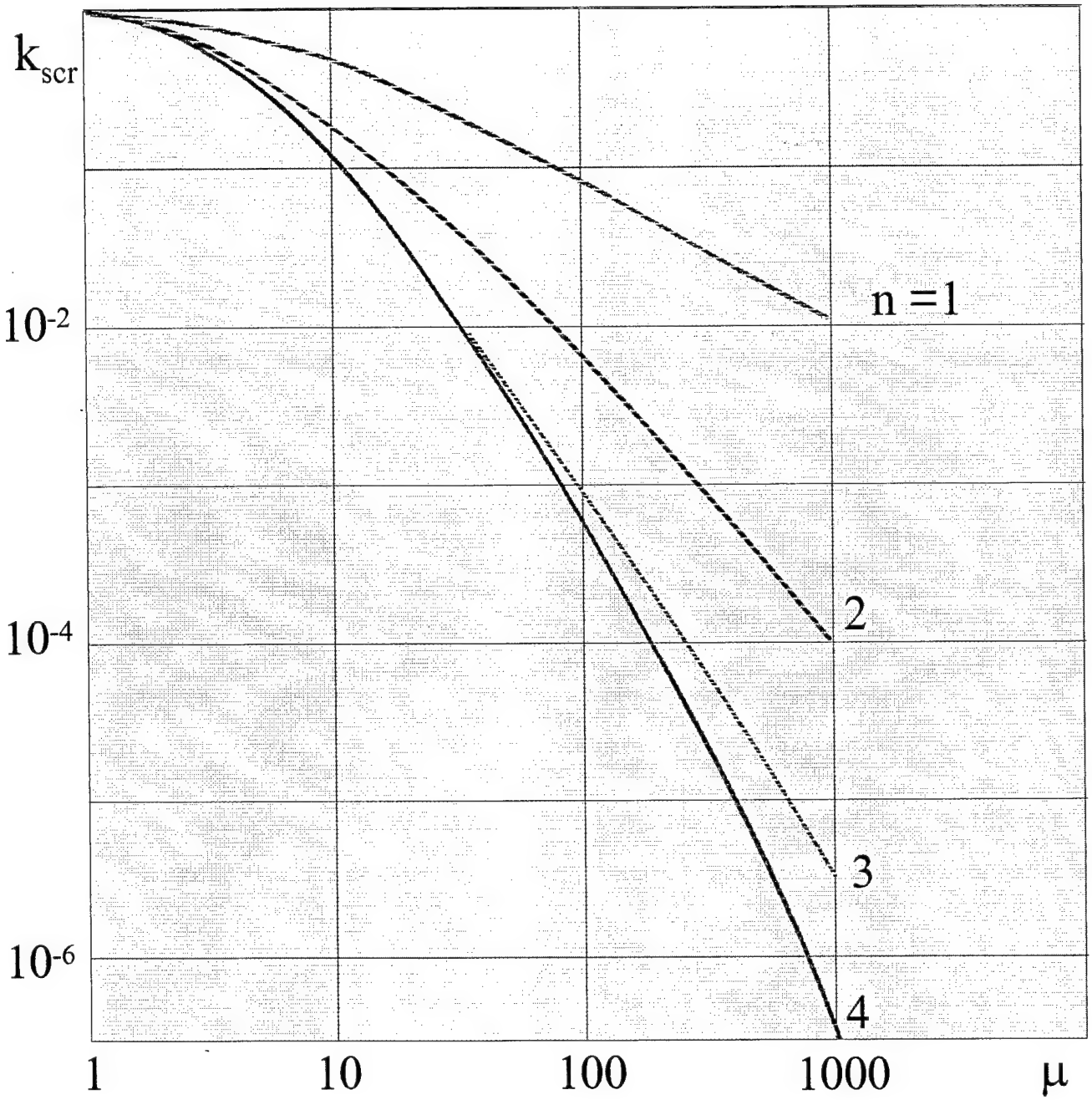

Fig.1.3.Evaluation of the screening coefficients of the multiple iron screens

It is possible to discuss as well a combination of magnetic and current-conducting screens. The theoretical evaluation, carried out for cylindrical shells shows both schemes are practically similar from the point of view of the screening ability, with slight preference of the scheme with the outer conducting screen. It is also beneficial from the point of view of the armature design. The conducting portion may be manufactured either of high purity beryllium or of HTSC and placed inside the cryostat at the intermediate temperature level. The outer metallic shell of the cryostat (the generator frame) may also play the role of such screen. It may be as well positioned on an outer surface at ambient temperature.

Figure 1.4. presents an axial cross-section of the armature of high-speed electrical generator employing cryogenic cooling system for the winding and iron screen. A double-layer helical armature winding *1* is laid down on the outer surface of cylindrical support structure made of fibre-glass laminate *2*. The construction is mounted on a cylinder *3* separating the armature cryogenic zone from the space, occupied by the generator rotor. The whole unit is then epoxy impregnated and baked. Thus, the winding with all the non-metallic elements form a single unit. The winding is connected to the current leads *4* fixed on the separating cylinder in the stator cryogenic zone as well. Above the winding there is the cylindrical ferromagnetic screen *5* wound of the amorphous steel tape, annealed, impregnated with epoxy and baked. Between the cylindrical ferromagnetic screen and armature winding there are the ducts for coolant circulation.

The ferromagnetic screen is fixed inside the *6* cylinder fabricated of a titanium alloy, which envelopes the stator cryogenic zone and serves as its outer generator frame. To eliminate thermal stresses, this shell incorporates an elastic element (sylphon) *7*. Both ends of the shell are welded to the end caps *8*, which are sealed with ring-shaped seals on the separating cylinder in the warm zone. The cryogenic zone is protected against heat fluxes from any side by vacuum insulation. The vacuumized shell is welded from above and from both faces, and the cavity wherein the generator rotor rotates is sealed with the help of stationary seals *9* placed between the end shields and the separating cylinder and with the hydrodynamic capillary-type seals *10* along the rotor shaft. The figure shows the simplified view of combined bearing-sealing unit.

The welded portion of vacuumized shell of the armature cryostat and the cavity for the rotor are supposed to be evacuated separately.

Liquid coolant is supplied into the cryogenic zone and the evaporated portion of the coolant is discharged from it via evacuated pipes *11* with pin-type connectors at their ends. Stator current leads *12* are located inside the pipes as well.

All the metallic design elements of the stator except current-carrying ones are made of a titanium alloy.

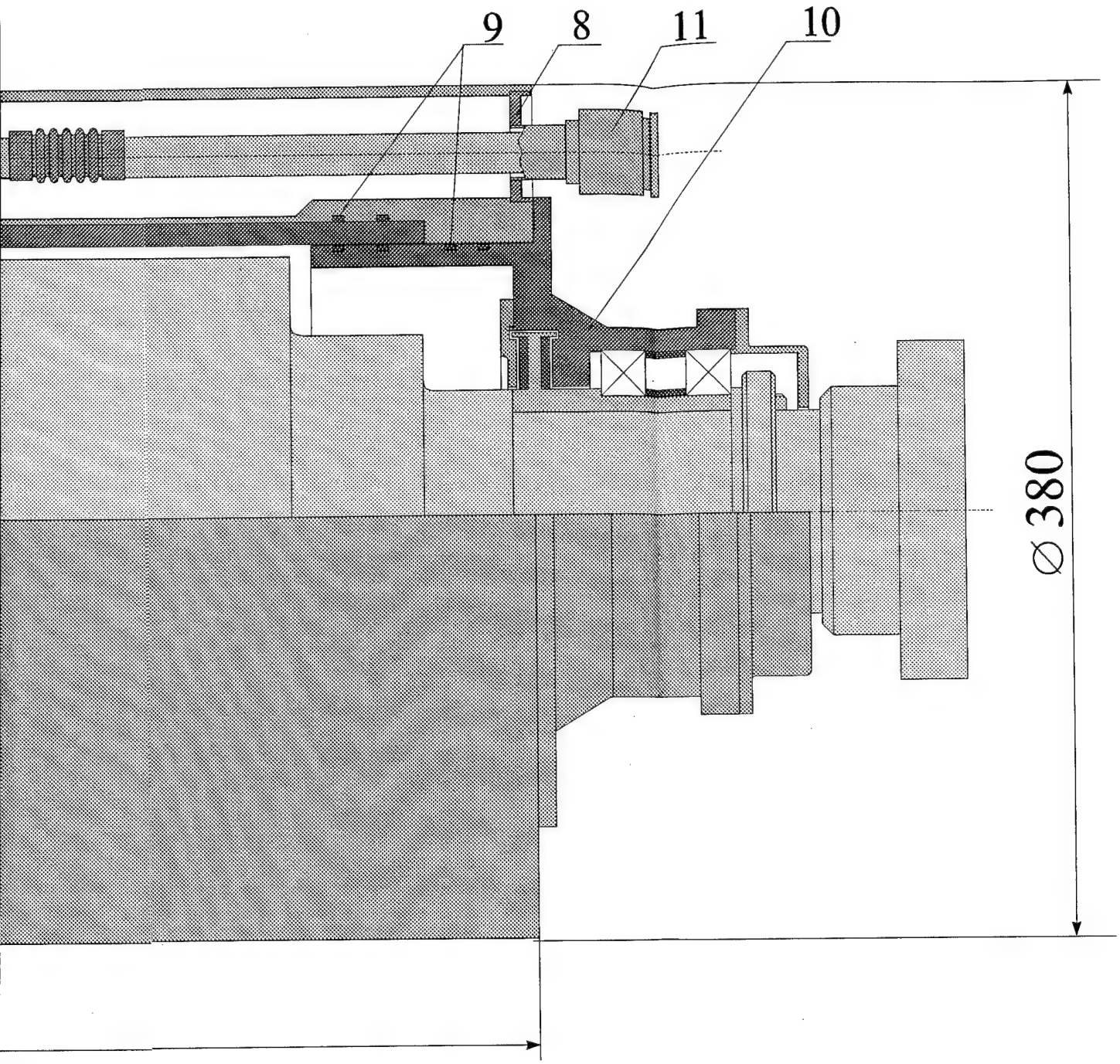

Fig.1.4. Hyperconducting armature of high-speed generator with iron core

1.3. Ironless type of hyperconducting armature

The generator armature without an iron screen may have several versions as well. It may be without an outer screen at all. Such a type of the armature is advantageous from the point of view of the generator mass but it is possible to use such a generator in practice only in case there are no restrictions on the outer stray magnetic fields, from one side, and that there is no danger of magnetization of the generator interior by the external magnetic fields, from the other.

The outer screen influence on the magnetic flux in the armature region and on the alternator parameters is determined by a coefficient

$$1 \pm \left(\frac{R_a}{R_0}\right)^{2p}, \tag{1.3}$$

where R_a - average armature winding radius, R_0 - interior radius of the outer screen, p - number of poles, sign "+" reefers to the iron screen, sign "-" - to the current-conducting screen.

The minimal winding mass (and cost because of high price of winding material) is achieved in case of an iron screen because the latter adds substantially to the value of the main magnetic flux. But in this case the generator is relatively heavy, though the metallic cryostat will be slightly cheaper than the fibre-glass laminate one.

In case of no outer screen at all the winding volume, mass (and cost) increase by approximately 60 %, but the armature is relatively light (by more than 30 kg). It is worth noting that the non-metallic cryostat will need constant vacuum pumping out during the generator operation.

The second version of the ironless armature type is the application of a current-conducting screen. As such a screen tends to demagnetize the main magnetic flux, the volume and mass of the armature winding will increase still further as compared to the previous case. To decrease the influence of the conducting shell it is necessary to increase R_0 (or to increase the pole number which will result in an increased rotor diameter), then it will be better to place the screen outside the cryostat. the mass of the winding will increase in accordance with (1.2).

The thickness of the conducting screen is determined as

$$h \leq 3\sqrt{\frac{2\rho}{\omega\mu_0}}, \tag{1.4}$$

where ρ - resistivity of the screen material, ω - angle frequency.

The screen mass is determined by the equation (1.2) as well.

Nevertheless the design of the cryostat will be one and the same for both versions of the ironless armature type and its description is presented below.

Figure 1.5. presents the armature version without a ferromagnetic screen. This peculiarity leads to consideration of the two design variants - either all the metallic shells enveloping the cryogenic stator zone and the vacuumized vessel should be located at a considerable distance from the armature winding in order to exclude heavy losses, or all these shells should be manufactured of a non-metallic material. The first variant results in a substantial increase of stator dimensions and of cryogenic zone volume. The second variant provides the possibility to somewhat decrease the outer stator diameter and its weight. That is why the second version was chosen, though its manufacturing cost is higher than that of the stator incorporating metallic shells.

Another typical feature of this stator type is its winding design. This is also a double-layer helical winding, but the layers are positioned on both outer and inner surfaces of the cylindrical support structure. The technological process of securing the winding layers onto both sides of cylindrical surfaces is undoubtedly much more complicated and labor consuming, but these drawbacks are offset by better cooling of the winding bars, their easier insulation process and absence of soldered interphase connections.

For the rest, both stator design variants are completely similar.

Table 1.3

Weight in kg of the armature by components (1-5 MW class generator)

N	Name of the armature element	With iron screen	Without iron screen
1	Armature winding	3.5	5.4
2	Winding support structure	9.5	11.0
3	Separating cylinder	25.6	19.0
4	Iron screen	20	0
5	Current leads	4.5	4.5
6	Fibre-glass laminate elements of the cryostat	0	30.0
7	Metallic elements of the cryostat	78.0	30.0
8	Total	141.1	99.9
9	End shields with bearing-sealing units	29.7	29.7
10	**Total**	**170.8**	**129.6**

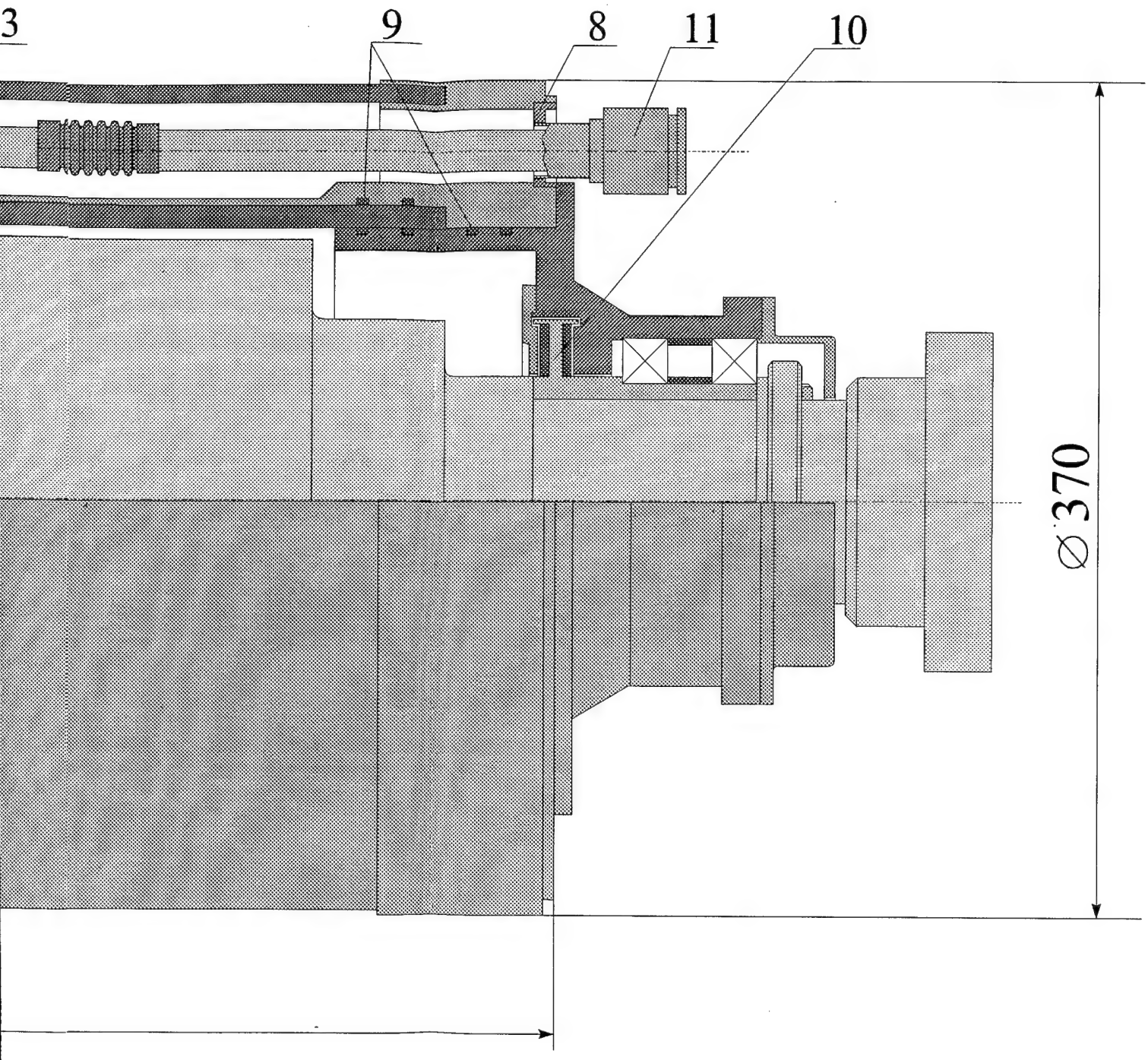

Fig.1.5. Ironless type hyperconducting armature of high-speed generator

To compare the variants of the armatures with the iron screen (Fig.1.4) and without any screen at all (Fig.1.5) in Table 1.3 there are given their weights by components and total.

1.4. Proposed armature manufacturing and assembly process

For the armature presented in Fig.1.4 there may be developed the following manufacturing process.

The winding support structure *2* is fixed rigidly on a separating cylinder *3*. The winding *1* is being laid out on the support structure. The volumes in the winding to form the cooling ducts are protected by special inserts with antiadhesive coating. The assembled unit is placed in a special form. The form is evacuated, filled with an epoxy and baked at 150° C for 1.5 hours. The withdrawn from the form monolithic unit is cleared from the inserts and extra epoxy. Then the current connecting elements *4* are fixed on a cylinder *3* and are connected to the winding terminals. The ferromagnetic screen *5* together with the shell *6* and the sylphon *7* is assembled on the winding outer surface. End caps with preliminary welded tubes for the coolant inlet and outlet and for the current leads are welded into the shell *6*. The assembled structure is covered by an outer cylinder (generator frame) and the end caps *8* are welded to it from both sides. Each welding procedure is being controlled for the absence of seal leaks at ambient and liquid nitrogen temperatures.

The end-shield of the alternator from the turbine side with assembled bearing and sealing unit *10* is preliminary rigidly fixed on the rotor shaft. The rotor is inserted into a separating cylinder and then the second shield unit is assembled on the rotor shaft. The bearing-sealing unit fit on the rotor shaft allows the shaft to have axial displacements when transmitting the torque. The armature winding bus are fixed by bolts and have static seals.

The process of assembly of the armature presented in Fig.1.5 is principally similar to the described above. The only difference is that the winding is at first laid out on a support structure, impregnated with epoxy and baked. After that it is fixed rigidly on a separating cylinder with a help of rings *13*. In this case the technological equipment for the winding impregnation and baking is more simple and cheap.

1.5. Peculiarities of electric insulation ageing at low temperatures

A hyperconducting winding has several peculiar features from the viewpoint of insulation operating conditions. First of all, an insulation system is a combination of solid insulating materials forming the main dielectric barrier washed with a cryogenic liquid (in particular, with liquid hydrogen) whose insulating properties are close to those of transformer oil. However, the cryogenic liquid alone can not be used as the only insulation, since at occasional temperature variations the

liquid may come to boil, which is accompanied by formation of gas bubbles with the reduced pressure inside a bubble. Electric strength of such a gas void is lower than that of the liquid by an order of magnitude, what results in a reduction of insulation reliability. The hyperconducting stator winding is helical, and all its possible design versions are drastically different from conventional winding designs. This calls for an adequate approach to choosing electrical insulating materials.

Peculiarities of polymer insulation ageing at cryogenic temperatures also require a special approach to choosing the insulation materials and their thickness, or to put it another way, operating electric strength. Earlier, when developing the cryogenically-cooled machines, we have conducted researches in this direction aimed at finding the optimum materials, elaborating new designs and efficient technologies. In the course of work reported herein we have gone through the results of our previous studies and analyzed them once more in order to make use of them when developing the hyperconducting stator winding insulation system.

The results of these researches are covered comprehensively in [1.3]. Here we will not go into the details of these, but will present only the main results obtained with single-layer PET film samples of two types. We hope that our future results obtained at liquid helium and liquid hydrogen temperatures will be at least not worse than the presented ones.

The DC and AC (50 Hz) tests were conducted on the single-layer PET film samples immersed into the liquid nitrogen medium. Two types of the PET film were used in the tests: 50 μm thick film fabricated in Russia and 11.5 μm film manufactured in Japan.

There were performed two types of DC tests. When performing the tests of the first type the linearly increasing voltage (in fact, the voltage increasing stepwise by 0.5 kV) was applied at various rates up to the breakdown of the sample. The tests of the second type were conducted at the fixed voltage providing the measurements of the time period necessary for a sample to be broken down. The AC tests were conducted only under the fixed voltage conditions. The samples were tested separately one after another to exclude the secondary effects.

The DC breakdown test results under the linearly-rising voltage conditions at various voltage rates taken at 293 K and at 77 K are shown in Fig.1.6. Presented in the figure are the results of the DC tests performed on the PET film 50 μm and 11.5 μm thick under the voltage increasing step by step up to the breakdown of the sample, at various rates of the electric strength rise at the indoor temperature (293 K) and at the liquid nitrogen temperature (77 K). Indicated in the diagram are the mean breakdown strength values, i.e. the values corresponding to 50% probability of the breakdown for the sample lots of 12-18 pieces. The presented data make it apparent that the functions of the electric strength on the voltage

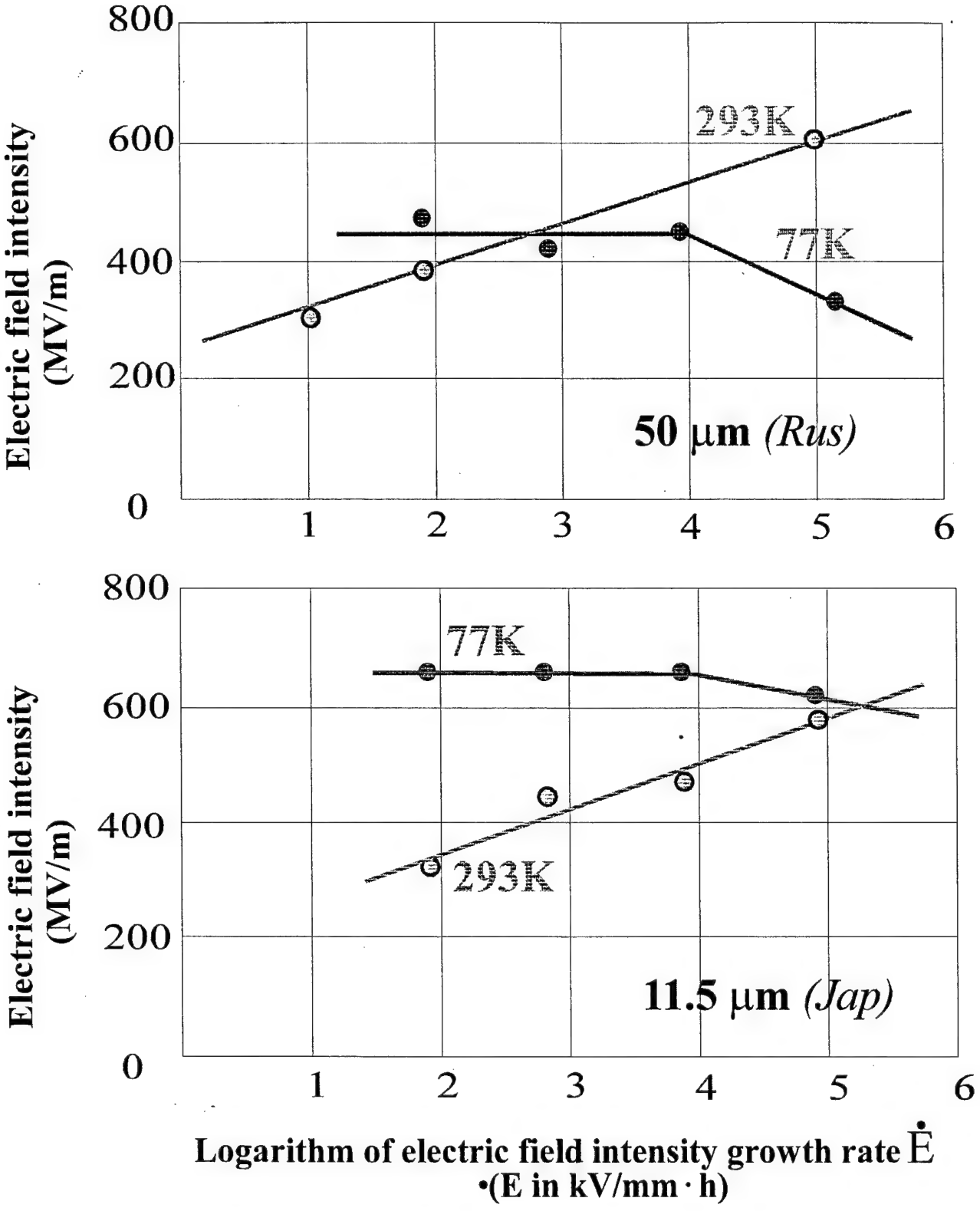

Fig.1.6. Dependence of average breakdown field intensity on the rate of electric filed intensity growth for PET samples

rate at 293 K and at 77 K are sharply different for the two types of PET film. At ambient temperature the electric strength of the test samples increases with the increase of the voltage rate, which can be explained by the shorter period of the field effect on the samples and slowing down of the polymer ageing. On the contrary, at liquid nitrogen temperature the electric strength does not depend on the voltage rate and even decreases with the increasing rate. Thus, we can conclude that polymer ageing at 77 K is significantly retarded.

Figure 1.7. shows the durability of the samples of PET film 50 μm and 11.5 μm thick in dependence of the electric field strength under DC conditions. In this diagram each point on the 293 K curve corresponds to the lifetime of the sample lot of 12...18 pieces, while at 77 K each point corresponds to the lifetime of each sample of the lot subjected to the tests. Fig.1.8. shows the same functions for AC (50 Hz) conditions. In this case, similarly to Fig.2, each point at 293 K indicates the mean lifetime of the sample lot and at 77 K for the Japanese film the lifetime of each sample is indicated, while for the domestic film each point corresponds to the mean lifetime of a lot. It should be noted that at 77 K the character of the $\tau(E)$ function changes: the slope of the straight lines reflecting the function $\tau(E)$ sharply increases for the films of both types, therewith for the PET films 50 μm this function turns almost into the vertical line at DC voltage, as under these conditions the samples are broken down either right after application of voltage (the corresponding points are marked with downward arrows), or are not broken at all during the whole session (the corresponding points are marked with the upward arrows).

Hence, confirmation of a strongly manifested durability dependence on the electric strength at 77 K can be regarded as one of the main experimental results. This is evident from the increasing slope of the straight lines illustrating this function. In other words, the dielectric ageing, i.e. deterioration of its electric properties under the effect of voltage, is considerably retarded even at the strength values close to the short-term dielectric strength which can be defined as the electric strength corresponding to $lg\tau = 0$. This means that the electric destruction at 77 K acquires critical character.

Discussing the practical significance of the experimental results it should be emphasized the following. It is commonly considered that the electric strength of the polymers and their lifetime increase as the temperature decreases. The results obtained indicated that in some cases the short-term dielectric strength can decrease at low temperatures. However, even for these polymers at comparatively low electric strengths (to the left from the vertical line) the durability at 77 K considerably exceeds that at the indoors temperature. The very sharp dependence of the polymer durability on the electric strength makes us accept an adequate approach to the choice of the allowable operating electric strength for the long-term insulation systems at the cryogenic temperatures. When choosing the operating electric strength for 293 K it is necessary to take into account the period of the electric field effect on the dielectric, as it would be

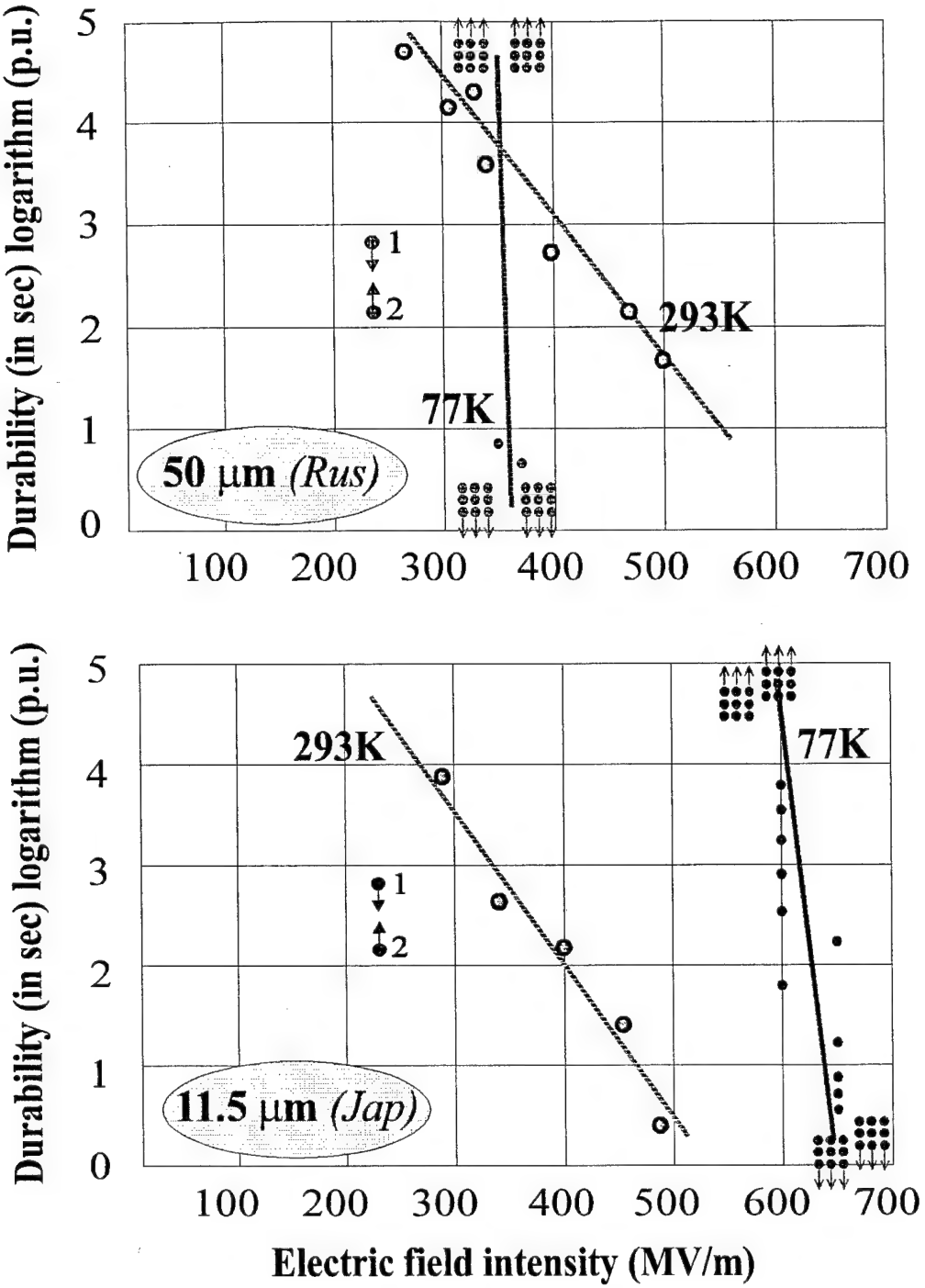

Fig.1.7. The PET samples durability as a function of DC electric field strenfth

point 1 - immediate breakdown upon voltage application
point 2 - no breakdown during test

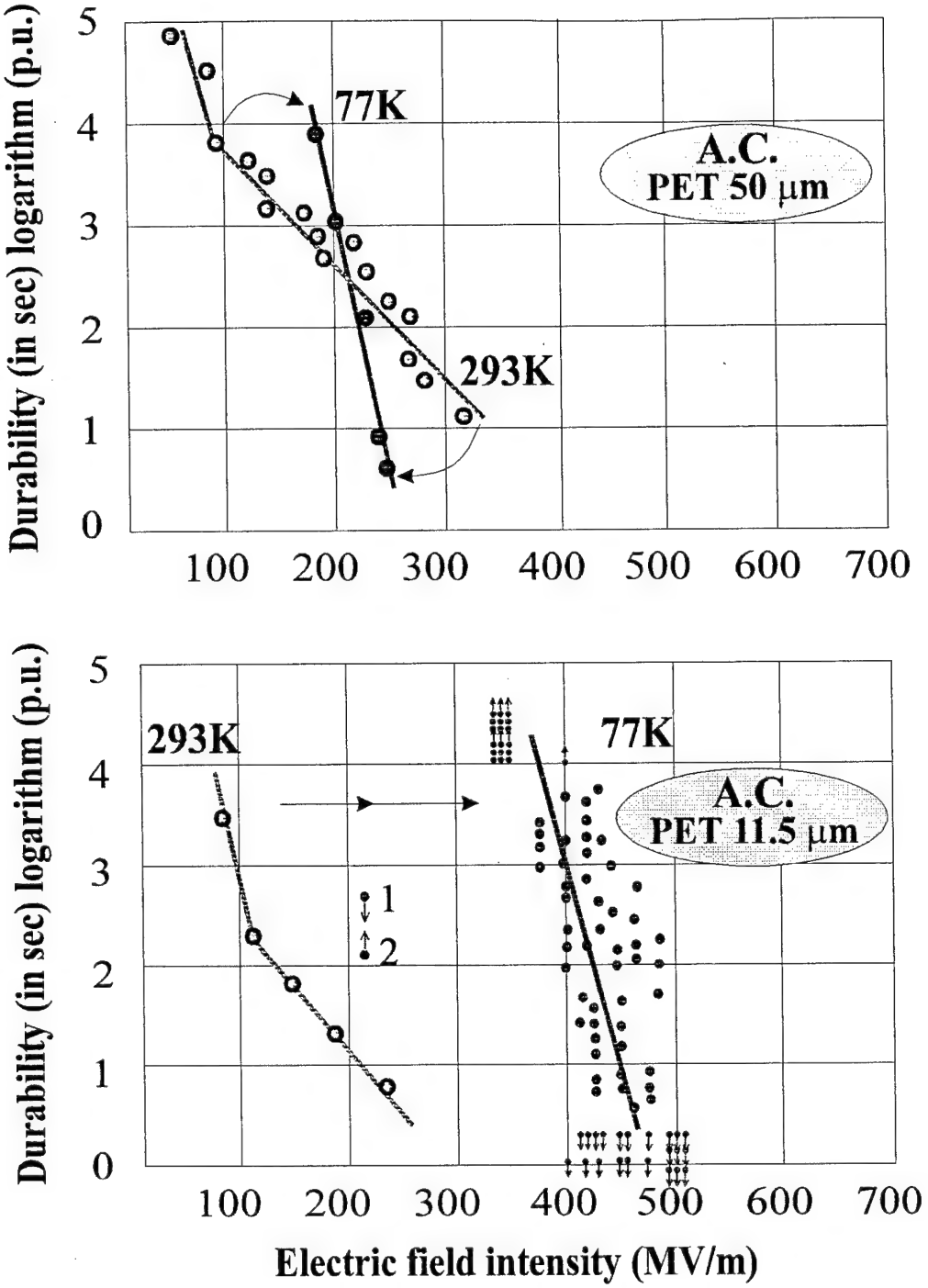

Fig.1.8. The PET samples durability as a function of AC electric field strenfth

point 1 - immediate breakdown upon voltage application
point 2 - no breakdown during test

no use to discuss the electric strength without consideration of the period of its exposure to electric field because of the kinetic character of the dielectric destruction. At 77 K the destruction becomes almost critical and the special care should be taken to keep the dielectric strength below the critical value under all the conditions including the short-term overvoltage duties which often take place in the electrical units, otherwise the dielectric would be broken down.

At the same time at 77 K and at the electric strength values not exceeding some "critical" value no deterioration of the dielectric performance was detected under the voltage applied. Therefore, in this case the required lifetime can be omitted when choosing the operating dielectric strength value.

1.6. High-voltage insulation scheme

The two possible versions of winding manufacturing were mentioned above. Below are presented considerations of their technological feasibility taking into account the aspects of insulation system design, i.e. choosing the proper materials and insulation intervals.

All the insulation intervals have been taken to be suitable to the more complicated modification of stator winding insulation system corresponding to the generator rated voltage of 10 kV.

In a design presented in Fig.1.4, the winding conductors of different phases intersect and due to the technological scheme of winding are located in practically one and the same plane. Epoxy impregnation and baking can be performed only after the winding manufacturing process is finished. Therefore the epoxy can be used as an insulation if the wires are insulated.

Two technological processes for insulation system formation are possible:

1. The conductors are insulated along their full length with porous non-impregnated insulation (e.g. annealed glass tape in half overlap, or cable paper, etc.) to provide the required thickness. Then, the winding is wound onto the frame with the help of a special attachment and evacuated, after which it is impregnated with one of the compounds based on epoxy resin developed at our Institute for cryogenic temperature range. Electric strength of the compound is about 100-140 kV/mm at liquid nitrogen temperature [1.4]. Field intensity between parallel conductors of different phases lying in the same plane in the interphase zone can be estimated from the equation:

$$E_{max} = \frac{0.45 \times U}{r \times ln\left((r + 0.5 \times S)/r\right)},$$

The same equation is valid for intersecting conductors as well [1.5]. The designations used in the formulae are illustrated by Fig.1.9 (a, b). Taking the

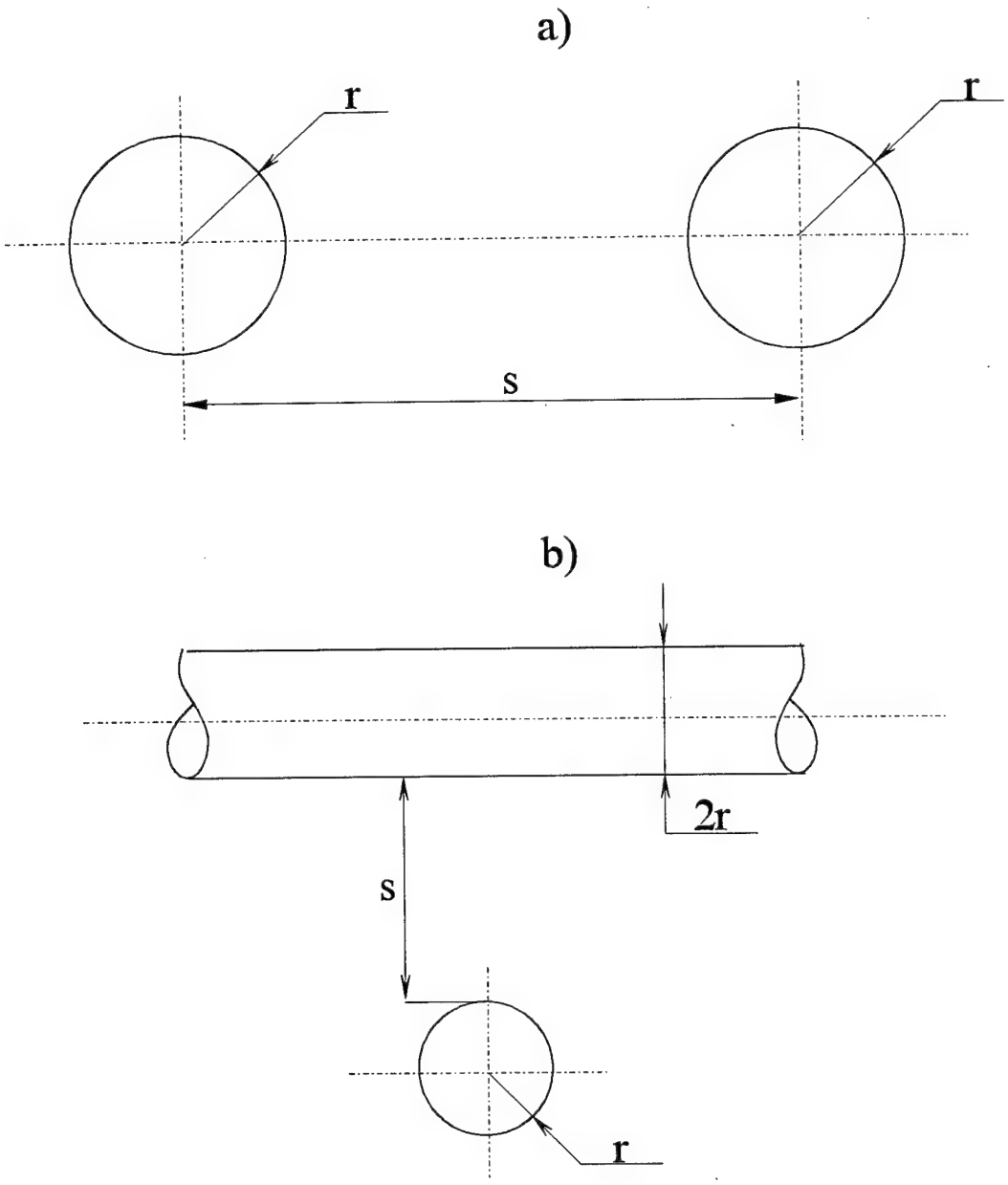

Fig.1.9. Explanatory drawing to the calculation of electrical stress in the insulation

diameter of described circumference to be approximately 5 mm, we get r = 2.5 mm. Let us assume that the conductor is insulated with an annealed glass tape in half overlap, i.e. S = 0.4 mm. Then E_{max} = 23.4 kV/mm. A close value of E is obtained for intersecting wires, too. Due to the presence of stress concentrators the maximum electric field intensity is about 1.5 times. This means that the estimated value of maximum intensity is about 40 kV/mm, what is 2.5 times less than the electric strength value given in [1.4]. Taking into account the peculiarities of dielectric ageing at low temperatures, may be considered as an admissible value, if only the level of overvoltage is not greater than that taken conventionally for electrical machinery (K_{over} = 2). It should be emphasized that compound impregnation and baking will deteriorate cooling efficiency of the winding because of the low thermal conductivity of the compound. So, an important point in the process of winding impregnating and baking is to make adequate cooling ducts.

2. In the other case the wires are insulated over their whole length using a polymer film with an adhesive sublayer, for example a lavsan film 50 μm thick laid in half overlap. Here we get E_{max} = 45.9 kV/mm. However, it should be borne in mind that dielectric strength of polymers, in particular of the lavsan film, is higher than that of epoxy compounds (Fig.1.8). Employing high-strength capacitor-type films, e.g. a 11.5 μm thick film wound in two layers in half overlap, we can obtain large margins in electric strength (Fig.1.8). Besides, heat removal from the winding conductors is significantly improved thanks to low insulation thickness. After the winding is wound, it is positioned onto the cylinder and secured by means of bandages made of glass tape impregnated with epoxy compound.

The design version presented in Fig.1.5 is a more convenient one from the viewpoint of insulation system manufacturing. Here, the cylinder separating the two winding layers serves as interlayer insulation. The cylinder thickness chosen in accordance with the requirements of mechanical strength and technological peculiarities meets the requirements from electric strength. Both on the inner and on the outer surface of the cylinder the wires do not intersect and run parallel to one another. It should be emphasized that the voltage between the adjacent conductors is the voltage of a single turn, except for the zones between phases. Interturn insulation may be made of a reduced thickness, contributing thereby to improvement of winding cooling. Insulation between phases (of the extreme conductors of adjacent phase groups) should be manufactured to withstand full phase voltage.

At the present stage of development, the second technological variant described above seems preferable for the specified winding version, i.e. the wired are insulated with thin capacitor-type polymer film having the adhesive sublayer. The interphase insulation is made with a 10 - 20 μm thick film wound in one layer in half overlap, and the extreme conductors of phases (semiphases) are insulated by 3-5 layers of this film wound in half overlap. After the winding process is finished, the winding is bandaged with strips of glass tape impregnated with epoxy compound, enhancing the mechanical rigidity of the whole structure. Of course,

there exists still another technology for insulation system manufacturing. The winding conductors of each phase are laid with small spaces between them. Dielectric barriers are positioned between the extreme conductors of adjacent phases (semiphases), and the whole winding is filled by a thin layer of compound, which in this situation provides both electrical and mechanical strength of the winding. We would like to emphasize that in case of placing the winding on both surfaces of the cylinder, a special attention is to be paid to ensuring adequate insulation in the zones between phases at the end faces of the cylindrical shell.

1.7. Determination of coolant type and armature operating temperature

The analysis of pure metal properties and effectiveness of employing them at low temperature (Fig.1.10 -1.11) gave evidence for the feasibility of applying pure aluminum and pure copper within the temperature range from 10 to 30 K, and pure beryllium at the temperature about 77 K, i.e. the liquid nitrogen temperature. To exploit properly the possibilities offered by application of pure metals at low temperatures, liquid hydrogen is to be chosen as coolant for electrical machine windings made of pure aluminum and copper, and liquid nitrogen - for the windings of pure beryllium. For cryogenically-cooled electrical machines with the windings made of pure aluminum and copper, liquid neon can be used as well. When deciding between liquid hydrogen and neon, one should bear in mind the optimization parameter of a machine: it may be either its total mass or volume. With liquid neon, the total mass of the coolant is 5 times greater than with liquid hydrogen, but its volume is 3 times less (Table 1.4.).

Table 1.4

Comparison of the coolant thermophysical properties

		N_2	He^4	H_2	Ne
Boiling temperature	K	77.36	4.2	20.38	27.102
Heat of evaporation	kJ/kg	198.4	20.4	481.5	86.2
Density	kg/m^3	804	125	70.8	1206
Specific mass flowrate	g/W·s	$5 \cdot 10^{-3}$	$4.9 \cdot 10^{-2}$	$2.1 \cdot 10^{-3}$	$1.2 \cdot 10^{-2}$
Specific volume flowrate	l/W·s	$6.2 \cdot 10^{-6}$	$3.9 \cdot 10^{-4}$	$2.96 \cdot 10^{-5}$	$9.95 \cdot 10^{-6}$

At the present stage of investigations, liquid hydrogen has been chosen as the main coolant for the cryogenic windings of pure aluminum. Liquid nitrogen and

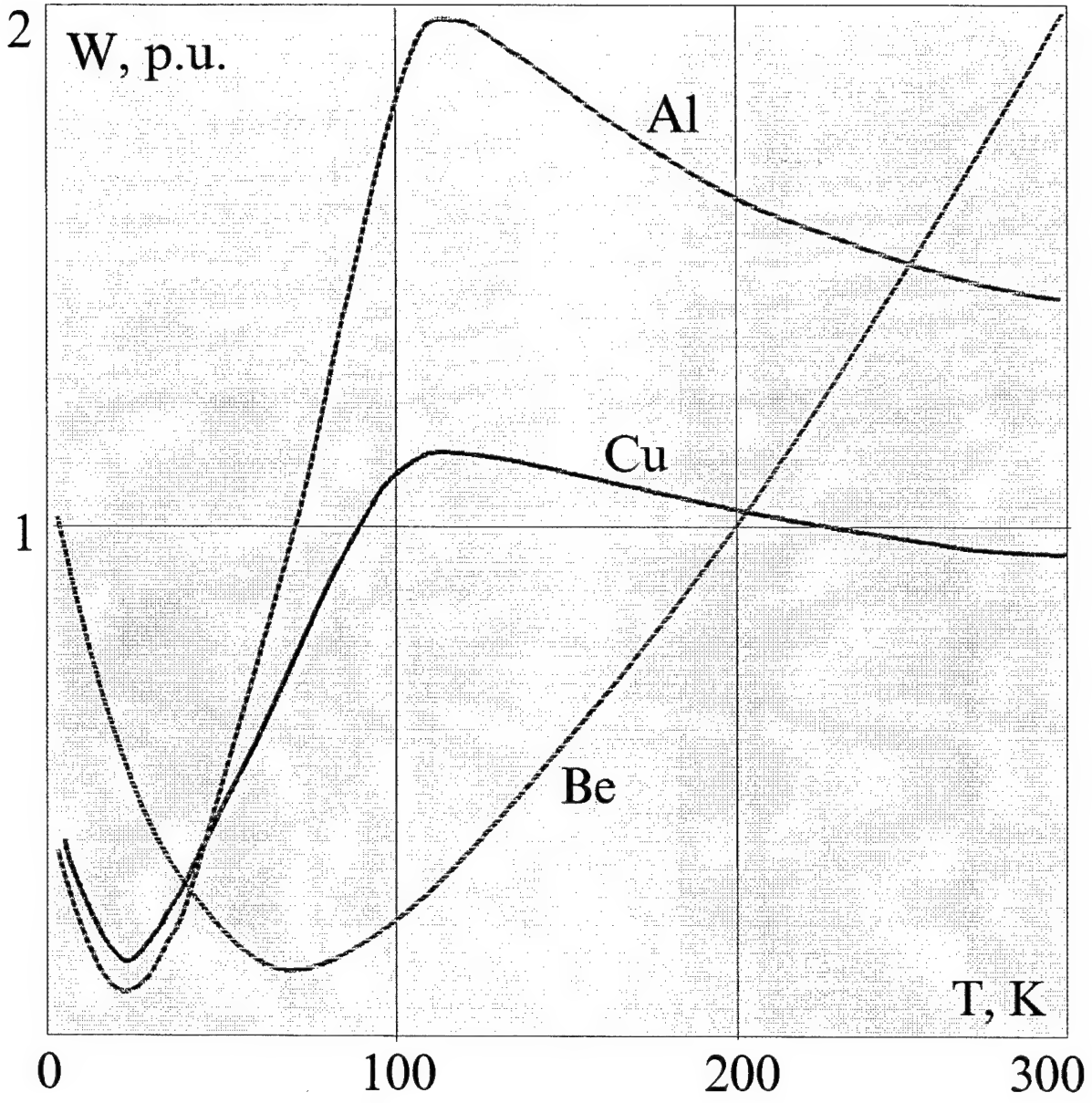

Fig.1.10.Effectiveness of the application of high-puritymetals at different temperatures

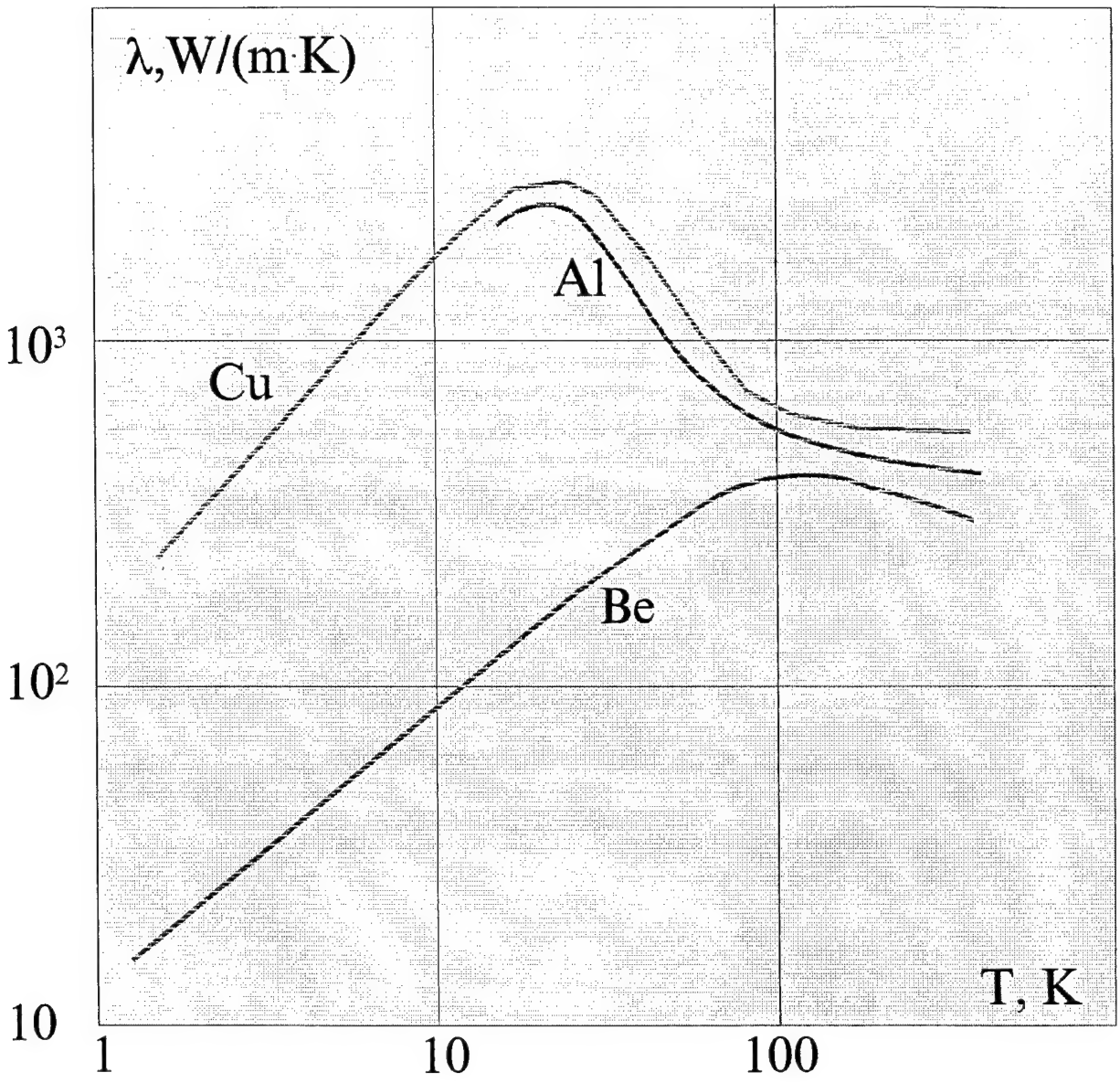

Fig.1.11.Temperature dependence of specific thermal conductivity for the high-purity metals

helium were used as coolants when testing the model bars at various temperature levels. It should be mentioned that though electrical resistance of pure aluminum and at liquid helium temperature is lower than at liquid hydrogen temperature, the effectiveness of cryostabilization by means of liquid hydrogen is much better, because its heat of evaporation, heat capacity and thermophysical boiling parameters are considerably higher.

For a developed design of cryoalternator armature, preliminary thermal calculations were performed for the non-blowed thermal bridges and current leads, the results of which are illustrated by Fig.1.12-1.13.

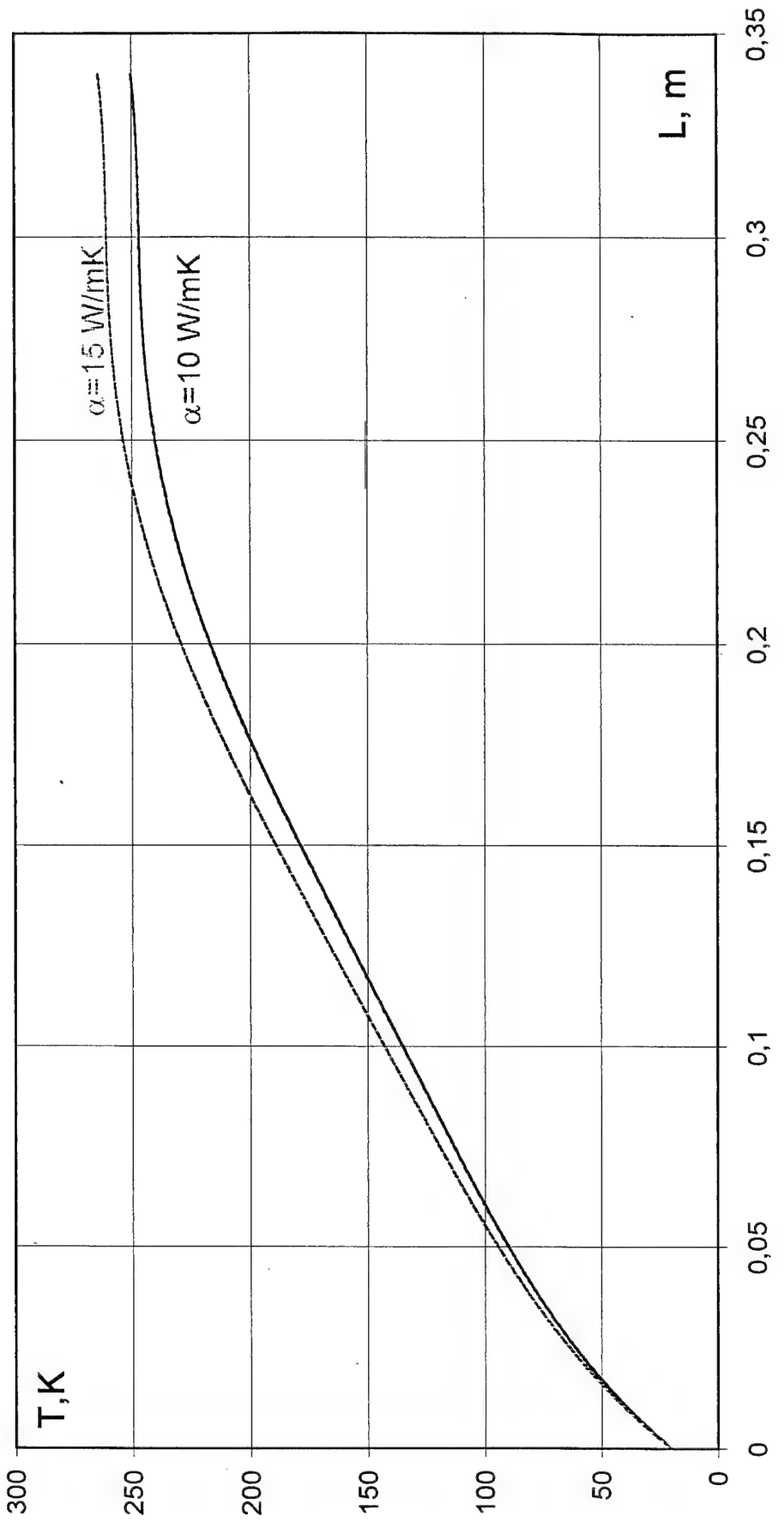

Fig.1.12. Temperature distribution along non-blown thermal bridge

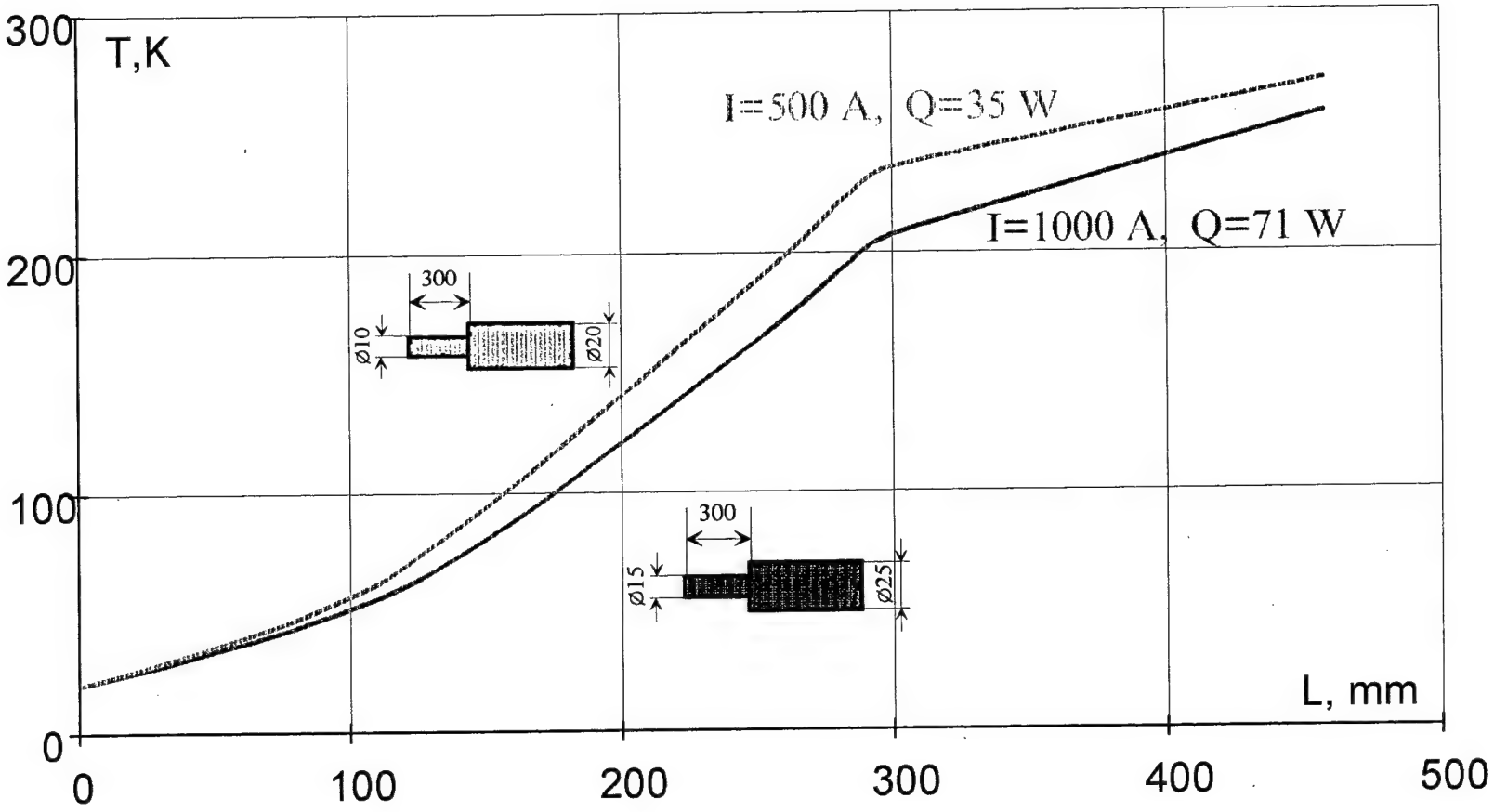

Fig.1.13. Temperature distribution along non-blown current leads of different design

2. DETAILED ARMATURE BAR DESIGN

2.1. Helical winding scheme

Helical winding is the one attractive for slotless armatures because of absence of end turns, small volume and weight and simplified manufacturing technology. Electrical scheme of helical winding is presented in Fig.2.1. Each armature bar is positioned along a helix, two layers of the winding represent two helixes opposing each other (Fig.2.2).

The winding coefficient of helical winding may be presented as [2.1, 2.2]

$$k_w = k_d k_h, \tag{2.1}$$

where k_d - winding coefficient, characterizing winding distribution around circumference, equal to

$$k_d = \frac{\sin\nu\frac{\pi}{2}\frac{s}{\tau}}{\nu\frac{\pi}{2}\frac{s}{\tau}}; \tag{2.2}$$

s - phase zone pitch, τ - pole pitch.

Coefficient k_h, specific for helical windings, characterizes its distribution along the winding length and is determined as

$$k_h = \frac{\sin\nu\frac{\pi}{2}\frac{l_a}{l_h}}{\nu\frac{\pi}{2}\frac{l_a}{l_h}}, \tag{2.3}$$

where l_a - active length of the alternator, l_h - total length of helical winding.

Finally the winding coefficient may be determined as

$$k_w = \frac{\sin\nu\frac{\pi}{2}\frac{s}{\tau}\sin\nu\frac{\pi}{2}\frac{l_a}{l_h}}{(\nu\frac{\pi}{2})^2\frac{s}{\tau}\frac{l_a}{l_h}}. \tag{2.4}$$

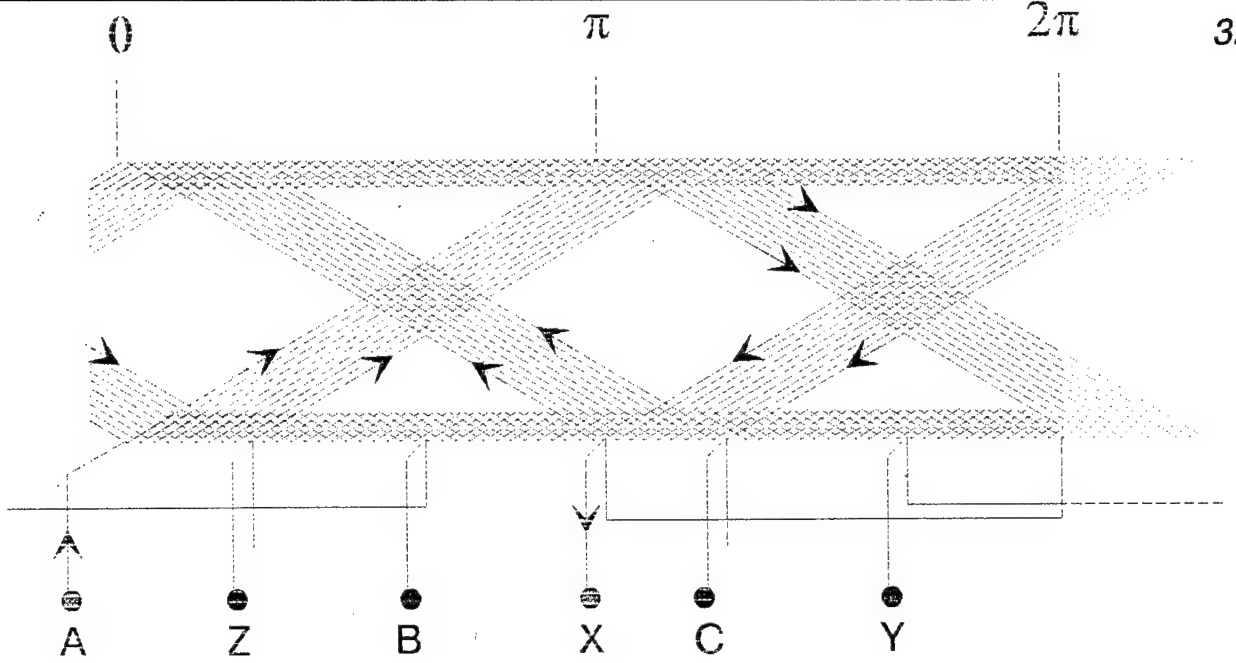

Fig.2.1. Principal electric scheme of helical winding

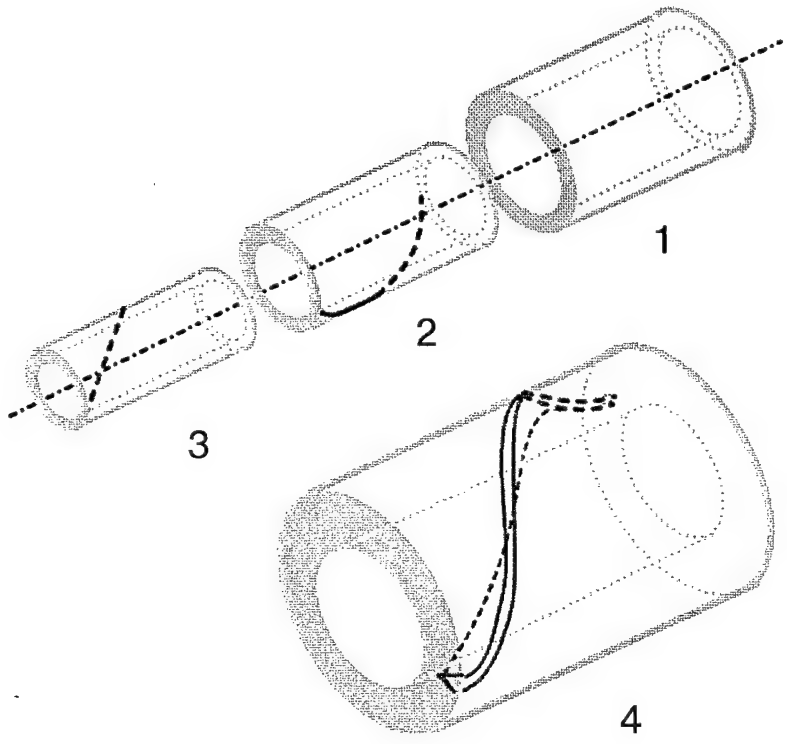

Fig.2.2. General construction of the armature with helical winding

1 - armature screen, 2 - bars of upper layer,
3 - bars of lower layer, 4 - cylinder with helical winding

In case the active length is equal to the full length of the winding the winding pitch of helical turn varies from $y = 0$ to $y = 2\tau$. Magnetic flux, linked with the turn is proportional to the area of quadrangle. In this case coefficient k_h equals

$$k_h = \frac{2}{\pi\nu}\sin\frac{\pi}{2}\nu,$$

and the winding coefficient for $\nu = 1$ is determined as

$$k_w = \frac{6}{\frac{2}{\pi}} = 0.608..$$

It may be reasonable to increase the length l_h of helical winding, making it $l_h > l_a$. Then the flux, linked with helical turn will be proportional to the area of a hexagon. The pitch of the turn will vary along the active zone from $y = y'$ to $y = y''$, where

$$\frac{y'}{y''} = \frac{l_h - l_a}{l_h + l_a}.$$

Thus the winding coefficient and electromotive force of helical winding increases with the growth of l_h .

To suppress higher harmonics in the electromotive force curve of helical winding one has to vary the ratio l_a/l_h. To suppress harmonics, divisible by ν, it is necessary to introduce the ratio:

$$\frac{l_a}{l_h} = \frac{\nu - 1}{\nu}.$$

The detailed electric scheme of helical winding accepted for one of the variants of the developed armature of the high-speed alternator is presented in Fig.2.3. It represents a 4-pole three-phase double layer winding with 108 armature bars in each layer. The total amount of the bars equals 216 with 36 turns in each phase.

The final electric scheme of the winding is dependent from the magnetic flux produced by the excitation winding in the armature winding region and may be settled only after the rotor detailed design development.

2.2. Variants of individual bar design

When discussing the individual bar design it is necessary to take into account the following. In conventional electrical machines the bar of the armature winding represents the part of the winding between two end clips, connecting this bar with the

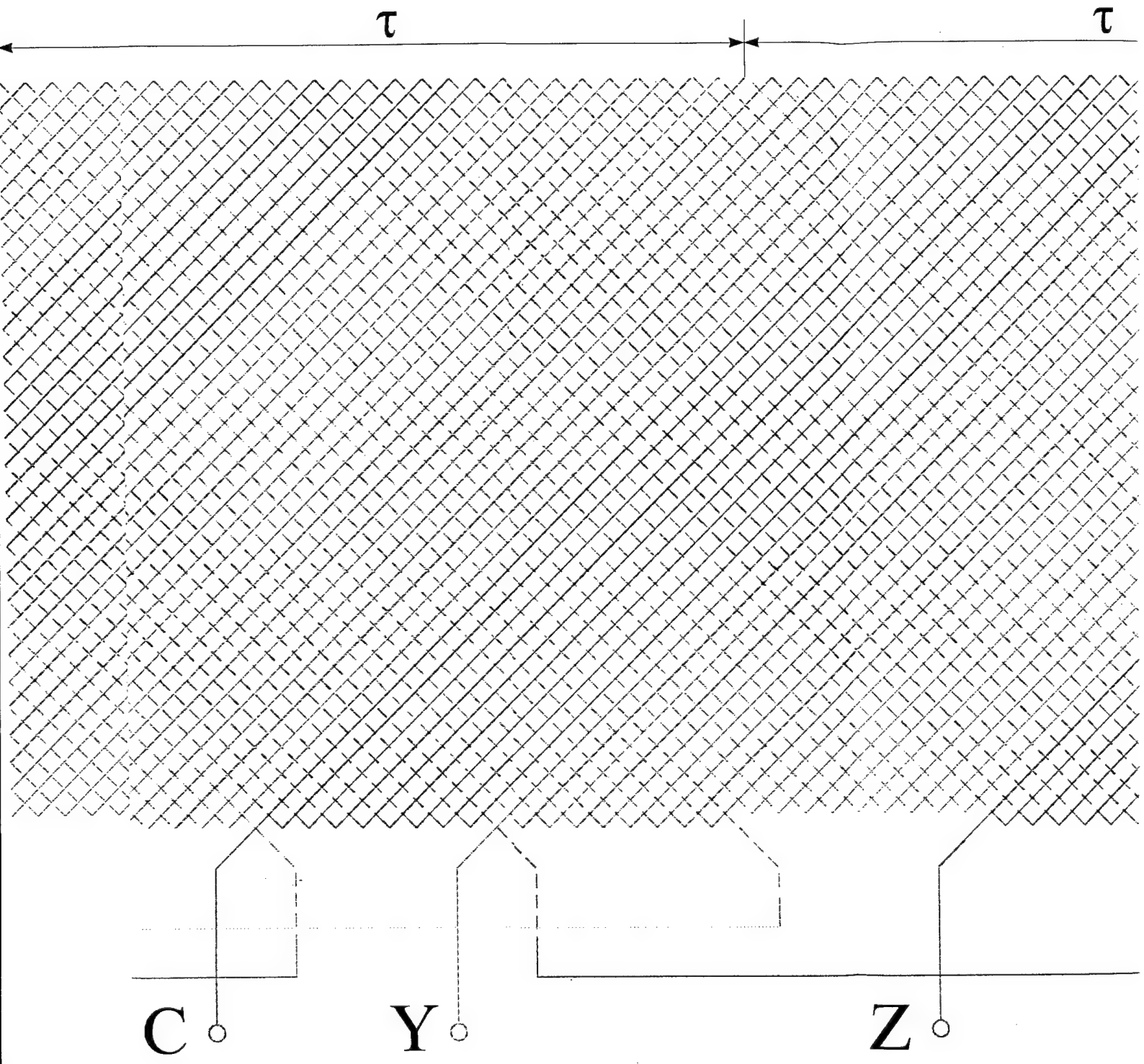

Fig.2.3. Electrical scheme of the

two adjacent ones. If there is no soldered connection between the two bars, they are called a turn.

It is always desirable with the armature winding characterized by low electric resistance to minimize the amount of the interphase electric connections. Therefore it is reasonable to develop the winding manufacturing process with an introduction of continuous winding laying out along the length of a phase, semi-phase or at least a part of a phase zone. Then the winding will be subdivided into a number of turns (or one turn) and each turn will comprise two semi-turns which will be later on named bars (though they differ from the real bars of conventional alternators). In our case the bar is the element of helical winding occupying one helical slot of the support structure.

The bar is subdivided into elementary wires. They may be insulated high-purity aluminum wires with the diameter of at least 0.1 mm (the less the better). Then the elementary wires should be twisted into strands with further manufacturing of multifilumentary strands of rectangular cross-section. These multifilumentary strands will represent the armature winding bar. The elementary wires in such a bar have a double-stage transposition. They will be characterized by low circulating current loss and relatively high eddy-current loss. Moreover such bars are to be handled with care because of a low mechanical strength of high-purity aluminum.

In the second variant the basic elementary wire is a composite with high-purity aluminum fibers in a reinforcement matrix. The fibers have a complex twist of 7×7 within the composite wire. The composite wires are then twisted in a strand with further manufacturing of multifilumentary transposed bars of rectangular cross-section. The elementary wires (fibers) have finally a three or four stage transposition scheme within the bar. When manufacturing the bars from the composite wires it is necessary to pay attention to their relatively high rigidity as compared to high-purity wires without a matrix. The bars will have relatively low eddy-current loss and practically zero circulating current loss.

The bars of helical armature winding, positioned in the upper and lower layers (Fig.2.2), are to have different lengths and different direction angles, corresponding to the angles α_1 and α_2:

$$\alpha_1 = \arcsin \frac{z(b + b_i)}{2\pi D_{h1}}, \quad \alpha_2 = \arcsin \frac{z(b + b_i)}{2\pi D_{h2}},$$

where z - number of armature bars in two layers, b - bar width, b_i - insulation gap, D_{c1} and D_{c2} - correspondingly the inner diameters of the first and the second layer.

The average winding diameter and direction angle are determined by the relation

$$\alpha_{av} = \arcsin \frac{z(b + b_i)}{2\pi D_{av}}.$$

If y_{av} is an average winding pitch across the diameter D_{av}, the armature winding length equals to

$$l = \frac{y_{av} \sin\alpha_{av}}{\cos\alpha_1 + \cos\alpha_2},$$

and the length of helical armature bars in the layers is determined as

$$l_1 = \frac{D_{h1}}{D_{a\tau}} \left(\frac{y_{a\tau}}{\cos\alpha_1 + \cos\alpha_2} \right),$$

$$l_2 = \frac{D_{h2}}{D_{a\tau}} \left(\frac{y_{a\tau}}{\cos\alpha_1 + \cos\alpha_2} \right).$$

These relations help to optimize the packing factor of the alternator armature active zone.

2.3. Magnetic fields in the armature region

Magnetic fields acting in the armature region are produced by both excitation and armature windings. There exists a variety of methods for calculation of the 3D magnetic fields, induced by the superconducting field winding. The methods may be applied to a hyperconducting alternator as well in case ferromagnetic elements in the rotor are absent. The character of excitation magnetic field distribution is well known also. As for the helical armature winding, its 3D magnetic field is of interest.

A simplified but relatively accurate scheme of magnetic field calculations may be introduced. It is shown in Fig.2.4.

Current density in helical winding is characterized by two components - axial and tangential (Fig.2.5):

$$J_z = J_h \sin\alpha, \quad J_\Theta = J_h \cos\alpha..$$

whereas in conventional lap winding there is only an axial component of current density in the active zone.

It results in the three-dimensional field character of the helical winding in the active zone of the alternator.

Poisson equation for amplitudes of magnetic vector potential is

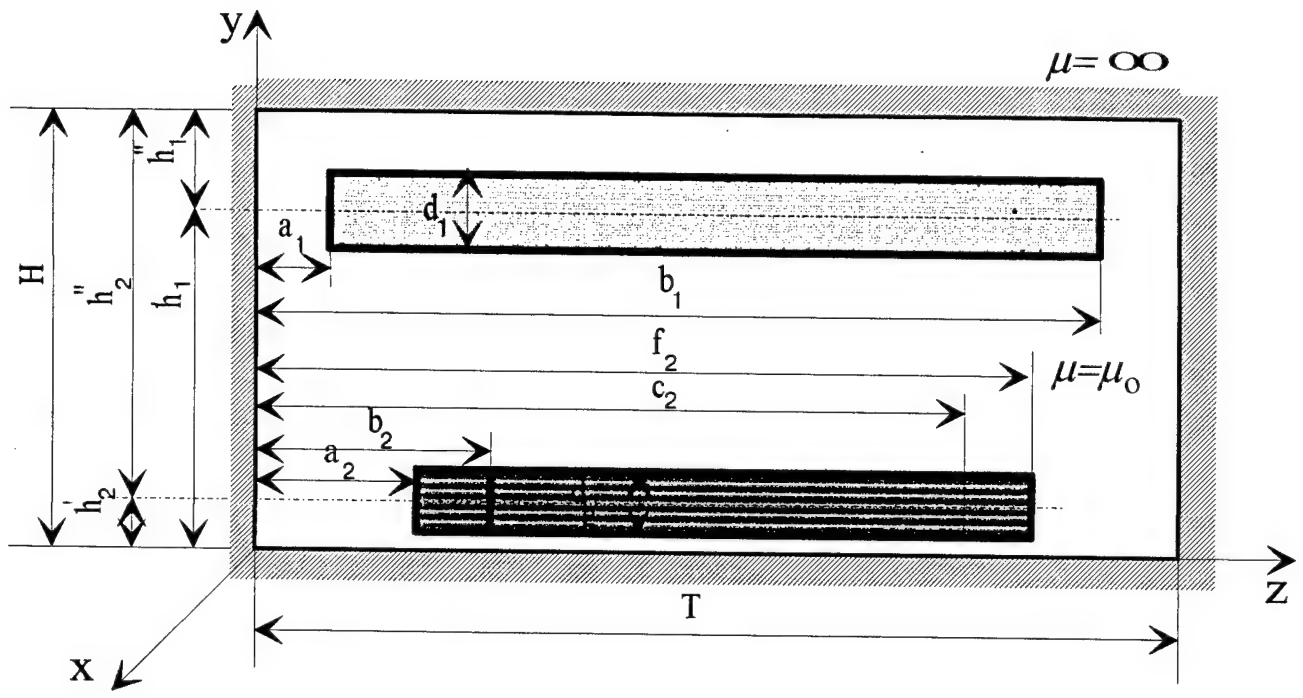

Fig.2.4. Scheme for calculation of 3D magnetic fields of helical winding.

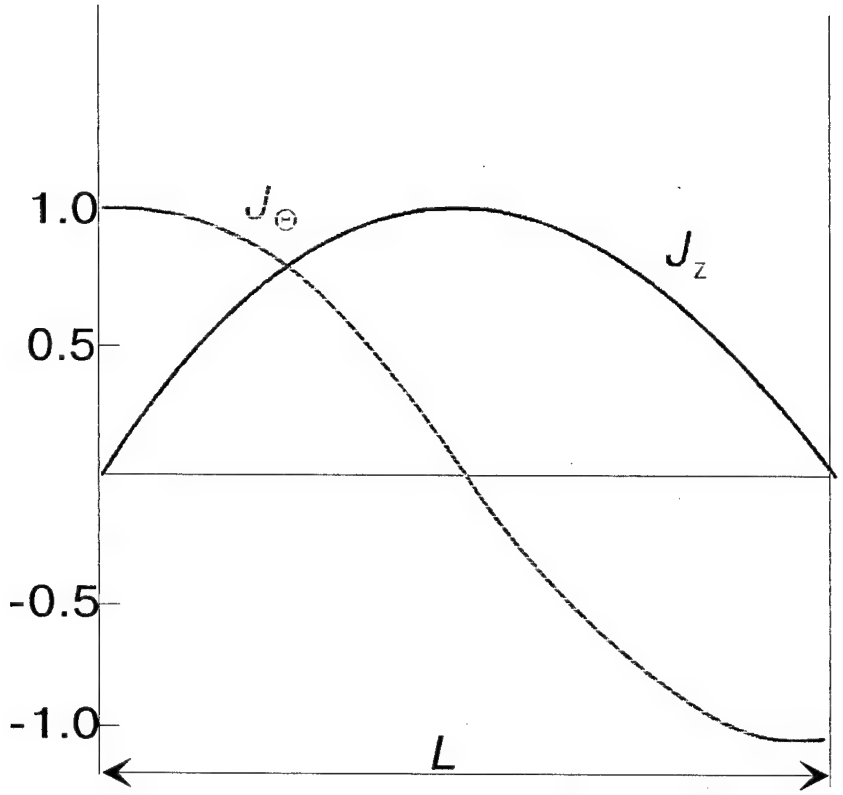

Fig.2.5. Components of current density of helical winding

$$\frac{\partial^2 U_i}{\partial y^2}+\frac{\partial^2 U_i}{\partial z^2}-\left(\frac{\pi}{\tau}\right)U_i=-\mu_0 J_i \quad (i=x,z),$$

where J_i - amplitude of current density.

Amplitudes of magnetic vector potential may be determined as:

$$P_{nsz}=J_h\frac{\sin\alpha}{\left(\frac{\pi}{l_h}\right)^2-\left(\frac{n\pi}{T}\right)^2}\left(\frac{n\pi}{T}\cos\frac{n\pi}{T}\alpha_1-\frac{\pi}{l_h}\sin\frac{n\pi}{T}b_1\right),$$

$$P_{nsx}=J_h\frac{\cos\alpha}{\left(\frac{\pi}{l_h}\right)^2-\left(\frac{n\pi}{T}\right)^2}\left(\frac{\pi}{l_h}\cos\frac{n\pi}{T}\alpha_1-\frac{n\pi}{T}\sin\frac{n\pi}{T}b_1\right). \qquad (2.6)$$

Components of magnetic flux densities are equal to:

if $0<y<h_1'-d_1/2$

$$U_x=\frac{4\mu_0}{T}\sum_{n=0,1,2,\ldots}^{\infty}P_{ncx}\frac{\mathrm{ch}\lambda\left(y-h_1'+\frac{d_1}{2}\right)}{\lambda^2\mathrm{sh}\lambda H}\cos\frac{n\pi z}{T},$$

$$U_z=\frac{4\mu_0}{T}\sum_{n=0,1,2,\ldots}^{\infty}P_{ncz}\frac{\mathrm{ch}\lambda\left(y-h_1'+\frac{d_1}{2}\right)}{\lambda^2\mathrm{sh}\lambda H}\sin\frac{n\pi z}{T},$$

$$B_x=\frac{4\mu_0}{T}\sum_{n=0,1,2,\ldots}^{\infty}P_{ncz}\frac{\mathrm{sh}\lambda\left(y-h_1'+\frac{d_1}{2}\right)}{\lambda\mathrm{sh}\lambda H}\sin\frac{n\pi z}{T},$$

$$B_y=\frac{4\mu_0}{T}\sum_{n=0,1,2,\ldots}^{\infty}\left(\frac{n\pi}{T}P_{ncx}-\frac{\pi}{\tau}P_{nsz}\right)sin\frac{n\pi z}{T}\frac{\mathrm{ch}\lambda\left(y-h_1'+\frac{d_1}{2}\right)}{\lambda^2\mathrm{sh}\lambda H},$$

$$B_z=\frac{4\mu_0}{T}\sum_{n=0,1,2,\ldots}^{\infty}P_{ncx}\frac{\mathrm{sh}\lambda\left(y-h_1'+\frac{d_1}{2}\right)}{\lambda\mathrm{sh}\lambda H}\cos\frac{n\pi z}{T},$$

if $h_1'-d_1/2<y<h_1'+d_1/2$

$$B_x=\frac{4\mu_0}{T}\sum_{n=0,1,2,\ldots}^{\infty}P_{szc}^{n}\frac{1}{\lambda\mathrm{sh}\lambda H}\sin\frac{n\pi z}{T}\times\left[\mathrm{ch}\lambda h_1''\,\mathrm{sh}\frac{\lambda d_1}{2}\mathrm{sh}\lambda y-\frac{1}{2}\mathrm{sh}\lambda H\mathrm{sh}\lambda\left(y-h_1'+\frac{d_1}{2}\right)\right],$$

$$B_y = \frac{4\mu_0}{T} \sum_{n=0,1,2,\ldots}^{\infty} \frac{1}{\lambda^2 \mathrm{sh}\lambda H} \left(\frac{n\pi}{T} P^n_{czc} - \frac{\pi}{\tau} P^n_{szc} \right) \sin \frac{n\pi z}{T} \left[\mathrm{ch}\lambda h_1'' \, \mathrm{sh} \frac{\lambda d_1}{2} \mathrm{ch}\lambda y - \mathrm{sh}\lambda H \mathrm{sh}^2 \frac{\lambda}{2} \left(y - h_1' + \frac{d_1}{2} \right) \right],$$

$$B_z = -\frac{4\mu_0}{T} \sum_{n=0,1,2,\ldots}^{\infty} P^n_{cxc} \frac{1}{\lambda \mathrm{sh}\lambda H} \cos \frac{n\pi z}{T} \times \left[\mathrm{ch}\lambda h_1'' \, \mathrm{sh} \frac{\lambda d_1}{2} \mathrm{sh}\lambda y - \frac{1}{2} \mathrm{sh}\lambda H \mathrm{sh}\lambda \left(y - h_1' + \frac{d_1}{2} \right) \right],$$

Magnetic fields of helical armature winding were investigated experimentally in the 5 MVA turbogenerator and on a model helical winding described in Part 4. Here are presented the results obtained during investigations of the 5 MVA machine. For comparison there are shown in Fig.2.6 magnetic fields of the slotless lap winding.

The magnetic flux density components B_ρ, B_z and B_6 when the cylinder with helical winding was inserted into the iron screen (Fig.2.7,a) and when there was no iron screen at all (Fig.2.7,b). The experimental data is in good relation with the calculated values of magnetic field components.

The components of magnetic flux, penetrating into the iron screen were measured as well. The axial component of flux density in the iron core is relatively small and its penetration does not result in substantial increase of iron losses. These results permitted to design the armature of the high-speed generator being developed with a ferromagnetic core positioned inside a cryostat.

Figure 2.8 presents distribution of electromagnetic forces in helical winding during the three-phase short-circuit. Axial component of electromagnetic force is equal to

$$F_z = J_\theta B_\rho;$$

radial one - to

$$F_\rho = F_{\rho 1} + F_{\rho 2},$$

where

$$F_{\rho 1} = J_\theta B_z, F_{\rho 2} = J_z B_\theta;$$

and tangential one - to

$$F_\theta = J_z B_\rho;$$

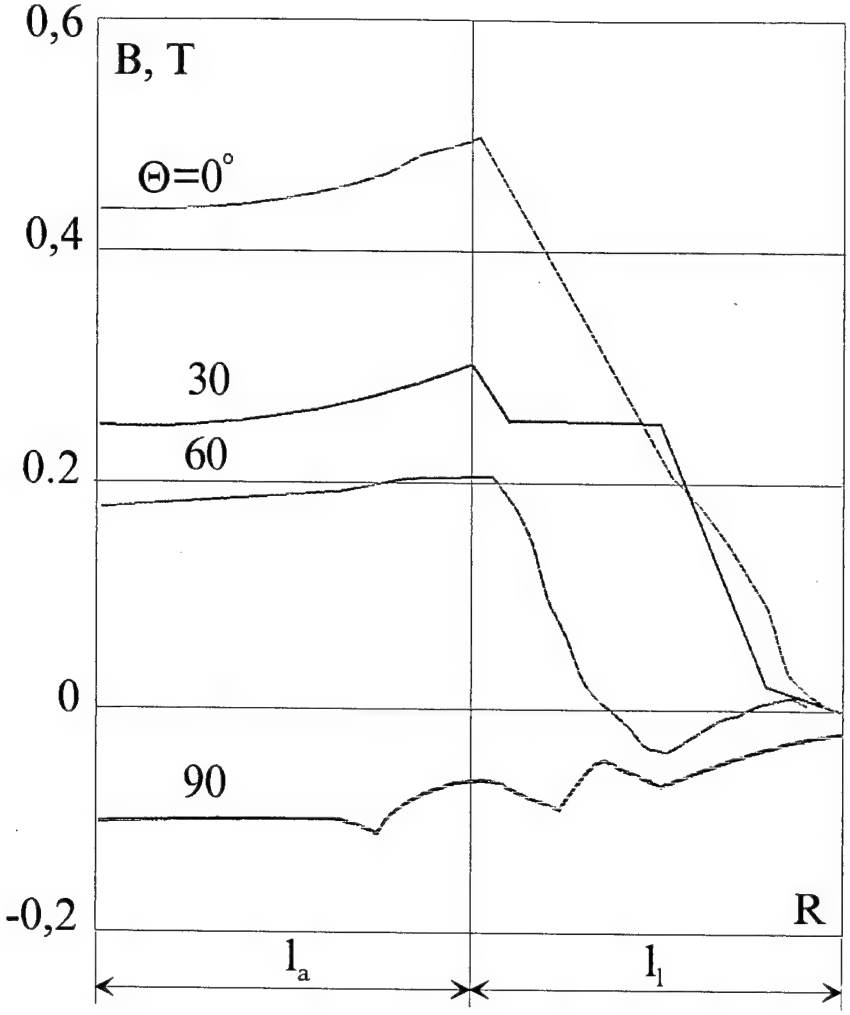

Fig.2.6. Magnetic flux, produced by the exitation winding in the armature winding rejion

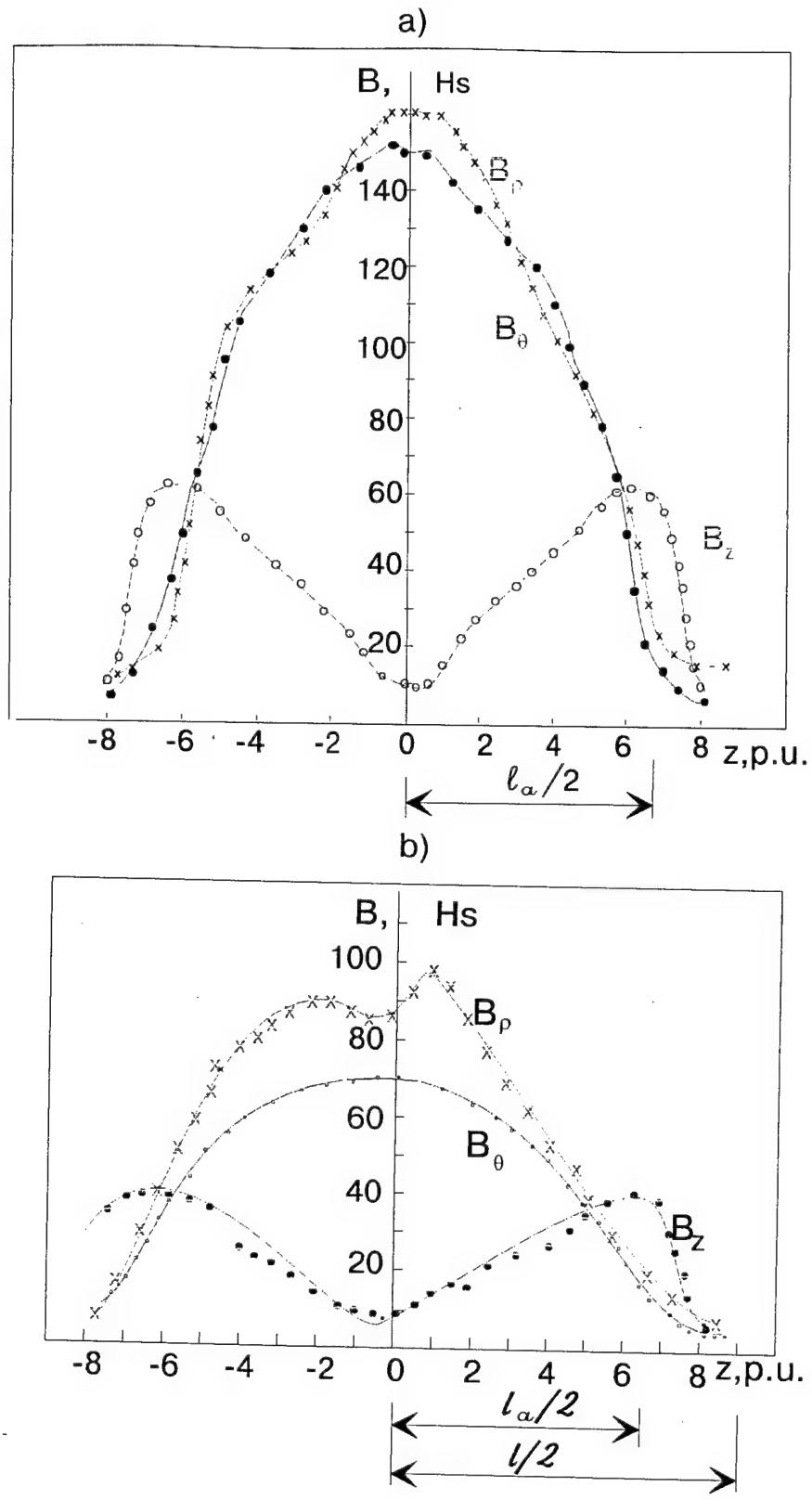

Fig.2.7. Components of magnetic flux density of helical winding with (a) and without (b) iron screen.

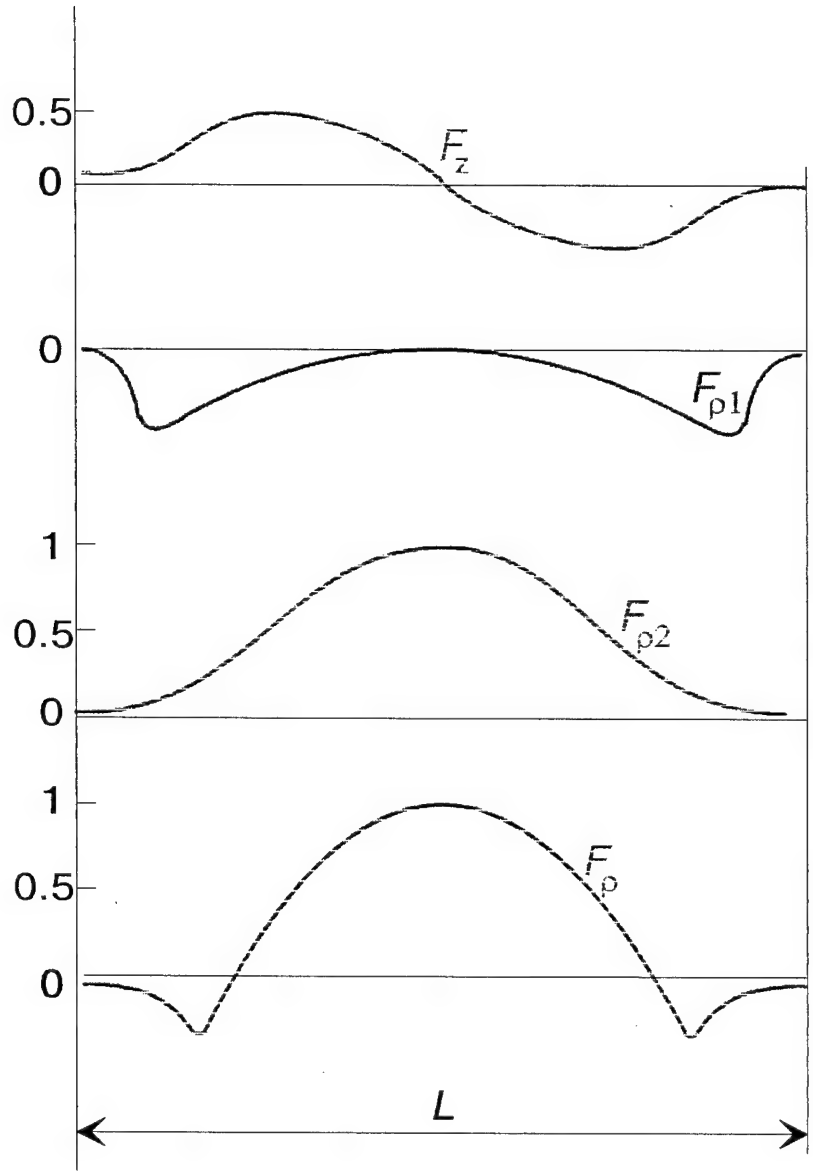

Fig.2.8. Components of forces acting in helical winding

2.4. Optimization of losses

There exist tree types of losses in the armature winding of a synchronous generator: ohmic losses, determined by the specific resistance of the winding material, current density value and volume of the winding material; eddy current losses, produced by the alternating magnetic fields acting in the winding region and circulating current losses, caused by the imperfection of the transposition scheme of the elementary wires inside the armature bar. There may be an extra component of current eddy losses due to the alternating currents flowing inside the elementary wires, but they are negligibly small for the wire diameters being discussed.

The eddy and circulating current losses are produced by both excitation winding and armature winding magnetic fields.

Let us consider a winding, in which the circulating current losses are negligibly small. It is possible in case of multi-stage transposition schemes development for the winding bar manufacturing. The sum of the ohmic and eddy-current losses then equals [3.3]

$$P_{\Sigma} = (J^2 \rho + k \frac{d^2}{\rho}) V, \tag{2.7}$$

where J - current density, ρ - resistivity, d - filament diameter, V - wire volume, k_1 - coefficient of eddy-current losses.

The volume of the wire depends on the current density:

$$V = \frac{k_2}{J},$$

therefore the losses may be determined as:

$$P_{\Sigma} = k_2 \rho J + k_1 k_2 \frac{d^2}{\rho J}. \tag{2.8}$$

With the temperature decrease the first component in the right side of the equation decreases and the second component - increases. The minimum value of losses may be obtained when

$$\frac{dP}{d\rho} = 0,$$

or it may be represented as:

$$\rho J = \sqrt{k_1} d = 1.11 f B d,$$

where $k_1 = \frac{1}{32}\omega^2 d^2$, $\omega = 2\pi f$, f- frequency, B - magnetic flux density.

The optimal filament diameter is obtained from

$$d = \frac{\rho J}{1.11 f B}.$$

Curves for determination of filament diameter for aluminum wires are presented in Fig.2.9.

The wire which is chosen for the armature bar manufacturing consists of high-purity aluminum filaments with diameter of about 0.03 mm. As it may be obtained from Fig.2.9 this wire may be used for the armature bars in a wide range of frequencies. Because of poor mechanical properties of high-purity aluminum the 49 filaments are twisted and embedded in a reinforcing matrix. The outer diameter of the composite wire is 0.3 mm.

Still when manufacturing the experimental armature bar described in Part 3 and 4 there were used different types of wires because it may be reasonable to have not an optimal value of losses but their optimal correlation in case of manufacturing costs restrictions.

2.5. Proposed bar manufacturing process

The armature winding bar of a helical winding, manufactured of high-purity metal or superconductor, is representing a part of either a turn or a semi-phase or a part of semi-phase being continuously wound to minimize the number of electrical connection. Therefore below is given a proposed manufacturing process of development of a bar of helical winding. The multifilumentary wire has the same cross-section as the winding bar to simplify the manufacturing process.

1. Manufacturing of a composite elementary wire with thin high-purity aluminum fibers and reinforcing matrix. The wire is to provide high current density at 20-30 K and decreased eddy losses at high (400-800 Hz) frequencies.

2. Insulating of the composite wire with a proper type of electrical insulation, characterized by good adhesion to the matrix material, stability to thermal cycling and good behavior during the winding impregnation and baking (no cracking and separation from the wire outer surface).

3. Manufacturing of the twisted strands of elementary wires.

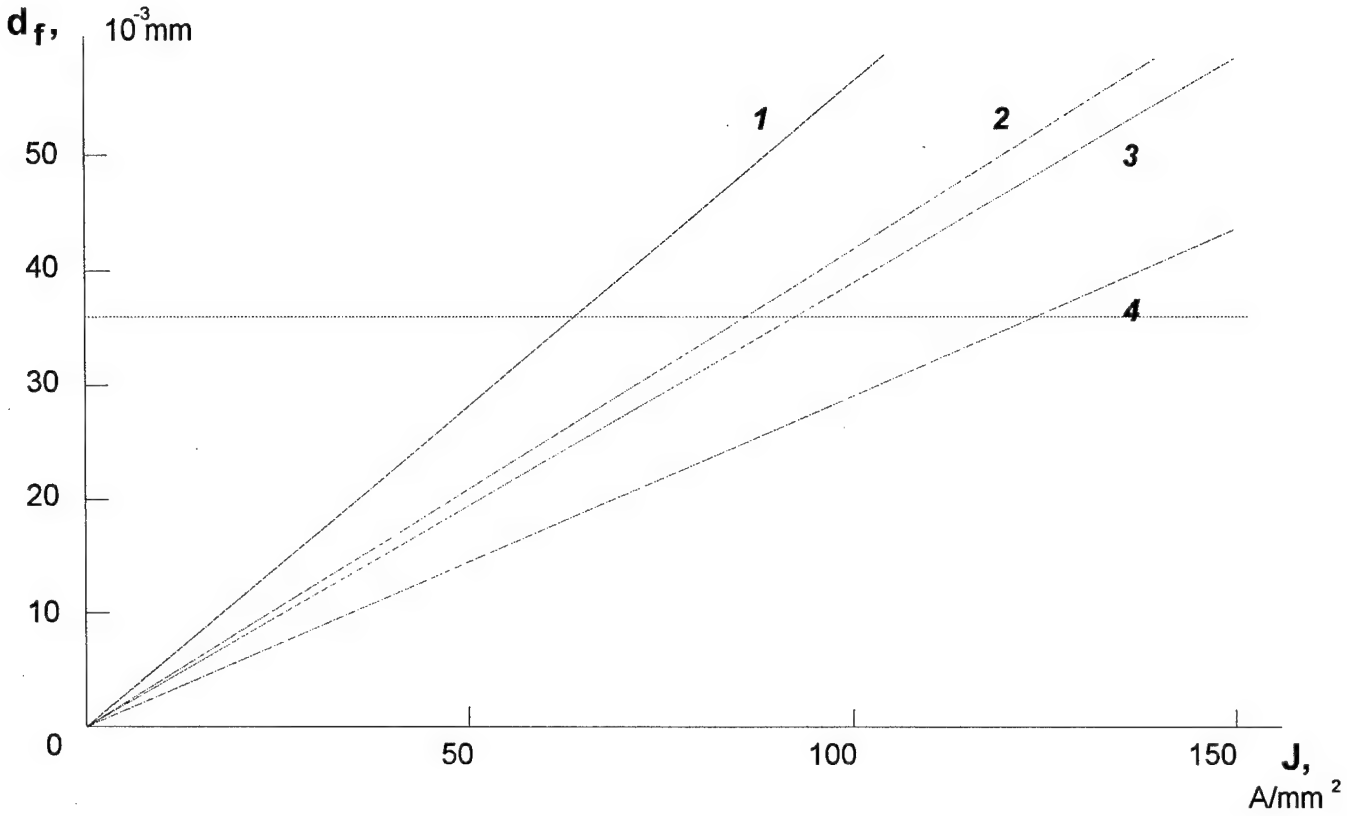

Fig.2.9. Aluminum filument diameter for minimal armature winding losses

1 - B=0.3 T, f=533 Hz

2 - B=0.4 T, f=533 Hz

3 - B=0.3 T, f=800 Hz

4 - B=0.4 T, f=800 Hz

4. Manufacturing of a mulifilumentary transposed wire with a square or rectangular cross-section.

5. Cutting of the wire into pieces equal to the length of the continuous winding element.

6. Checking of the quality of electrical insulation of elementary wires in the prepared mulifilumentary wire cuttings.

7. Preliminary soldering of the multifilumentary cutting ends by a special technological process, suitable for the obtained composite wire.

8. Manufacturing of special clips with a solder coating on the inner side intended for the electrical connections inside the winding.

According to the experimental results presented in Part 4 it is possible to manufacture the armature bar without the main insulation in case the bars are positioned in slots. The impregnation process is to be carried out only when the whole winding will be laid out in slots. The impregnation and baking provides obtaining of a monolithic construction stable to thermal and mechanical stresses. The cooling ducts for the bar cooling are to be organized in a way described in Par. 1.4.

3. ARMATURE BAR FABRICATION

3.1. Fabrication of elementary wires

Elementary wires were initially manufactured of three types:
- high purity aluminum wires 0.1 mm in diameter with enamel insulation 15 μm thick and break-down voltage 50 V;
- high purity aluminum wires 0.3 mm in diameter with enamel insulation 15 μm thick and break-down voltage 20 V;
- composite high-purity aluminum wires 0.3 mm in diameter with 49 filaments of 30 μm diameter, packing factor 0.65, matrix material - Al-Mn, matrix specific resistance $3.4 \cdot 10^{-8}$ Ohm·m (independent of temperature variation), with outer enamel insulation 10 μm thick and break-down voltage 25 V;
- electrotechnical copper wires 0.071 mm in diameter.

The copper wires were used to compare the experimental result and to evaluate the possibility of manufacturing of a relatively cheap armature winding for the cryogenic generator.

There is nothing special about the first, second and the last types of wires. The third one incorporates new technologies and therefore its investigations are of interest. They were carried out for a number of different composite aluminum wires to determine the mechanical parameters and probably to reject the circular composite wire in favour of rectangular one.

Mechanical properties of composite hyperconductors of circular and rectangular cross-section were investigated during tensile test. The composite wire from the point of view of mechanical properties represents a structure, comprising two phases: with a phase of a low mechanical strength, representing high-purity aluminum (mechanically - a matrix [3.1]) and a phase with improved mechanical strength, representing the reinforcement of the composite wire. The obtained stress-strain diagrams permitted to determine the ultimate strength σ and relative elongation. The typical stress-strain diagram of the composite is presented in Fig.3.1. The tests were carried out on a native stress machine 1231 U-10.

The experimental data for the investigated samples of hyperconductors is presented in Table 3.1. It contains the information abouut ultimate strength and relative alongation of four samples of composite wires of different cross-sections.

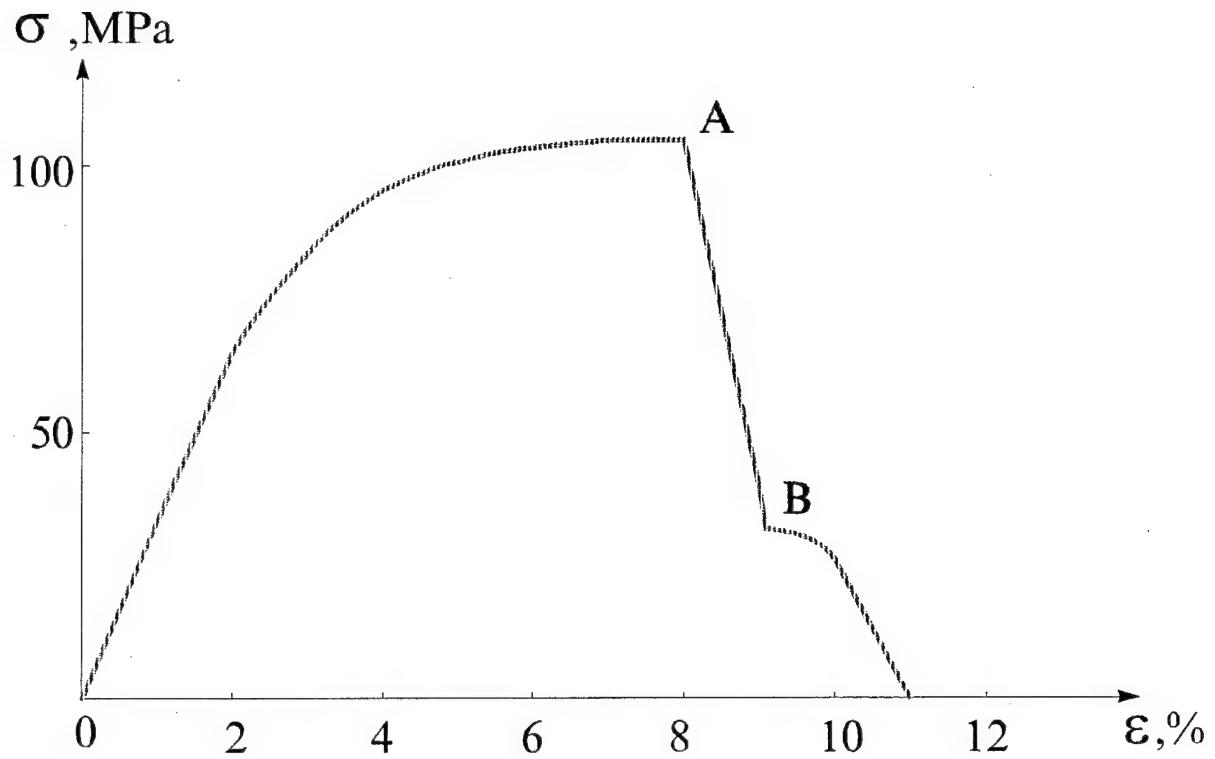

Fig.3.1. Stress strain diagram of a composite material

Table 3.1

Mechanical Strength of Hyperconducting Composite Wires

N	Cross-Section Geometry	Cross-Section Size, mm	Number of Filaments	Ultimate Strength, σ_b, MPa	Relative Elongation, ε, %
1	Square	2×2	7	51-77	10-14
2	Rectangular	2×4	7	84	Not determined
3	Rectangular	2×1	1	93-108	6-11
4	Circular	∅=0.3	49	51-83	Not determined

The fracture load acting over the total cross-section of the composite, was determined. The total fracture load of the hyperconductor P_{hc} represents a sum of the phase load corresponding components:

$$P_{hc} = P_{Al} + P_S \tag{3.1}$$

where P_{Al} - the load acting on the high-purity aluminum and P_S - the load acting on the composite shells.

Accounting for strength σ and area S of the corresponding cross-sections the equation (3.1) may be rewritten as

$$\sigma_{hc} S_{hc} = \sigma_{Al} S_{Al} + \sigma_S S_S \tag{3.2}$$

or

$$\sigma_{hc} = \sigma_{Al} \frac{S_{Al}}{S_{hc}} + \sigma_S \frac{S_S}{S_{hc}} \tag{3.3}$$

Ratios $\frac{S_{Al}}{S_{hc}}$ and $\frac{S_S}{S_{hc}}$ represent the volume fractions of the matrix and of the reinforcement and are equal to V_{Al} and V_S correspondingly.

Therefore equation (3.3) may be presented as

$$\sigma_{hc} = \sigma_{Al} V_{Al} + \sigma_S V_S \tag{3.4}$$

Equation (3.4) is usually referred to as the rule of mixtures.

To evaluate the strength of the high-purity aluminum and of the shells it is possible to apply the datum on micro hardness. It is known that to perform the strength express-

analysis of the metals σ_B under the conditions when the strength cannot be determined directly it is possible to use the ratio

$$\sigma_B = kH_V, \tag{3.5}$$

where k- coefficient of proportionality, H_V- micro hardness as determined by the Vickers method [3.2].

When investigating composite aluminum wires the micro hardness was determined by the transverse and longitudinal grindings on a native micro hardness gauge NT-3. The indentor load was 50 g. A diamond scaffold Vickers pyramid was used with a vertex angle 136°. the micro hardness was then calculated by the formula

$$H_V = \frac{1854P}{d^2}, \tag{3.6}$$

where P - indentor load in grams, d - print diagonal in μm.

For instance in a composite with a single fibre in a matrix (pos.3 of the Table 3.1) the micro hardness of high purity aluminium equals 200 MPa and of the matrix - about 450 MPa. Substituting (3.5) in (3.4) we have

$$\sigma_{hc} = kH_{V_{Al}}V_{Al} + kH_{V_s}V_S, \tag{3.7}$$

and as a result:

$$k = \frac{\sigma_{hc}}{H_{V_{Al}}V_{Al} + H_{V_s}V_S} = \frac{108}{200 \times 0.6 + 450 \times 0.4} \approx 0.33.$$

Therefore the hardness of high purity aluminum $\sigma_{Al} = 0.33 \times 200 \approx 66$ *MPa* and of the matrix material $\sigma_s = 0.33 \times 450 \approx 149$ *MPa.*

The results of fracture deformation of composite high purity aluminum wires of different cross-sections at liquid nitrogen temperature are presented in Fig.3.2-3.5. The process of the composite destruction is characterized by a ductile origin at both ambient and liquid nitrogen temperatures.

3.2. Fabrication of multifilumentary strands

A variety of multifilumentary strands was manufactured to form the bars for investigations in the test-fixtures.

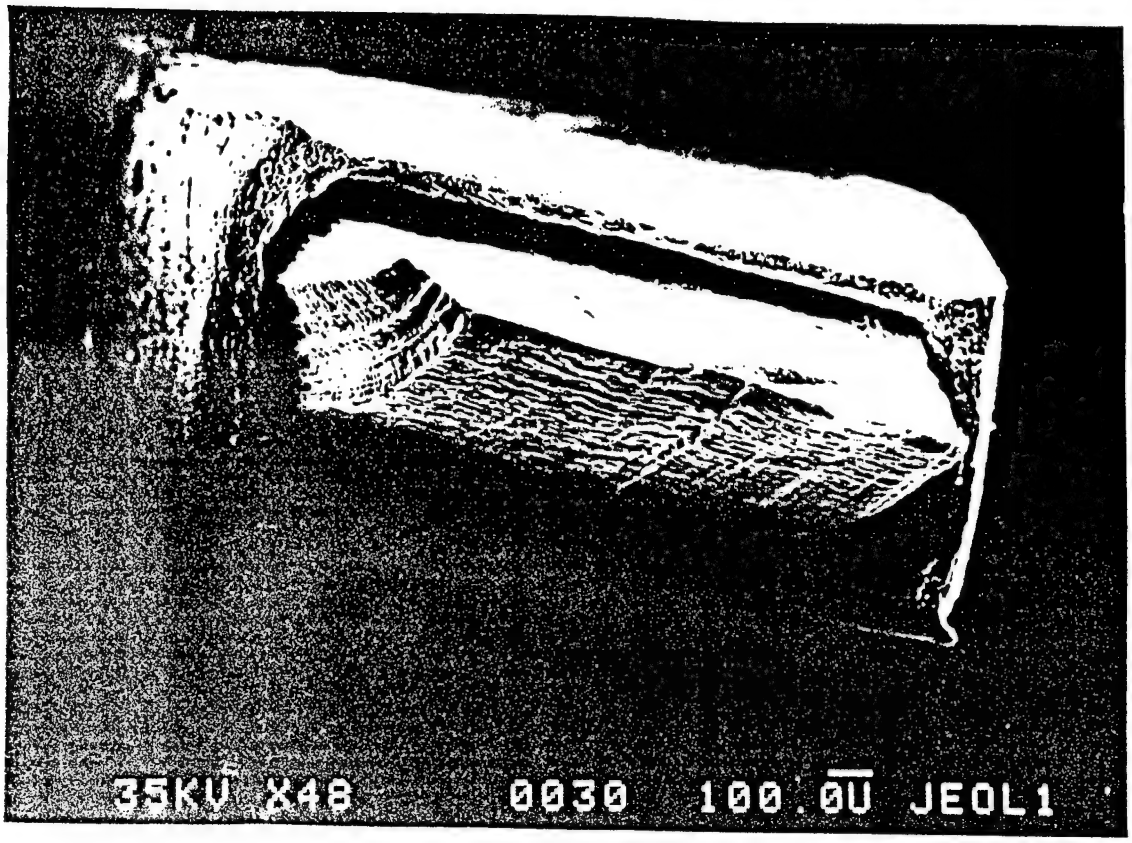

Fig.3.2. Surface fracture of the composite wire with a single fibre at 20° C.

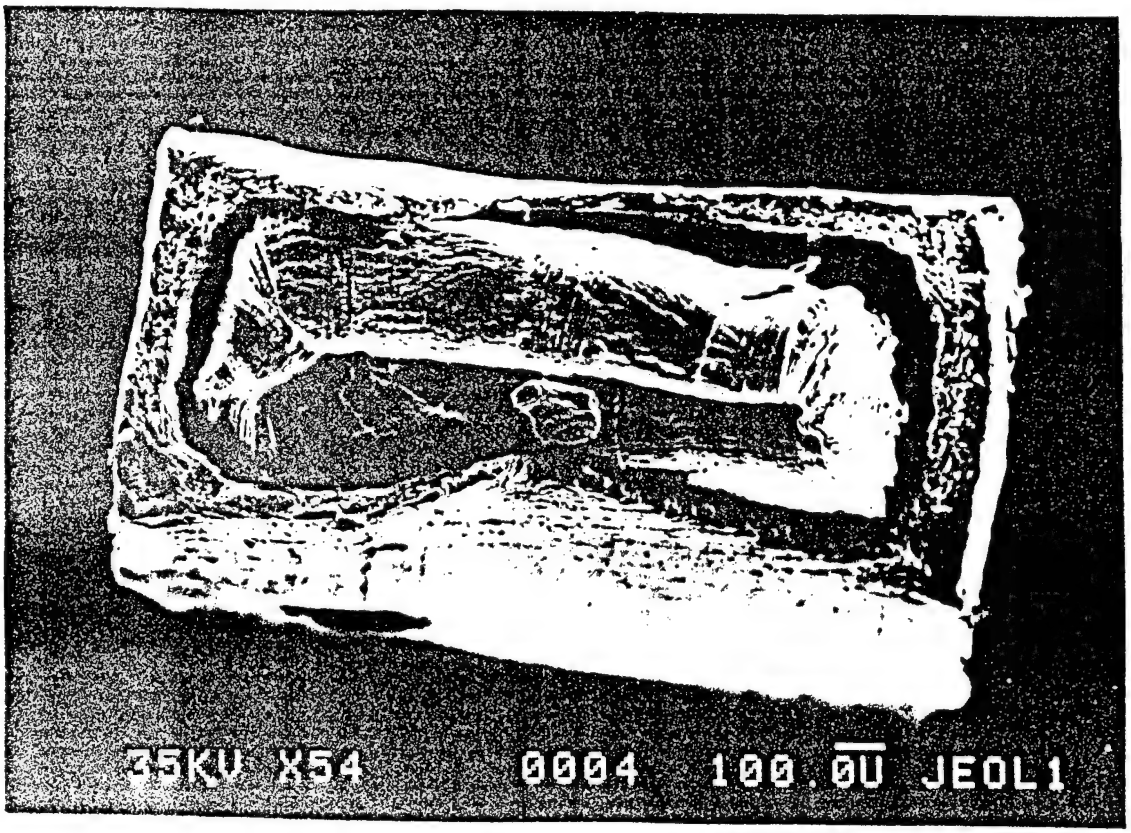

Fig.3.3. Surface fracture of the composite wire with a single fibre at 77 K.

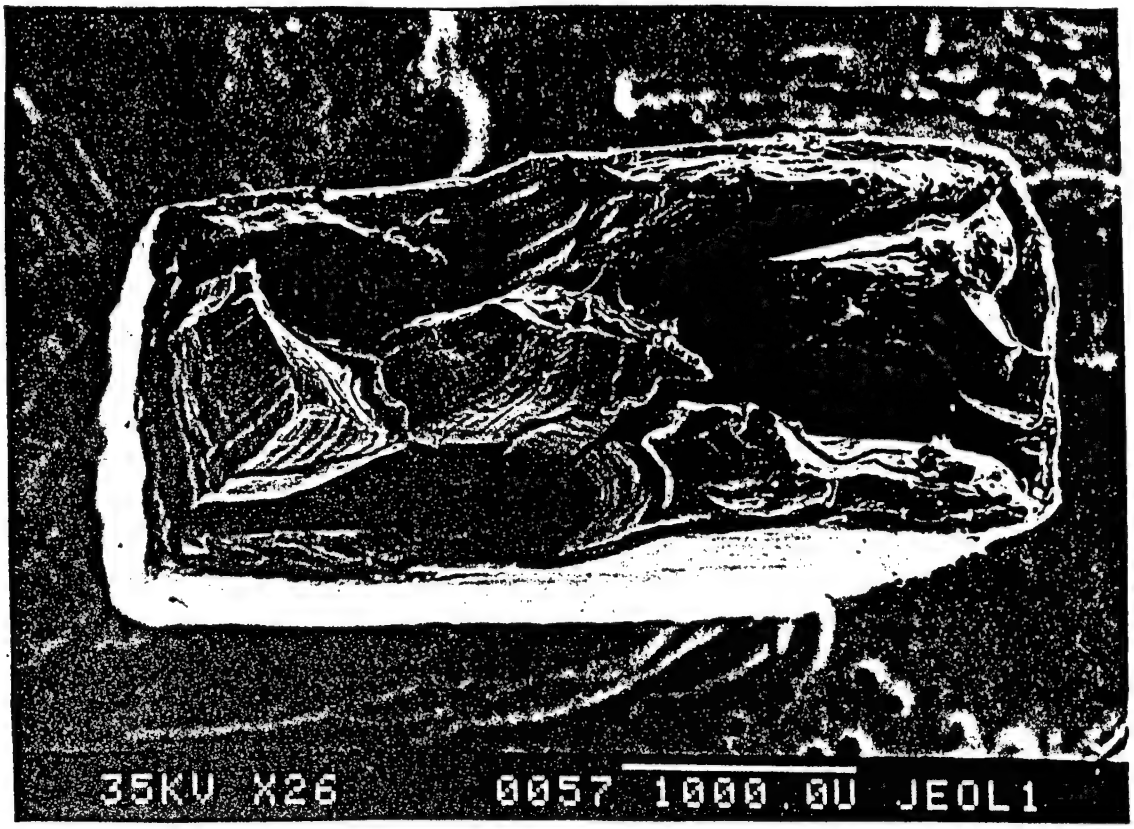

Fig.3.4. Surface fracture of the composite wire with 7 fibres at 77 K.

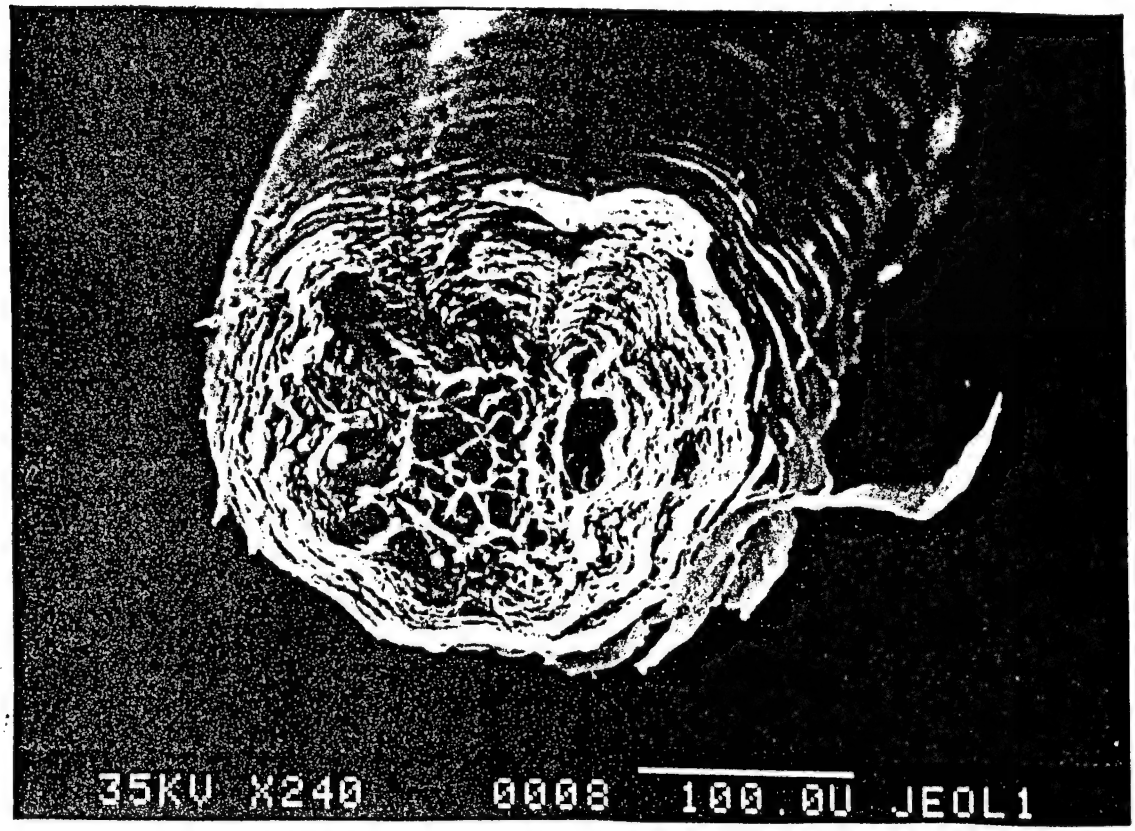

Fig.3.5. Surface fracture of the composite wire with 49 fibres at 77 K.

Sample 1. High-purity aluminum wires of 0.1 mm diameter form a strand with 28 elementary wires and a twist pitch of 35 mm. Twenty four strands are transposed in a flat braid with a pitch 32 mm and a final size 8×2 mm^2. Effective cross-section of high purity aluminum equals 5.28 mm^2, packing factor is 0.33. The wire is presented in Fig.3.6.

Sample 2. High-purity aluminum wires of 0.1 mm diameter form a strand with 28 elementary wires and a twist pitch of 35 mm. Twenty four strands are transposed in a square multifilumentary wire with a pitch 50 mm and a final size 4.5×4.5 mm^2. Effective cross-section of high purity aluminum equals 5.28 mm^2, packing factor is 0.26. The wire is presented in Fig.3.7.

Sample 3. Composite high-purity aluminum wires of 0.3 mm diameter form a strand with 4 elementary wires and a twist pitch of 15 mm. Twenty four strands are transposed in a square multifilumentary wire with a pitch 50 mm and a final size 4.5× 4.5 mm^2. Effective cross-section of high purity aluminum equals 4.4 mm^2, packing factor is 0.21.

Sample 4. Copper wires of 0.071 mm diameter form a twisted strand with 60 elementary wires. The strands have a silk insulation. Twenty four strands are transposed in a square multifilumentary wire with a pitch 50 mm and a final size ~4.5× 4.5 mm^2. Effective cross-section of copper equals 4.75 mm^2, packing factor is approximately 0.2. The wire is presented in Fig.3.8.

Sample 5. Copper wires of 0.071 mm diameter form a twisted strand with 27 elementary wires. The strands have a silk insulation. Twenty four strands are transposed in a flat braid with a pitch 25 mm and a final size 6×3 mm^2. Effective cross-section of copper equals 3.2 mm^2, packing factor is approximately 0.18. The wire is presented in Fig.3.9.

3.3. Fabrication of aluminum armature bars

The samples of multifilumentary wires described above were used to manufacture experimental armature bars. There were manufactured two groups of bars:

- of high purity aluminum for the main tests,
- of copper for basic comparison of test results.

The total variety of the manufactured bars equals 14. They are (the first figure in brackets means the sample of the multifilumentary wire, the second - the variant of the bar manufacturing process):

Bar 1-1 (aluminum). To be placed in slot without epoxy impregnation and external electrical insulation.

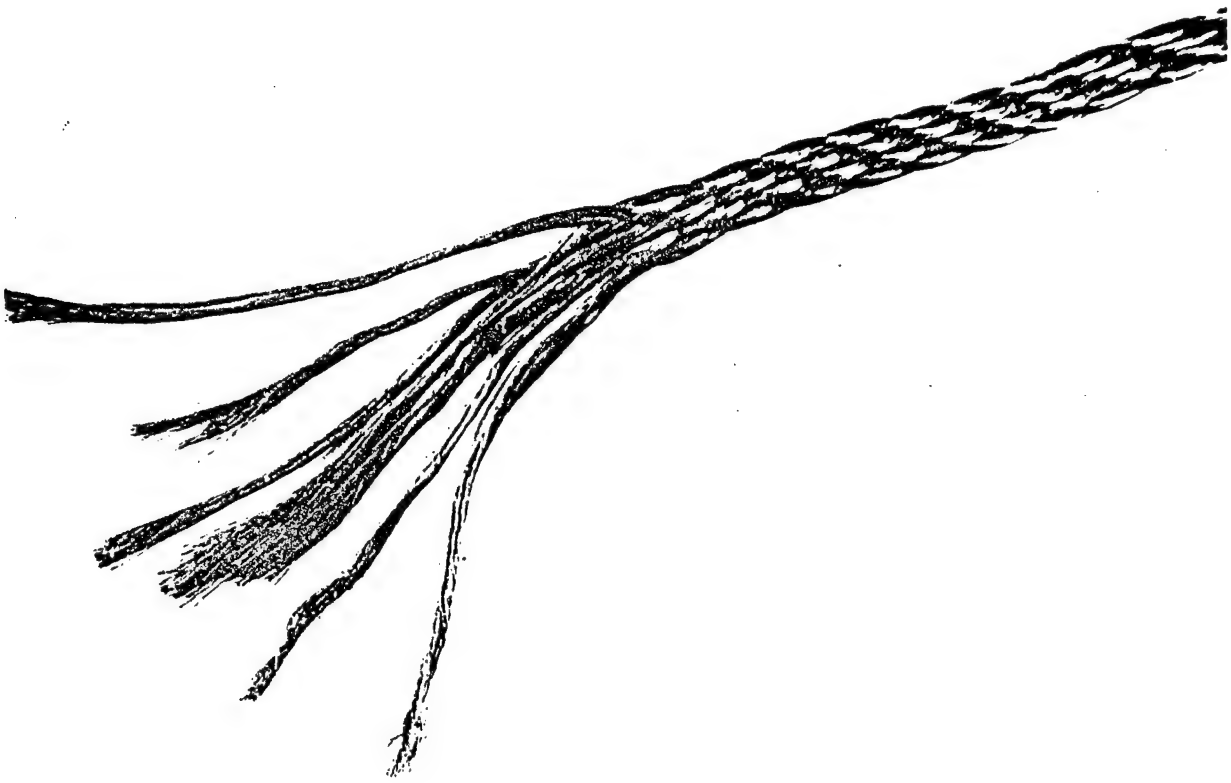

Fig.3.6. Multifilumentary high-purity aluminum braid (Sample 1).

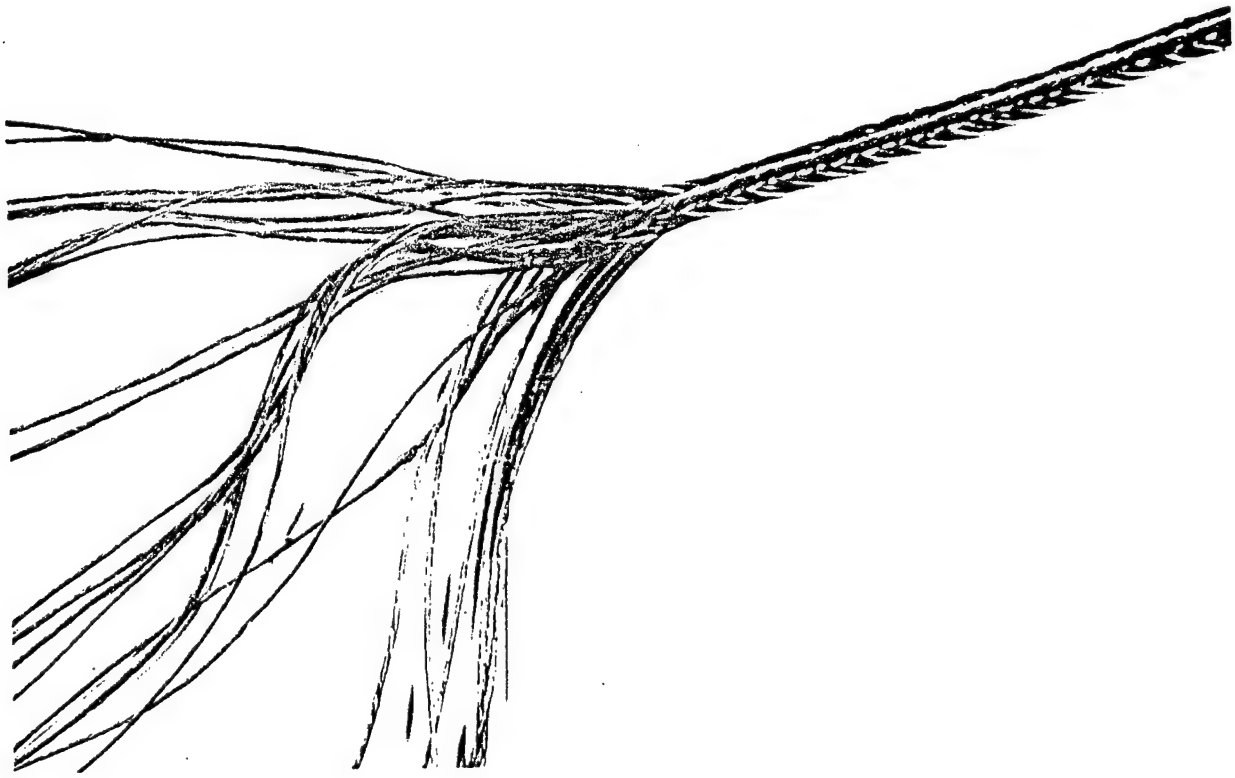

Fig.3.7. Multifilumentary high-purity aluminum rectangular wire (Sample 2).

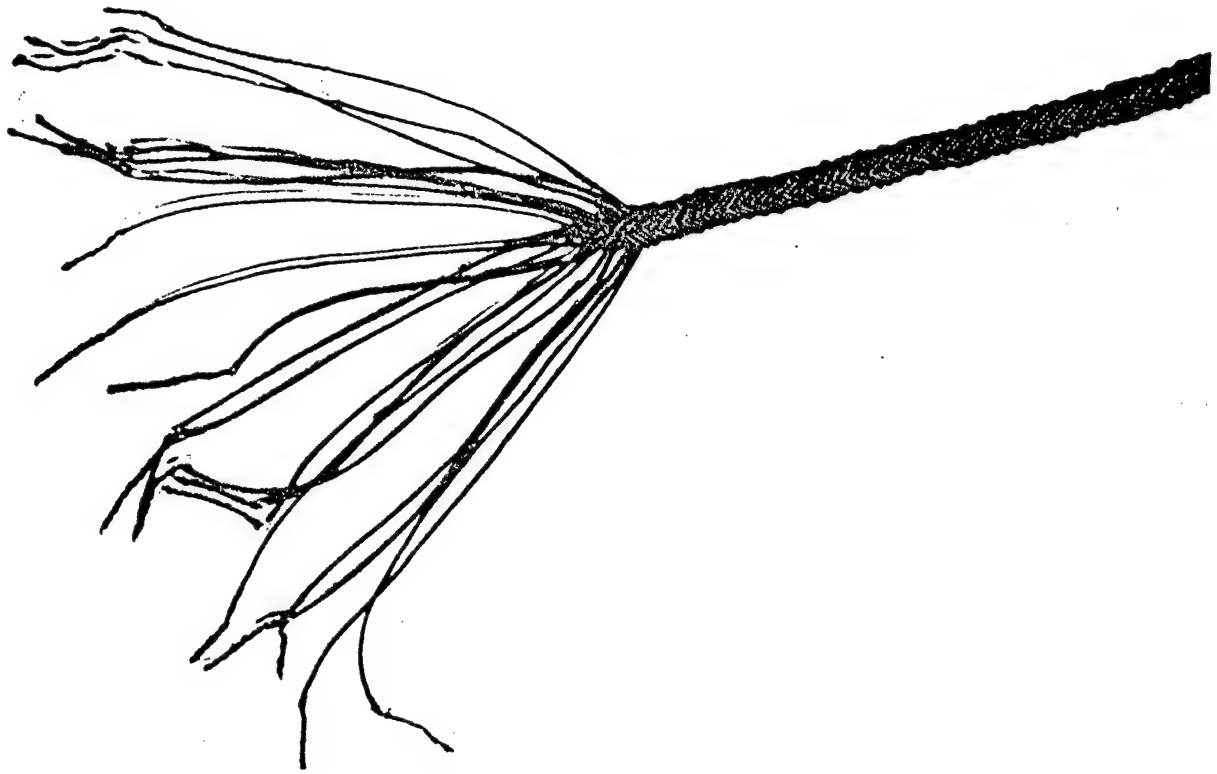

Fig.3.8. Multifilumentary copper rectangular wire (Sample 4).

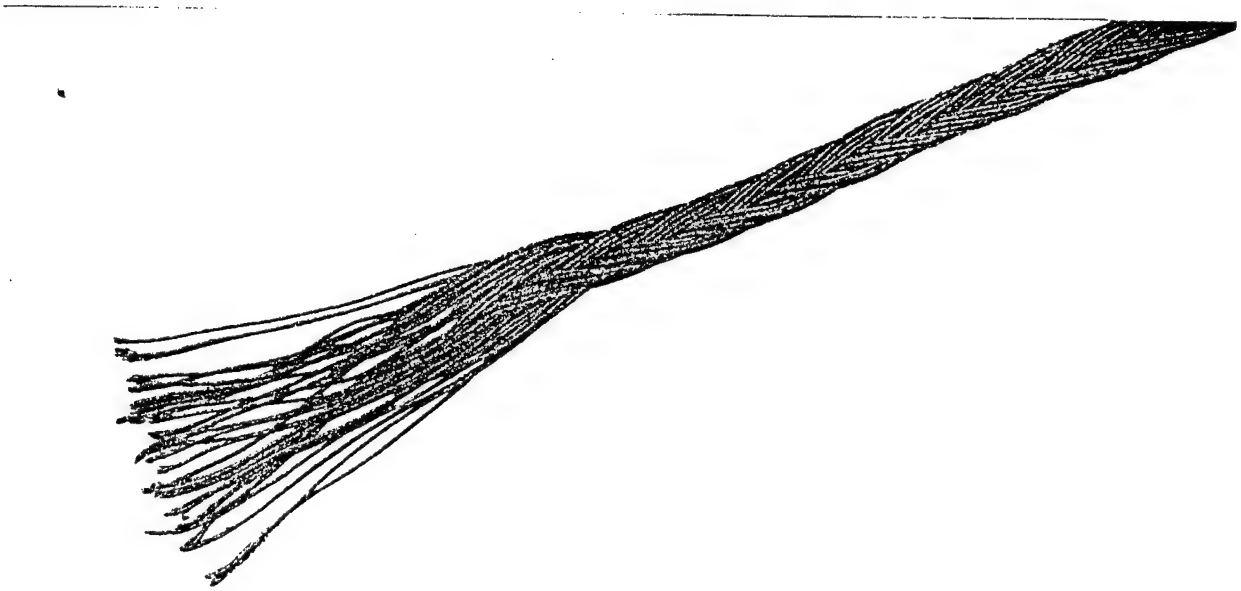

Fig.3.9. Multifilumentary copper braid (Sample 5).

Bar 1-2 (aluminum). Impregnated with special cryogenically stable epoxy ET-10 and baked.

Bar 1-3 (aluminum). Impregnated with epoxy ET-10 and BN filling agent (30% of the epoxy volume) and baked.

Bar 2-1 (aluminum). To be placed in slot without epoxy impregnation and external electrical insulation.

Bar 2-2 (aluminum). Impregnated with epoxy ET-10 and baked.

Bar 2-3 (aluminum). Impregnated with epoxy ET-10 and BN filling agent and baked.

Bar 2-4 (aluminum). Insulated in semi-lap by a lavsan ribbon 50 μm thick and 20 mm wide.

Bar 3-1 (aluminum). Impregnated with epoxy ET-10 and baked.

Bar 3-2 (aluminum). Impregnated with epoxy ET-10 but with a different pressing procedure as compared to the previous case.

Bar 4-1 (copper). Impregnated with epoxy ET-10 and baked.

Bar 4-2 (copper). To be placed in slot without epoxy impregnation and external electrical insulation (except the silk insulation of the strands).

Bar 5-1 (copper). To be placed on a fixture surface with 3 sides contacting with the coolant.

Bar 5-2 (copper). Insulated in semi-lap by a lavsan ribbon 50 μm thick and 20 mm wide.

Bar 5-3 (copper). Sheathed by a glass cloth 50 μm thick. Impregnated with epoxy ET-10 and baked.

The total amount of the manufactured bars equals 25 because some versions were several times repeated for the disc and cylindrical fixtures. The bars were investigated to acquire the information of the thermal behaviour at different temperature levels, of stability to thermal cycling, of electrical insulation behaviour. The test results are presented in Part 4.

3.4. Fabrication of the test fixture

It was decided to carry out experimental investigation of the bars with a help of two test fixtures: a disc one and a cylindrical one. The relatively complicated procedure was accepted mainly for the liquid helium experiments. The disc model provided a guarantee that all the parts of experimental bars would be immersed in liquid helium. Moreover their damage during the tests for the maximum current density determination was less painful than that of the cylindrical model.

The test fixture comprises a support structure with the slots for the armature bars, special clips connecting the bars with the current leads and current leads connecting the elements at ambient and cryogenic temperatures. The fixture is being suspended during the cryogenic experiments in a special test cryostat.

In both cases the bars were positioned in slots machined in fibre glass textolite and impregnated with special epoxy, stable to the temperature cycling. One side of each bar was opened to the coolant, because the cooling scheme of the armature being developed is based on a system of channels on one side of each layer of the helical winding. Some of the bars had outer electrical insulation and some had none.

The temperature was controlled by special high accuracy temperature-sensitive resistors intended for the low temperature measurements. They were fixed on the bar surface from the side facing the slot bottom.

The fixture of a disc type (Supplement I, Fig.S.1) has the diameter 230 mm and is 20 mm thick. The slots are positioned on the average diameter 205 mm and occupy both sides of the disc. There are two slots on each disc model. The slot cross-section equals 5×5 mm^2 or 8×3 mm^2. The length of the bar on a disc model is 550 mm. Each stator bar is connected to the current leads with a help of special copper clips. They are soldered to the copper bars and have a bolt connection with the current leads. In case of high-purity aluminum bars the connections were performed immediately after the enamel insulation pickling. The bolts are made of brass. The contact electrical resistance was equal to Rc=12 μOhm at 300 K and practically no temperature dependence was observed during the cold experiments.

The fixture of a cylindrical type (Supplement I, Fig.S.2, S.3) represents 1/3 of a cylinder, the slots occupy approximately 1/4 part of a cylinder (in accordance with the armature winding scheme presented on Fig.2.3). The cylinder has ID=290 mm and OD=310 mm. After evaluation of the results of the liquid nitrogen tests it was decided to continue experiments with only 4 types of the armature bars. Therefore there are only four slots on a cylindrical fixture. The slot cross-section equals 5×5 mm^2. The bars are 500 mm long, the cylinder is about 580 mm long. The system of current connections for the bars represented a single copper bus of the cross-section 35×5 mm^2 on one side of the model. On the other side the bars were connected to special copper clips.

There are three current leads from the current supply to the cold zone of the cryostat (Supplement I, Fig.S.4). They are capable to carry the currents up to 5 kA. The leads are cooled by the coolant vapour. Two of the current leads represent themselves coaxial hollow copper tubes. The cooling gas flows through the inner ducts. The third lead is a copper braid inside a tube of stainless steel. Each cold experiment allowed to test two bars. After that the cryostat was opened and the test fixture was exchanged for a new one.

4. ARMATURE BAR TESTS

4.1. Configuration of cryogenic test-bed

The cryogenic test-bed was organised within the cryogenic test facility of the Department of Non-Conventional Electrical Machines (Fig.S.5,a and b).

It comprised the cryostat for the low temperature experiments with the diameter of the cold part 300 mm and the volume of cryogenic liquid up to 100 l. The cryostat was equipped by currentt leads and by a special level meter, incorporating superconducting elements and providing continuous measurement of the cryogenic liquid level along the height of the cryostat.

To supply the cryogenic liquid during experiments there were used a 500 l liquid nitrogen tank and a 500 l liquid helium tank, both equipped with level meters. A variety of vacuum pumps was involved in preparation of the cryogenic system for the low temperature experiment. The exhausted gas was stored in gasholders and transferred to the recivers with the help of compressors.

There were used two types of current supply sourses during experiments. A DC one allowed to determine the current-carrying ability of the bars and an AC one provided initial data for the loss evaluation.

The first sourse of current supply represented a DC electrical machine with the current up to 4 kA and a transistor system of excitation current regulation. The second one had lower current but possesed a wide range of freguency variation from 20 to 1000 Hz.

The test-bed was equipped with an IBM PC of AT-286 type, responsible for the experimental data aquisition, processing and presentation in visual and graphical form. It reffered to the electrical current, voltage drop anf temperature on the bottom side of the tested bar. The computer also provided regulation and control of the excitation current of the power supply and transformation of DC into pulses of different duration. The bar protection function was performed by the computer as well. The resistance and the rate of its increase were controlled with a fast de-excitation of the power supply in case the rate exceeded the restricted value.

4.2. Preliminary tests of aluminum wires and coils

Tests of elementary wires described in Par.3.1 include:

1. Experimental determination of conductor specific electrical resistance as a function of temperature; the results are given in Fig.4.1. Calculations based on experimental results were carried out for temperature dependence of eddy-

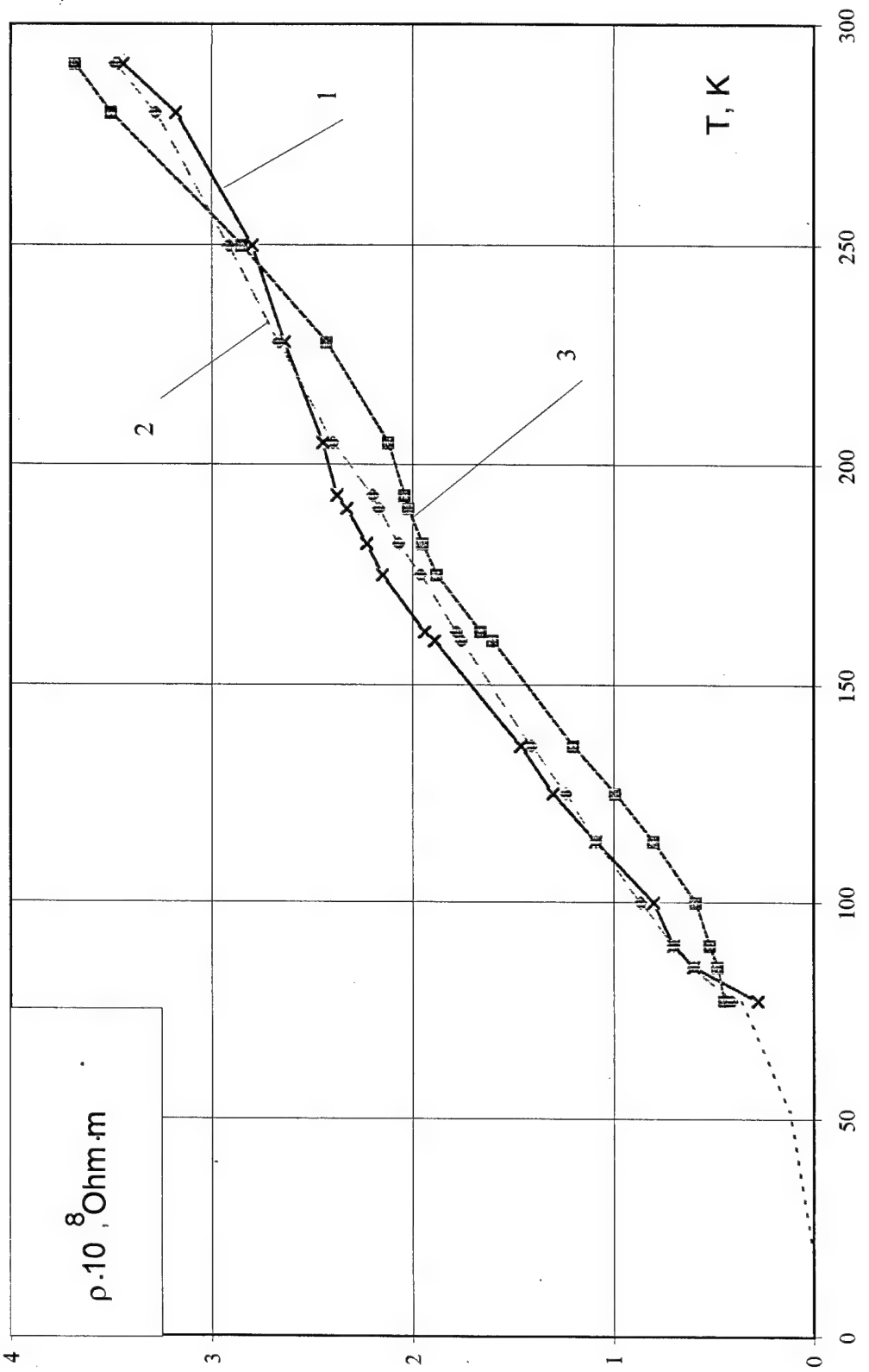

Fig. 4.1. Temperature dependence of specific electrical resistance.

1 - high-purity aluminum wire 0.1 mm in diameter, 2 - high-purity aluminum wire 0.3 mm in diameter, 3 - aluminum composite wire 0.3 mm in diameter , containing 49 filuments of high-purity aluminum.

current losses for the windings manufactured of high-purity aluminum composite wires 0.3 mm in diameter and of solid wires 0.1 mm in diameter at 400 Hz frequency and magnetic field amplitude equal to 0.1 T and 0.5 T. Results of calculations are shown in Fig.4.2.

2. Determination of heat behavior of the elementary wires with their whole surface exposed to cooling medium. For this purpose specific resistance as a function of current density has been measured at three temperature levels, namely 300, 160 and 77 K; the results are presented in Fig.4.3.

To study the variation of wire heat behavior under different heat removal conditions, the test coils were fabricated and tested at 77 K (See Fig.4.4). Test coil dimensions are: outer diameter - 50 mm, inner diameter - 28 mm, height - 7 mm. The coils wound of aluminum composite wire 0.3 mm in diameter and of copper conductor 0.071 mm in diameter were not impregnated, but the coils wound of pure aluminum wire 0.1 mm in diameter were impregnated. Test results are presented in Fig.4.5.

After preliminary testing of elementary wires and the coils, the wires manufactured of high-purity aluminum 0.1 mm in diameter, of aluminum composite of 0.3 mm and of copper of 0.071 mm were chosen for manufacturing of experimental bars to continue studies (See Par.2.2 and 3.3).

4.3. Tests of aluminum armature bars of simplified geometry

During experiments with the disc test fixtures (Supplement, Fig.S.6), 14 samples were tested at ambient temperature and in liquid nitrogen, and 6 samples - in liquid helium. From the point of view of current-carrying capacity, comparison was made between the two methods of bar transposing: either flat or square cross-section; between the two impregnating epoxies: either containing 30% volume of BN filler or no filler at all; between the non-insulated bar and the bar wound with a lavsan film strips. This comparison was performed for the bars composed of three types of elementary conductors.

Results of tests performed at liquid nitrogen temperature prove that the bar transposing method and type of the epoxy used to obtain monolith structure have practically no effect on bar current-carrying capacity. From the viewpoint of mechanical properties, i.e. retaining its shape at bending and stretching, preference was given to the bar with a square cross-section.

During the tests at 77 K, the maximum current for the impregnated bars of high-purity aluminum was about 600 A, of copper - 370 A, for the bar made of high-purity aluminum and insulated with a lavsan film strips - 200 A, for the copper bar with lavsan film strips - 300 A. Current-carrying capacity of non-impregnated bars of high-purity aluminum and aluminum composite wire is over 1000 A, same of copper wire is 700 A.

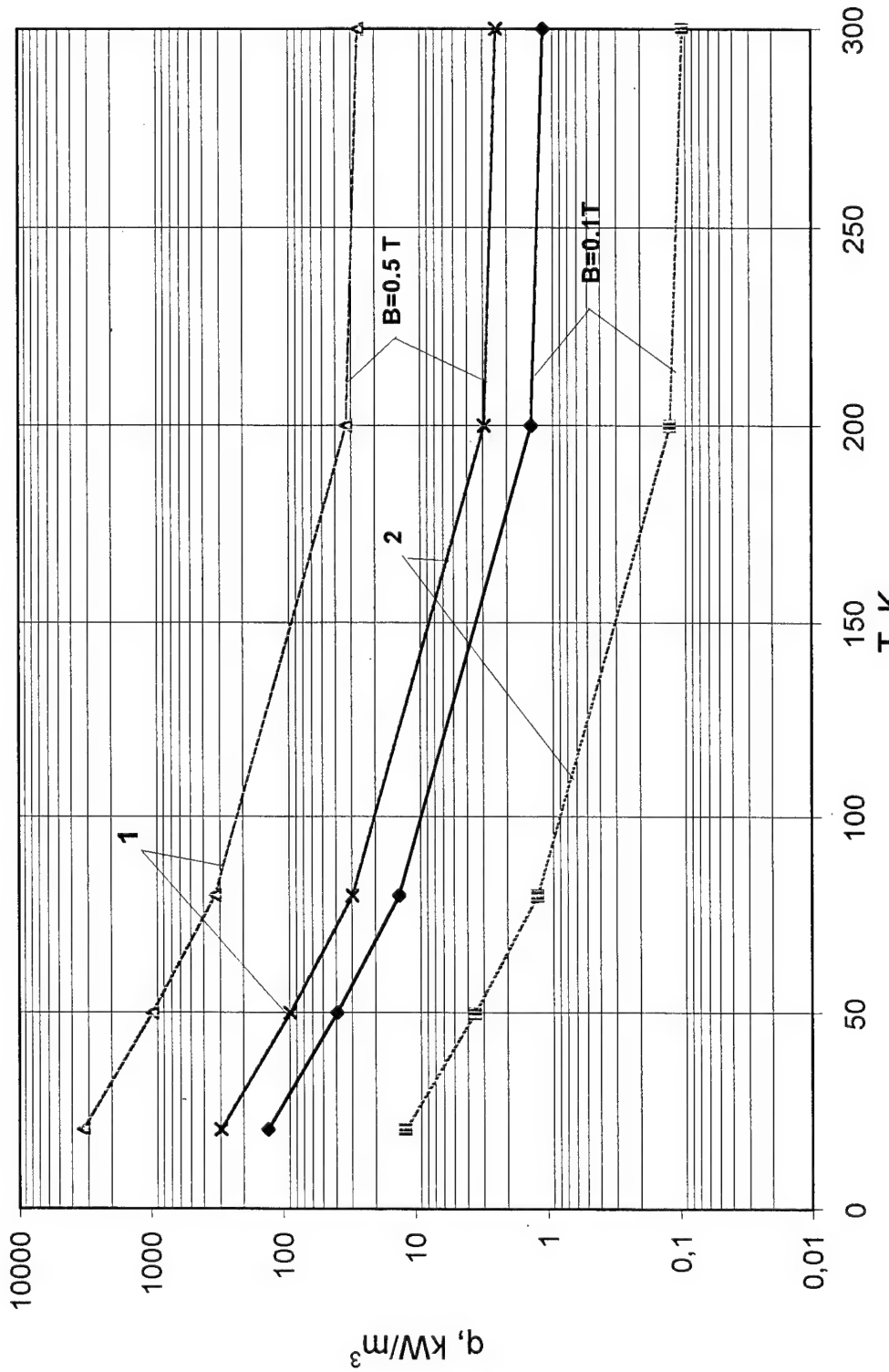

Fig. 4.2. Temperature dependence of the eddy current losses at 400 Hz

1 - high-purity aluminum 0.1 mm, 2 - composite wire 0.3 mm.

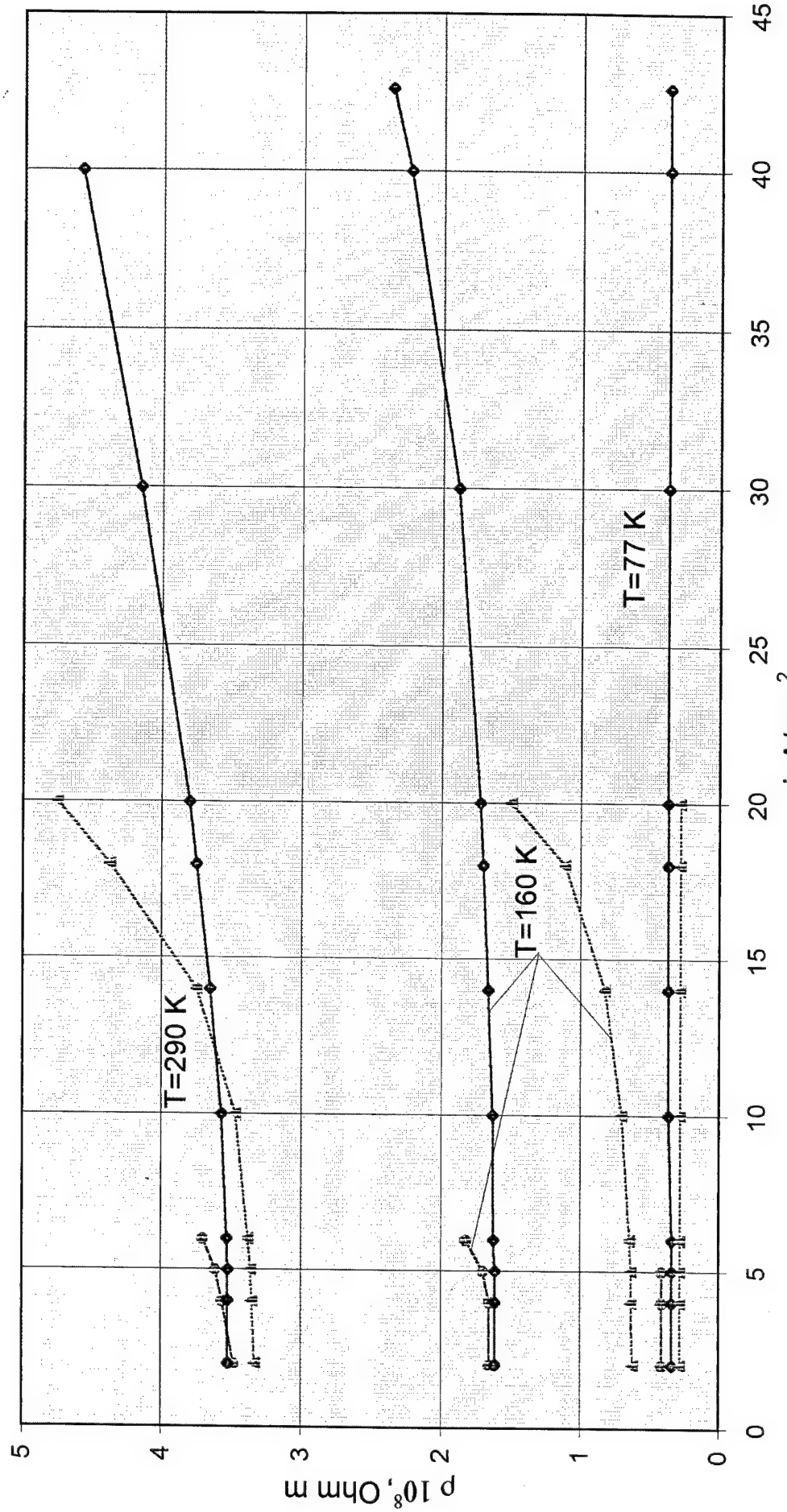

Fig. 4.3. Current density dependence of elementary wire specific resistance at three temperature levels.

1 - high-purity aluminum 0.1 mm, 2 - high purity aluminum 0.3 mm, 3 - aluminum composite 0.3 mm.

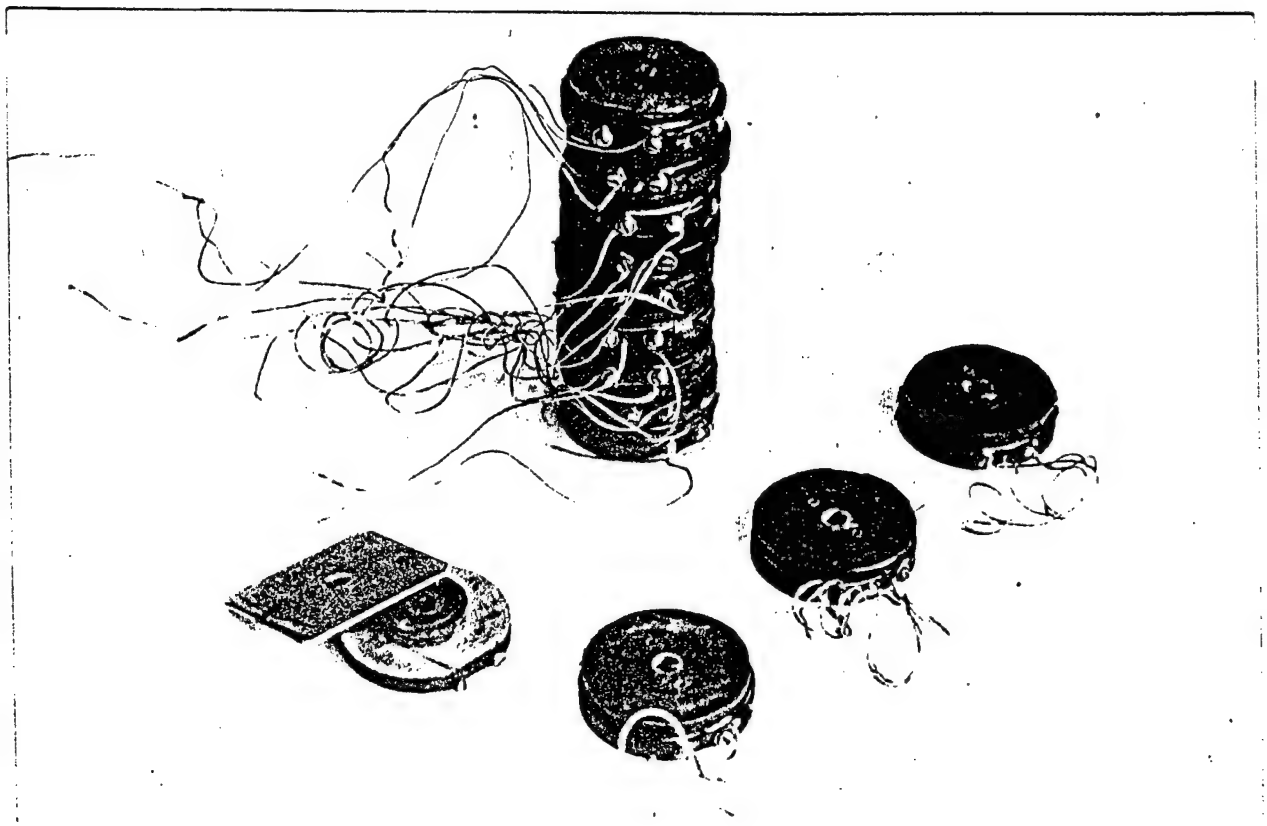

Fig.4.4. Coils for investigation of heat behaviour of elementary wires.

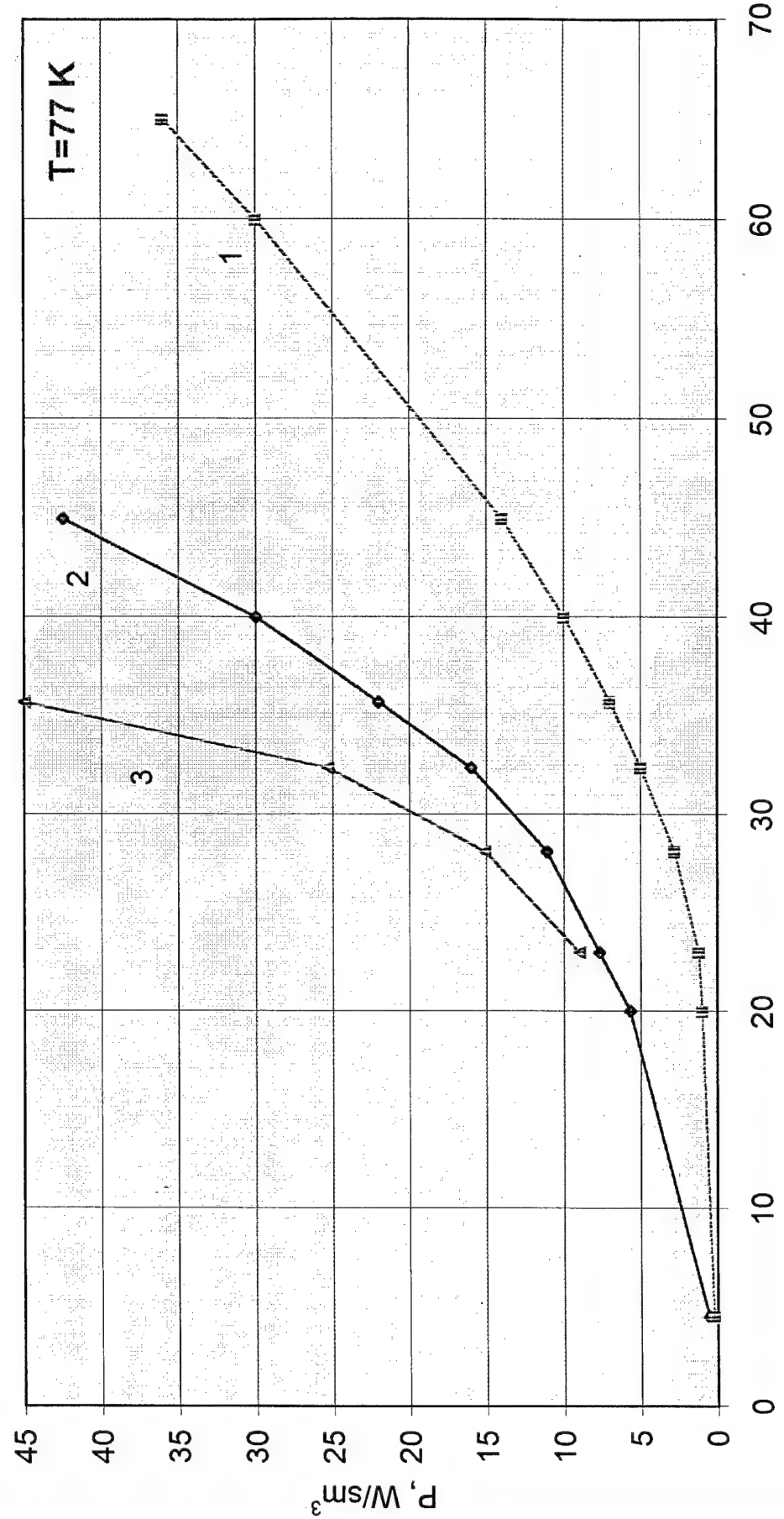

Fig. 4.5. DC losses as a function of current density at liquid nitrogen cooling.
Coils: 1 - of aluminum composite, 2 - of high-purity aluminum wire 0.1mm impregnated with epoxy, 3 - of copper wire.

The results of studying the bars on disk fixtures are presented in Figs.4.6-4.12. Here the test conditions were more heavy than those with a full-scale cylindrical test-rig. In the course of testing the sample 3-1 (tests 1, 2, 3 illustrated by Figs.4.6 - 4.8) the protection tripping was chosen to be functioning with a time lag, what resulted in burning-down of the bar (the diagram of burn-down process is not given herein). After-test inspection of the samples and the curves $R=R(t)$ suggest that bar degradation and burn-down can be explained by a combined action of heating and impact thermodeformation, leading to elementary wire brittle failure.

At 4.2 K the current-carrying capacity of an epoxy-impregnated bar made of pure aluminum is 1330 A, that of the impregnated bar made of aluminum composite is 1870 A, and of the copper bar - 1100 A.

4.4. Tests of full-sized aluminum armature bars

Four epoxy-impregnated bars were chosen to be tested at full-scale cylindrical test fixture, namely two bars of aluminum composite with different methods of the bar pressing during epoxy impregnation, one copper bar and a bar of high-purity aluminum.

Figure 4.13 illustrates the process of a full-scale cylindrical model cooling-down with liquid helium. Presented in Fig.4.14 and 4.15,a are the results of testing the full-scale bars in a test-fixture in liquid helium. These tests revealed no drastic difference from the results obtained during the studies using the disc test fixture. Some stages of the low temperature experiments are presented in Fig.S.7 of the Supplement. During these tests with cylindrical test-fixture a more accurate protection mode of operation was chosen. Current-carrying capacity of the bar manufactured of aluminum composite at liquid helium temperature was determined as equal to 1870 A, similar to the tests with disc fixtures.

4.5. Tests of full-sized copper helical winding

Till now we possesed experience with experimental investigations of the relatively large armature with helical winding as a part of the 5 MVA, 3000 rpm turbogenerator. To obtain experimental values of magnetic fields and parameters for a much smaller armature an experimental copper helical armature winding intended for a 4-pole high-speed alternator was manufactured and tested (Fig.S.8). The main parameters of the model are presented in Table 4.1.

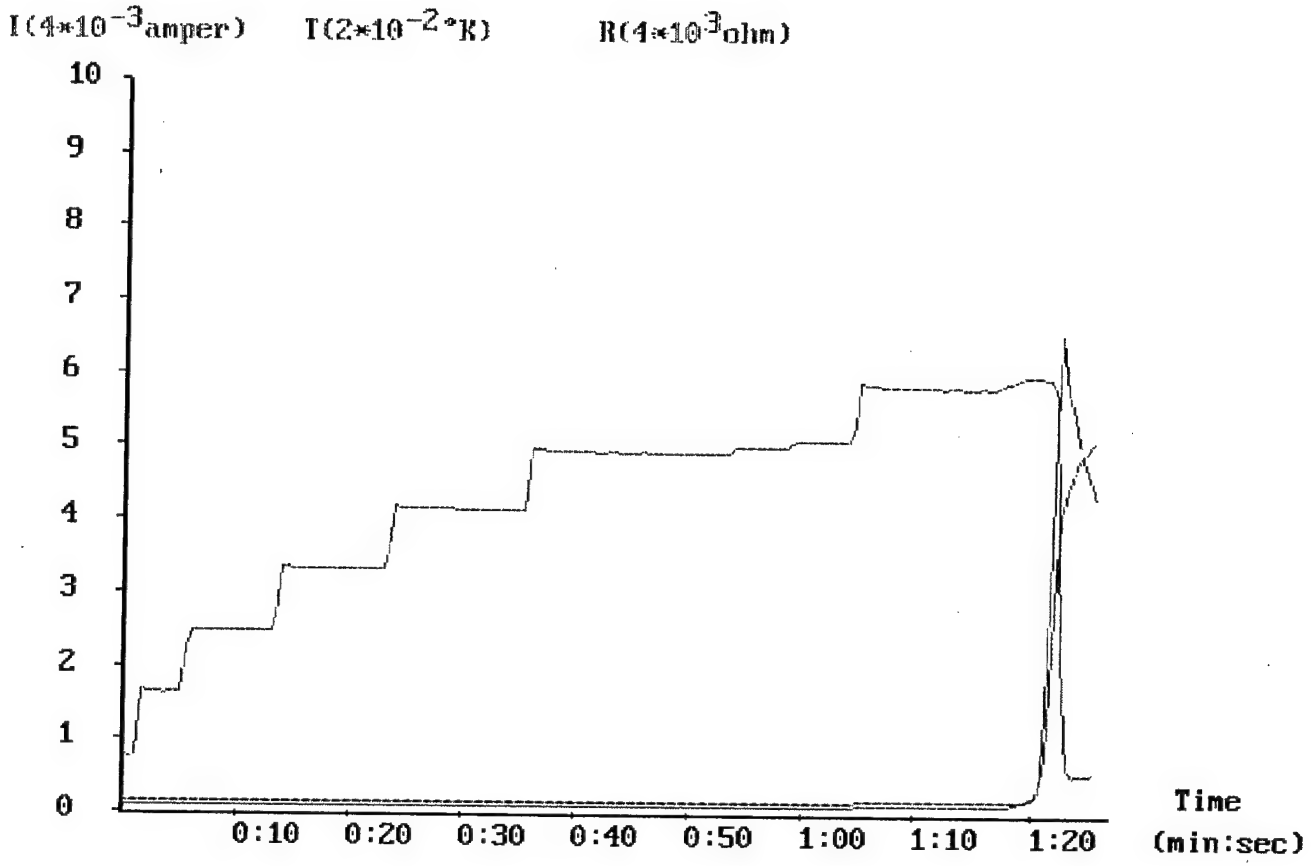

Fig. 4.6.Experiment with current variation in the composite bar (bar 3-1, test 1).

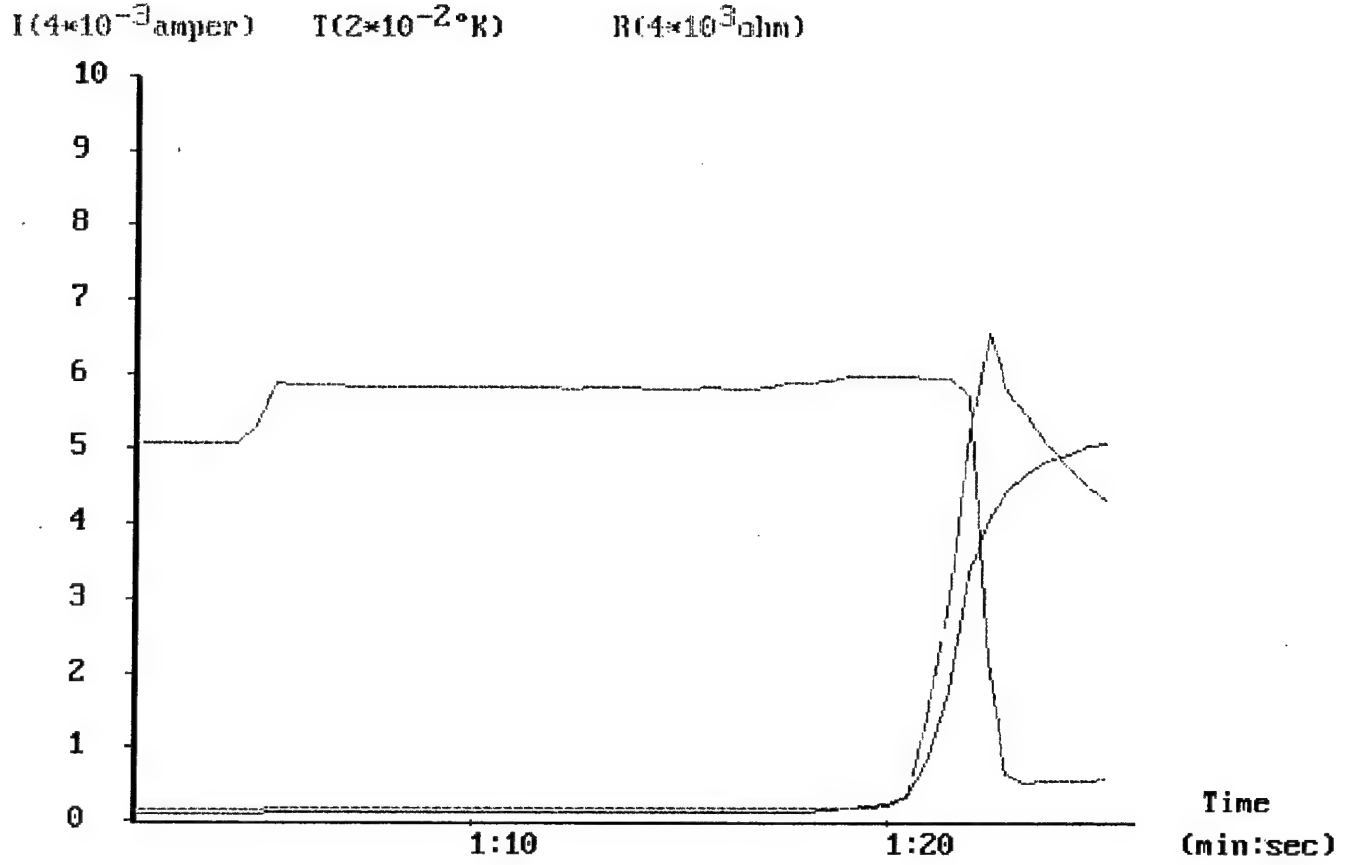

Fig. 4.6a. The avalanche-type heating process of the composite bar (bar 3- 1, test 1) at the current of 1490 A.

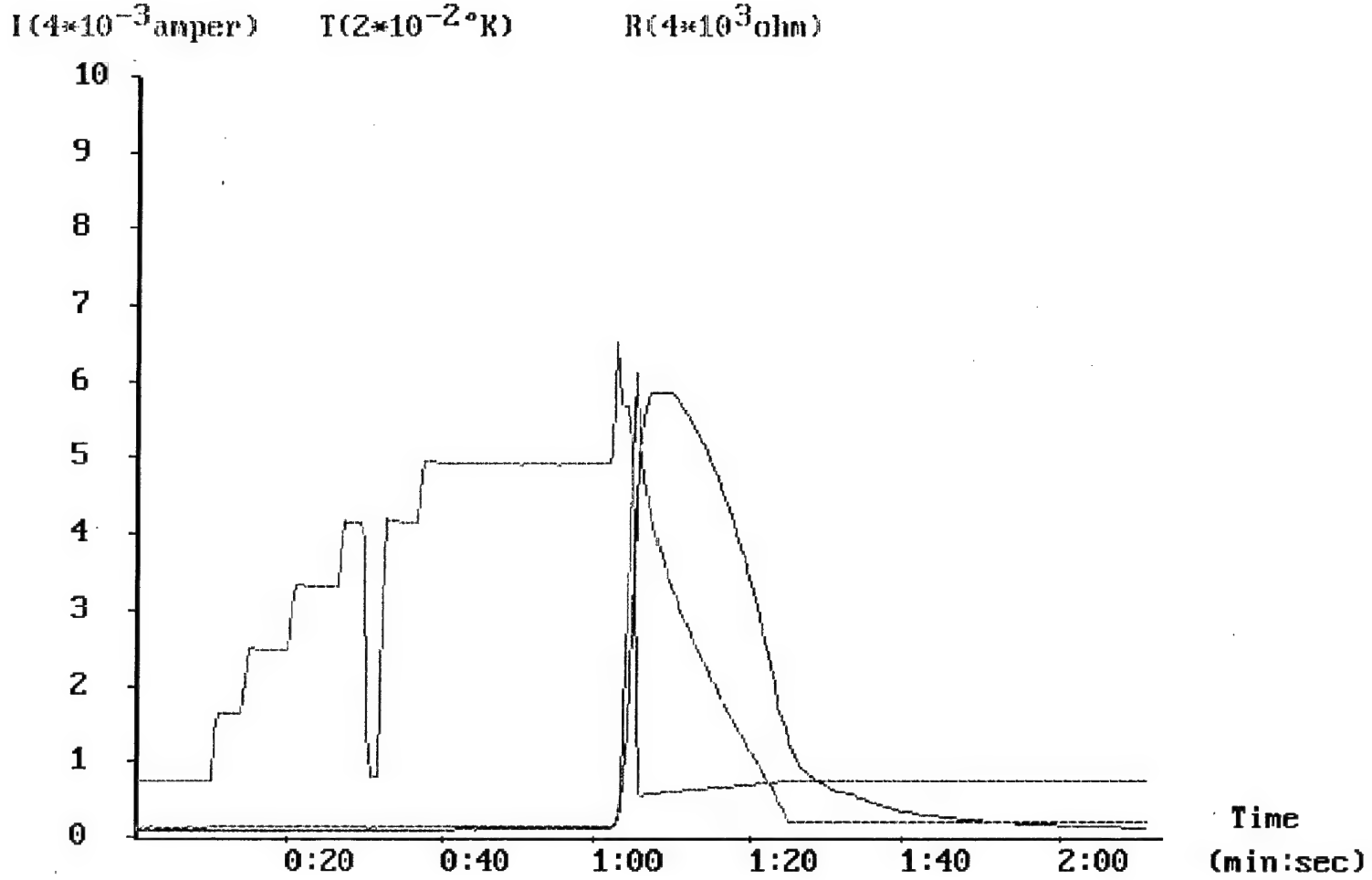

Fig. 4.7. Experiment with current variation in the composite bar (bar 3-1, test 2) and its avalanche-type heating above 1500 A.

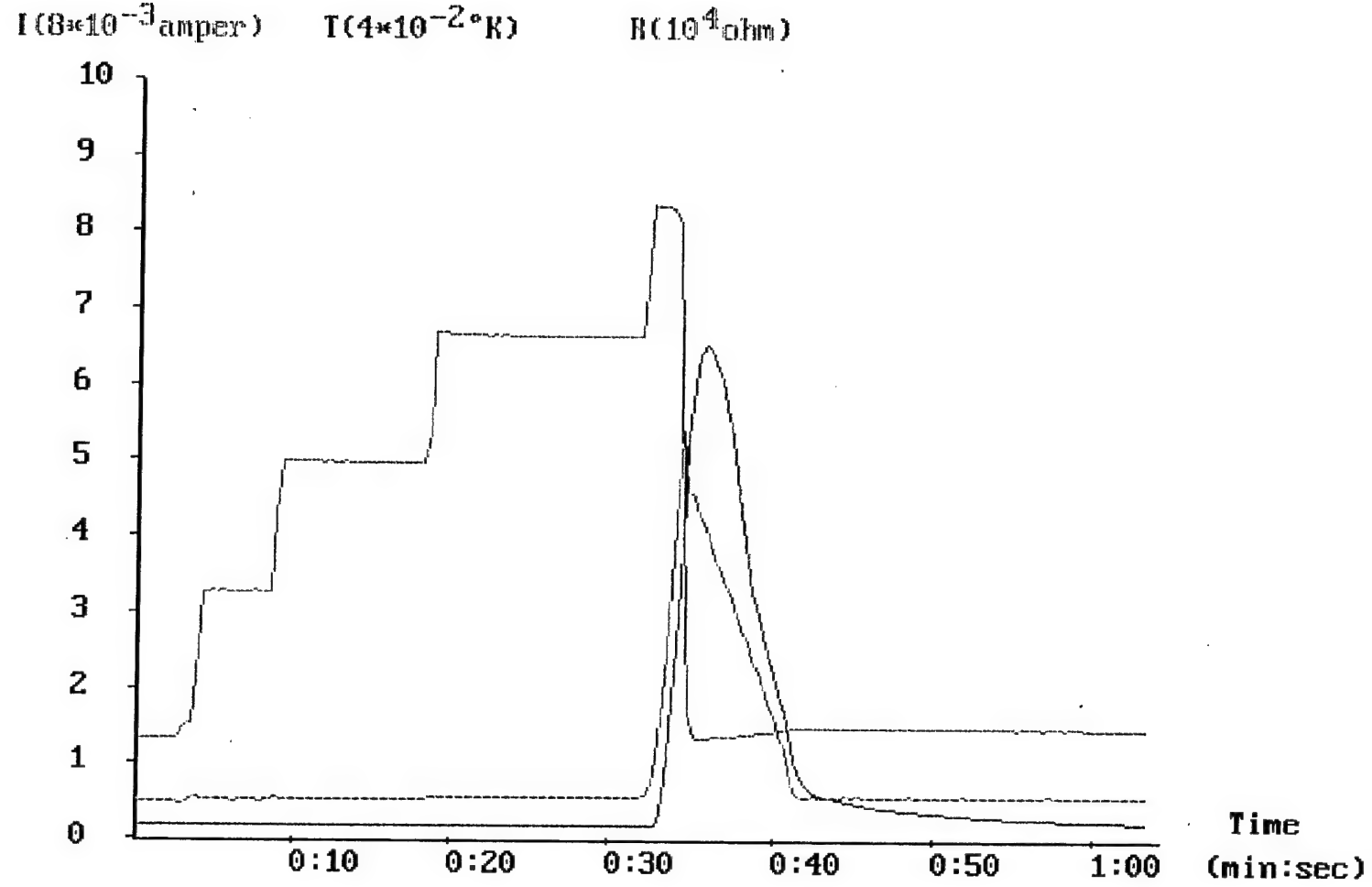

Fig. 4.8. Experiment with current variation in the composite bar (bar 3-1, test3) and its avalanche-type heating above 1100 A.

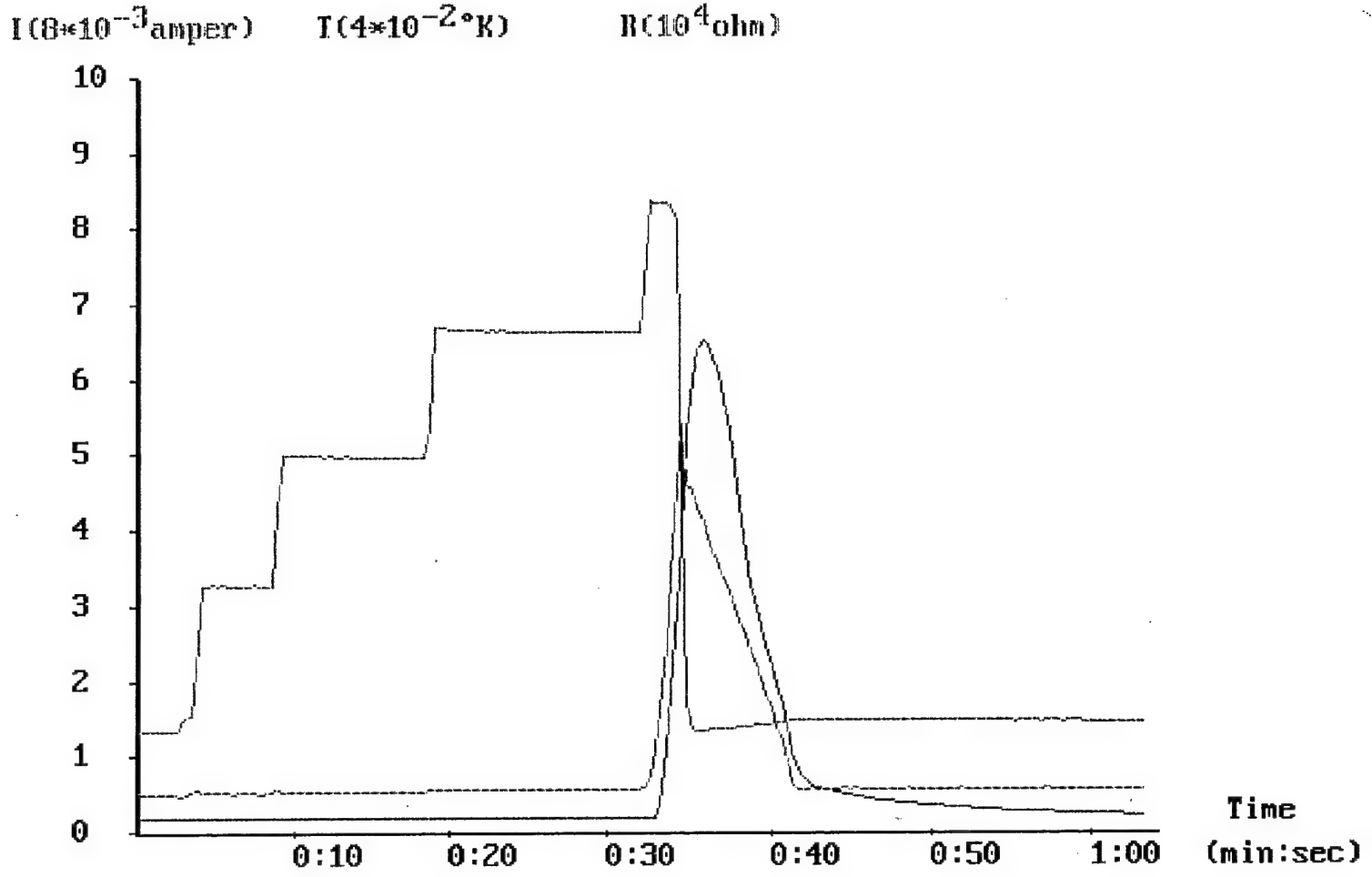

Fig. 4.9. Change current the bar of high purity aluminum (bar 2- 2, test 1), with avalanche-type heating at 1330 A and its cooling-down after protection system operation.

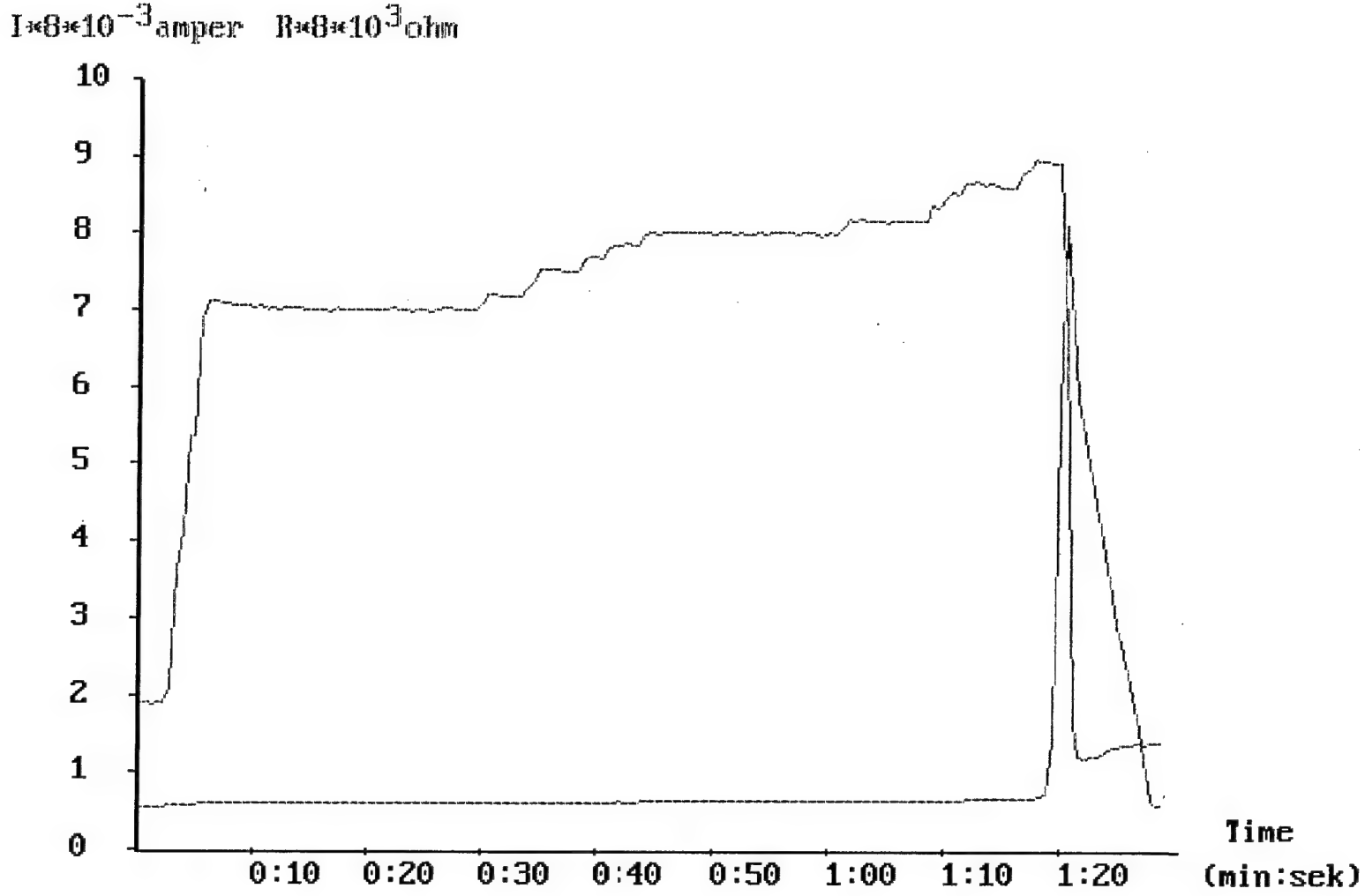

Fig. 4.10.Change current of the bar of high purity aluminum (bar 2-3, test 1), with avalanche-type variation of resistance at 1115 A and after protection system operation.

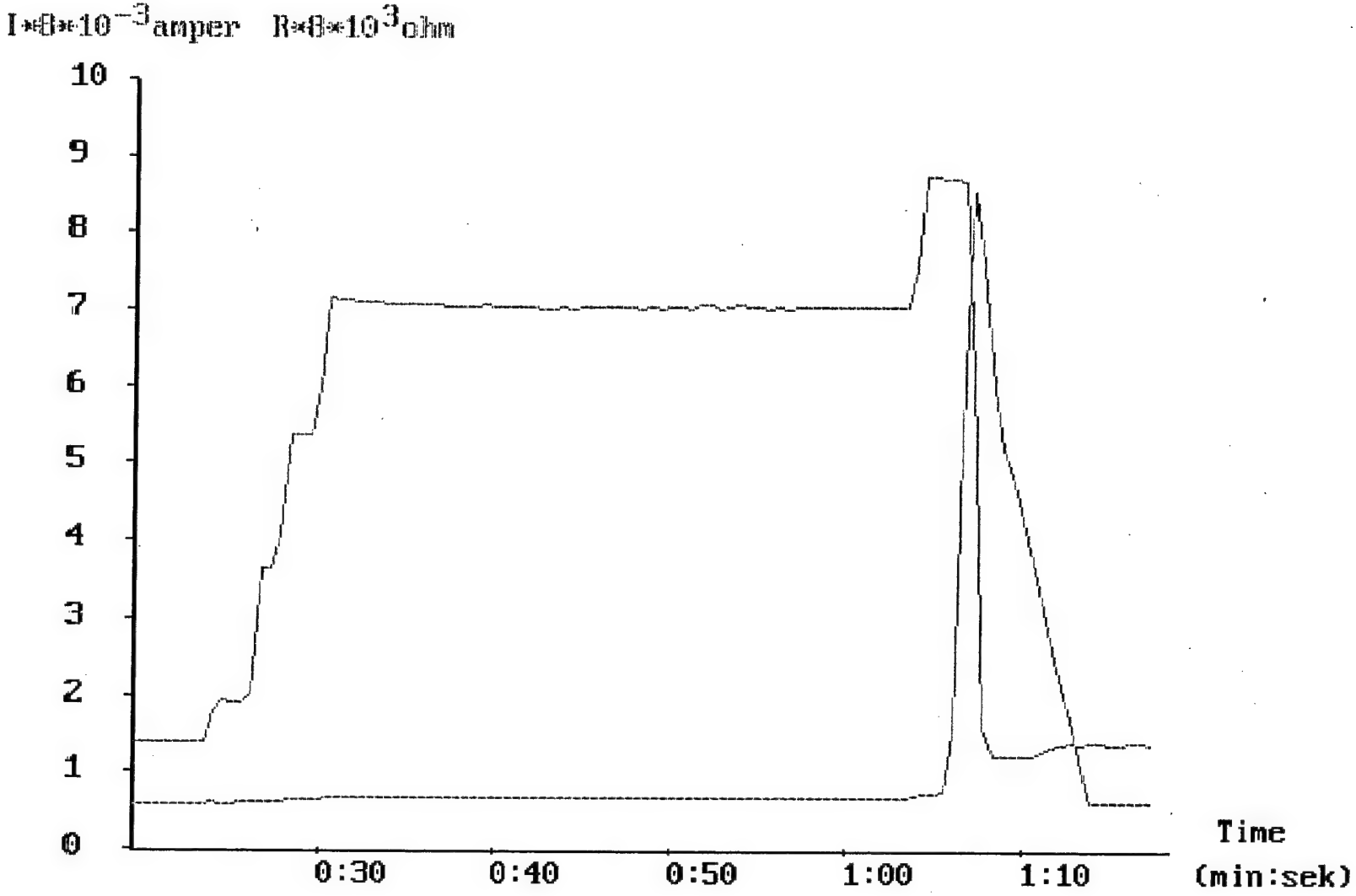

Fig. 4.11.Change current of the bar of high purity aluminum (bar 2-3, test 2), with avalanche-type variation of resistance at 1110 A and after protection system operation.

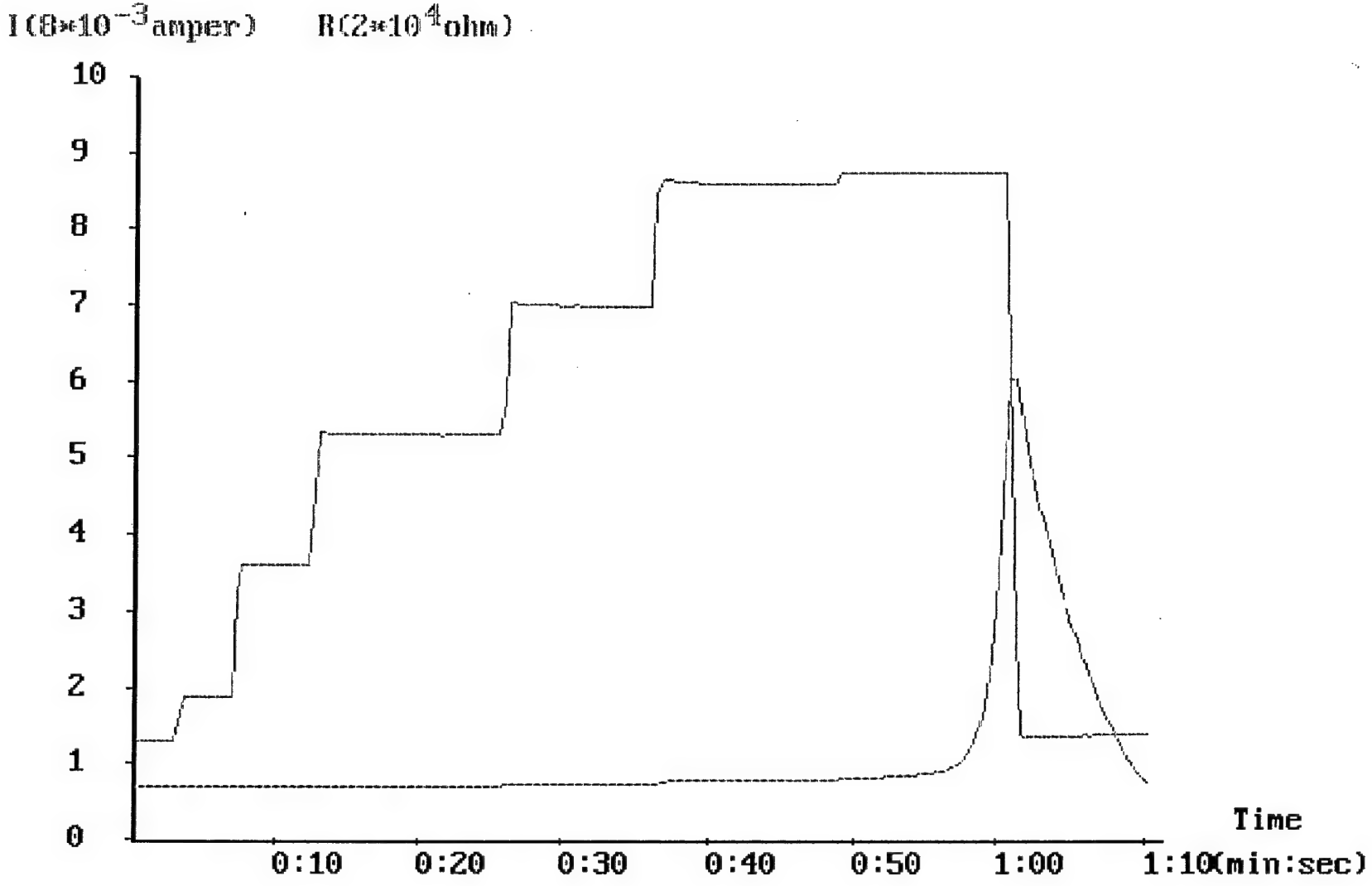

Fig. 4.12.Change current of the bar of copper, with avalanche-type variation of resistance at 1100 A and after protection system operation.

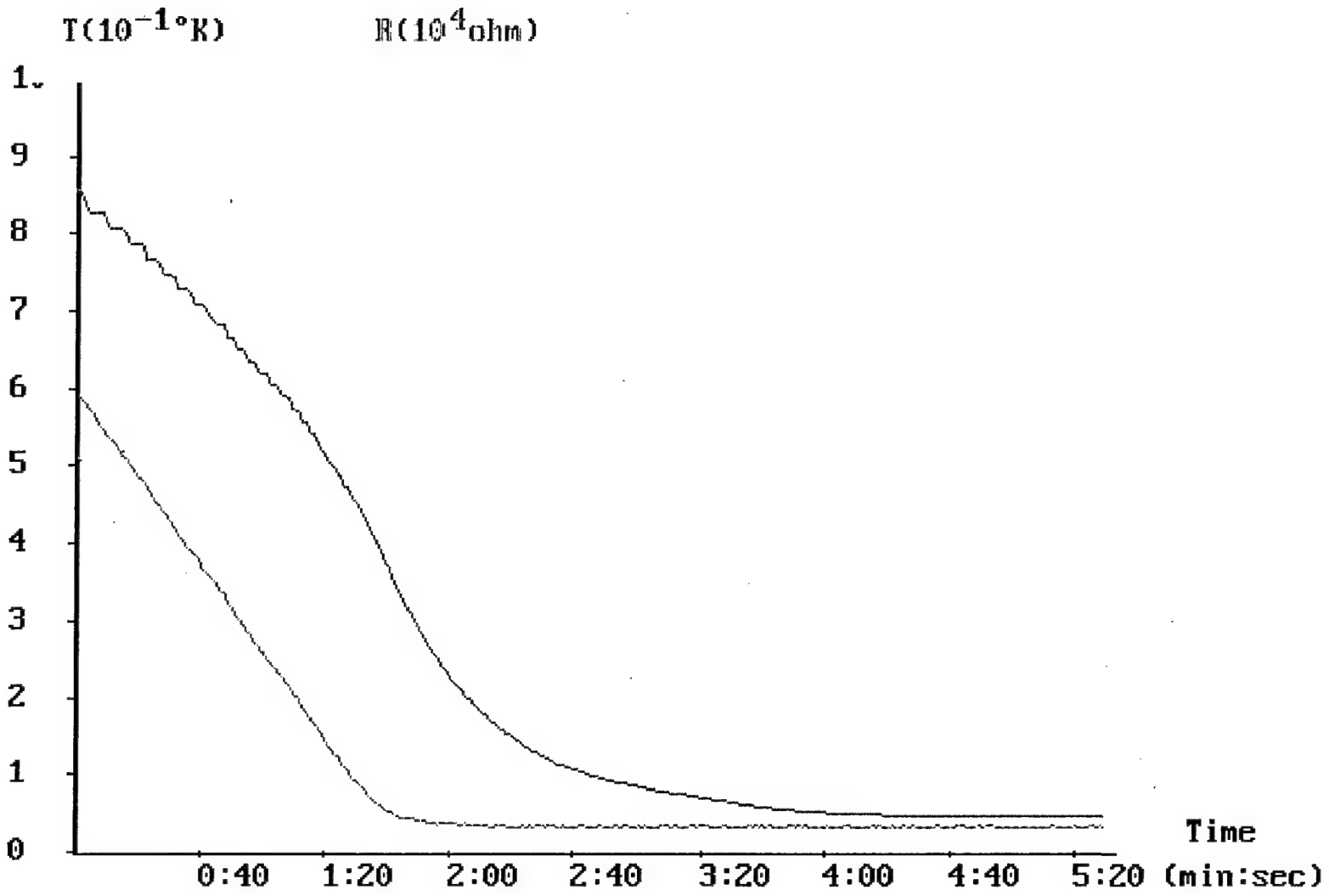

Fig.4.13. Variation 0f composite bar resistance and temperature during cryostat filling-in with liquid helium

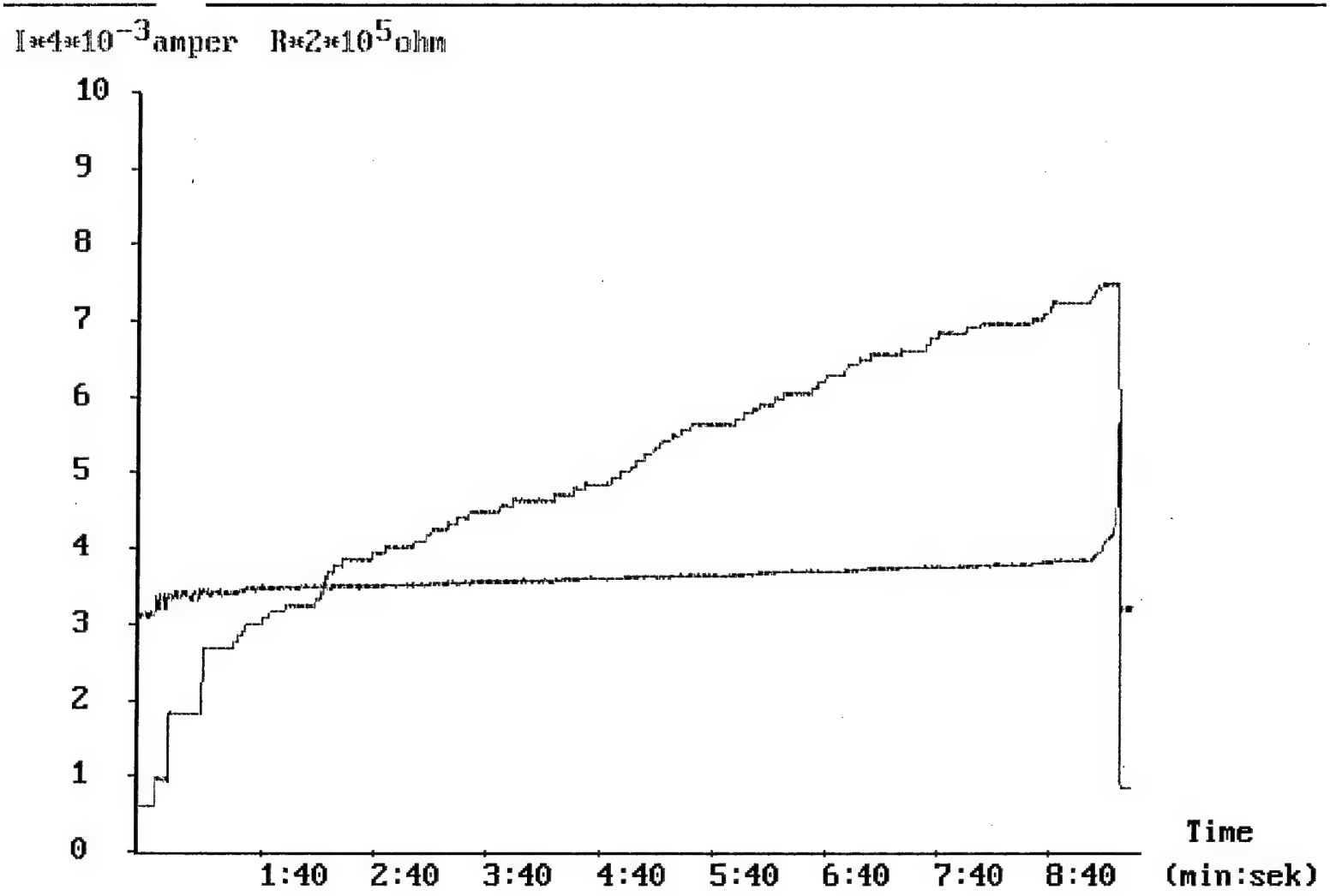

Fig. 4.14.Experiment with current variation in the composite bar (bar 3-2, test 1).

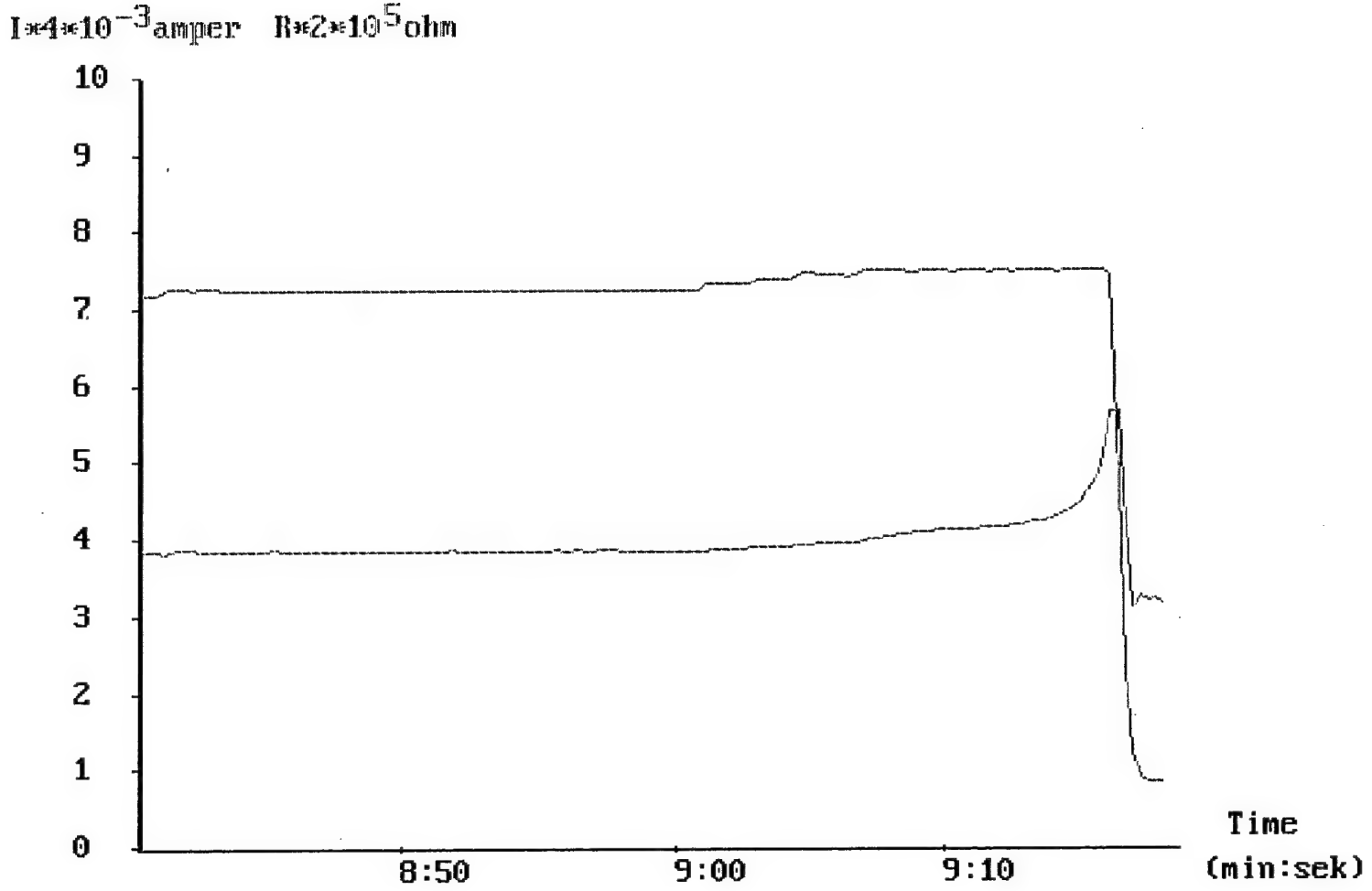

Fig. 4.14a. Process of an avalanche-type increase of the composite bar (bar 3- 2) resistance at 1870 A and its abrupt drop after protection system operation.

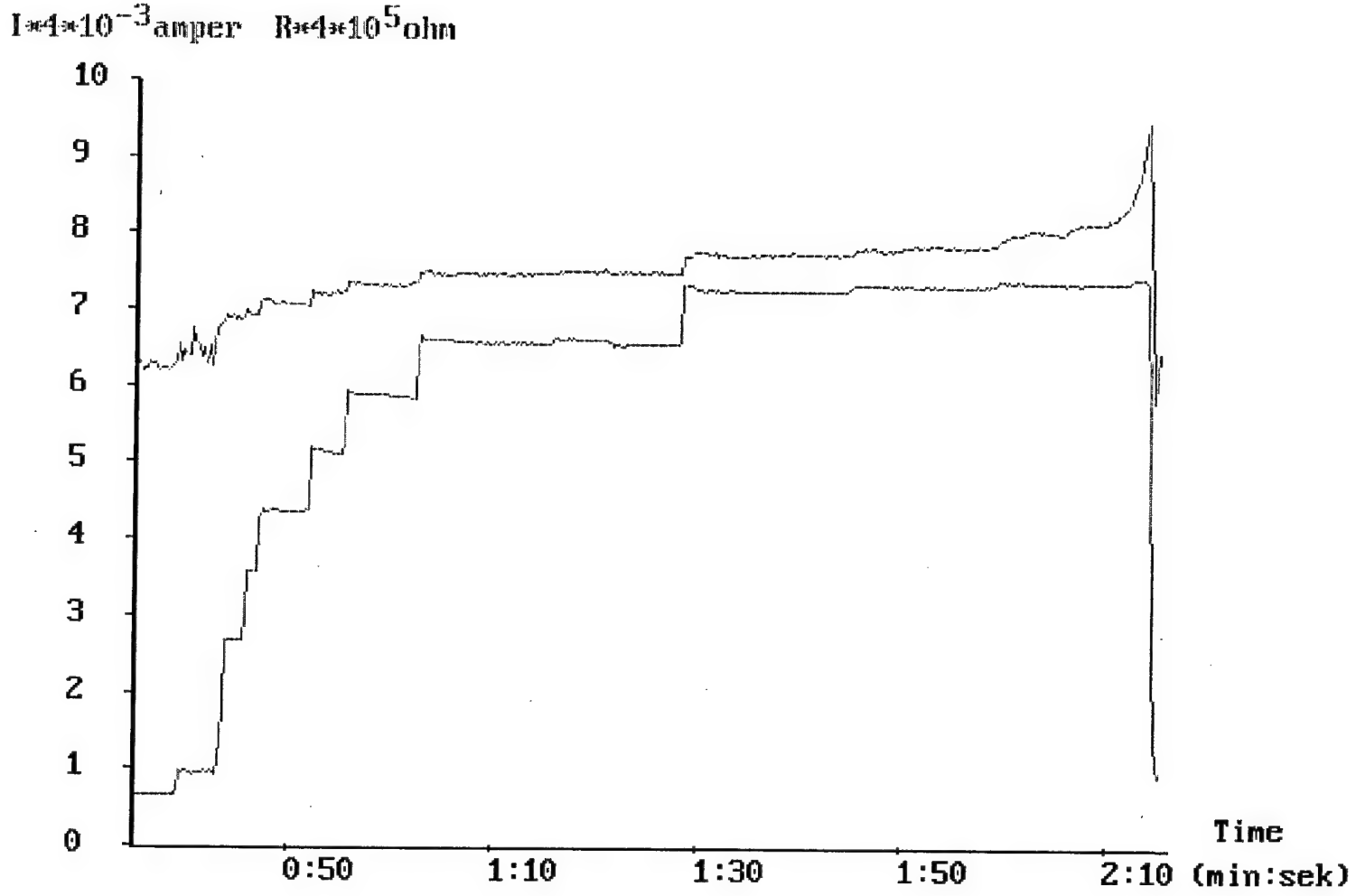

Fig. 4.15. Experiment with current variation in the composite bar (bar 3-2, test 2).

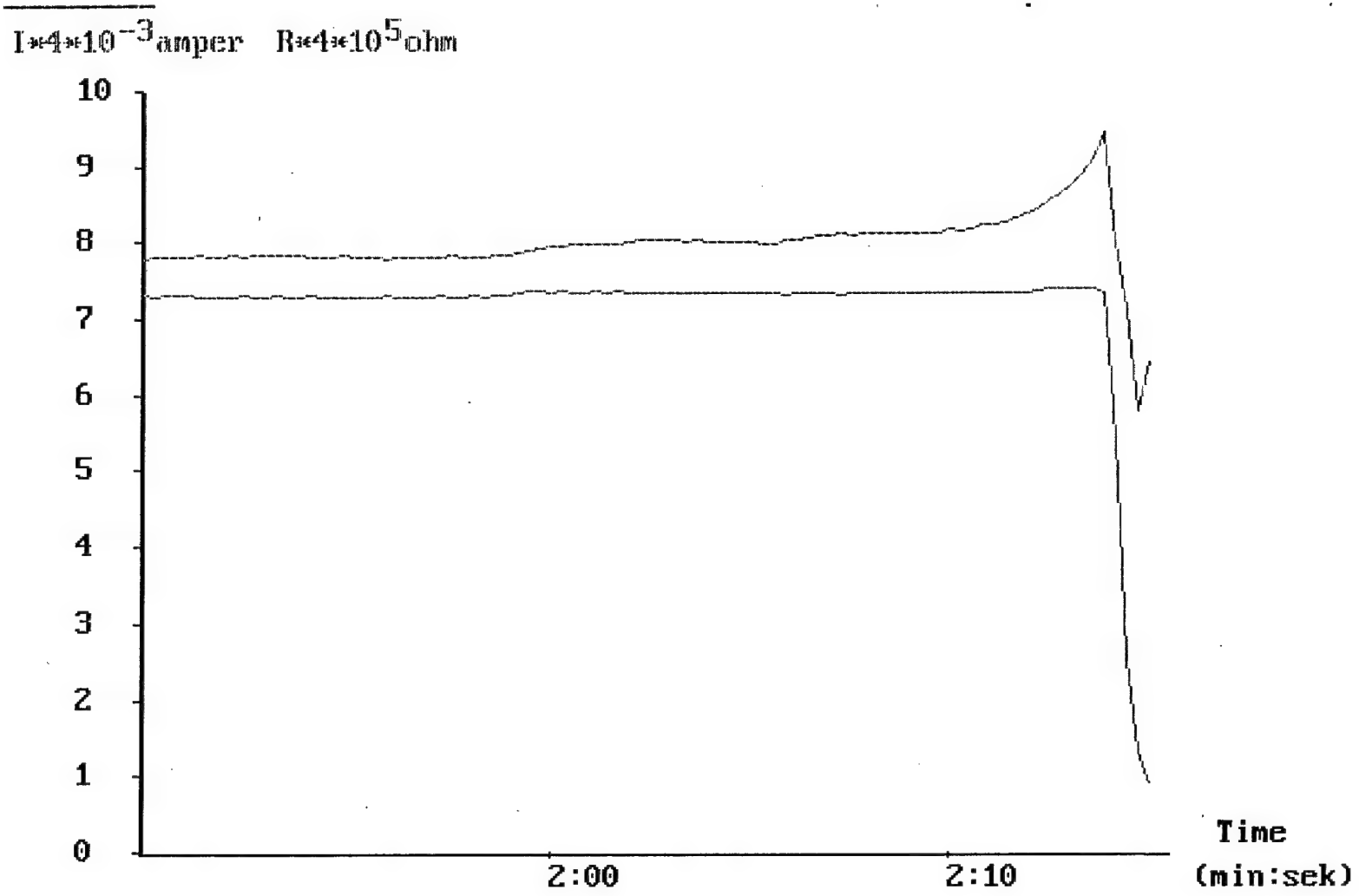

Fig. 4.15a. Process of an avalanche-type increase of the composite bar (bar 3- 2) resistance at 1850 A and its abrupt drop after protection system operation.

Table 4.1

N	Parameter	Value
1	Winding inner diameter, m	0.310
2	Winding outer diameter, m	0.345
3	Winding axial length, m	0.35
4	Total number of bars in two layers	216
5	Number of turns per phase	36
6	Numper of poles of the alternator	4
7	Number of phases of the armature	3
8	Phase Ohmic resistance, Ohm	0.19
9	Phase inductance, mH	0.11

Results of magnetic field measurements are shown in Fig.4.16 - 4.21.

The harmonic contents in the magnetic field of the helical winding was measured with the help of special sinusoidal meters, having the pitch of the corresponding harmonics. the winding was subdivided along its axial length into three zones: zone 1 - side of bus and teminals, zone 2 - in the middle of the winding, zone 3 - side of turbine. The test results are presenred in Table 4.2. They show that though the high harmonic contents varies along the winding length, it cannot influence substantially the alternator parameters.

Table 4.2

Harminic order	Zone number	Star connection	Delta connection
1	1	100 %	100 %
1	2	100 %	100 %
1	3	100 %	100 %
3	1	0 %	0 %
3	2	0 %	0 %
3	3	0 %	0 %
5	1	11.4 %	11.2 %
5	2	1.6 %	2.4 %
5	3	5.3 %	9.2 %
7	1	<4 %	0 %
7	2	<1 %	0 %
7	3	<3 %	0 %

High-voltage tests in liquid nitrogen showed that the winding can operate at 10 kV. It has withstood the high-voltage tests up to 25 kV. It is important for the

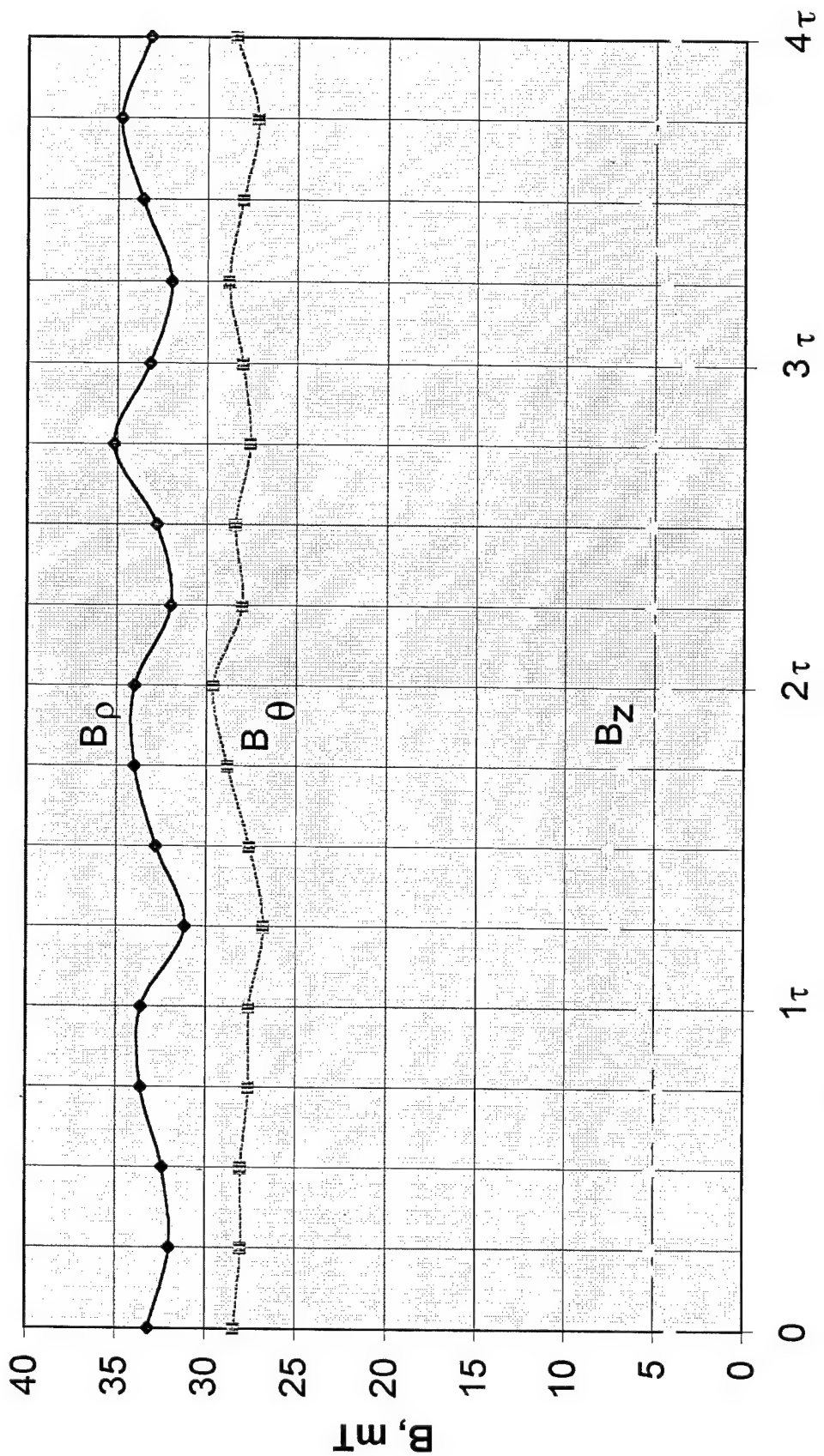

Fig .4.16. Distribution of magnetic induction on the inner surface of supporting cylinder of helical winding.

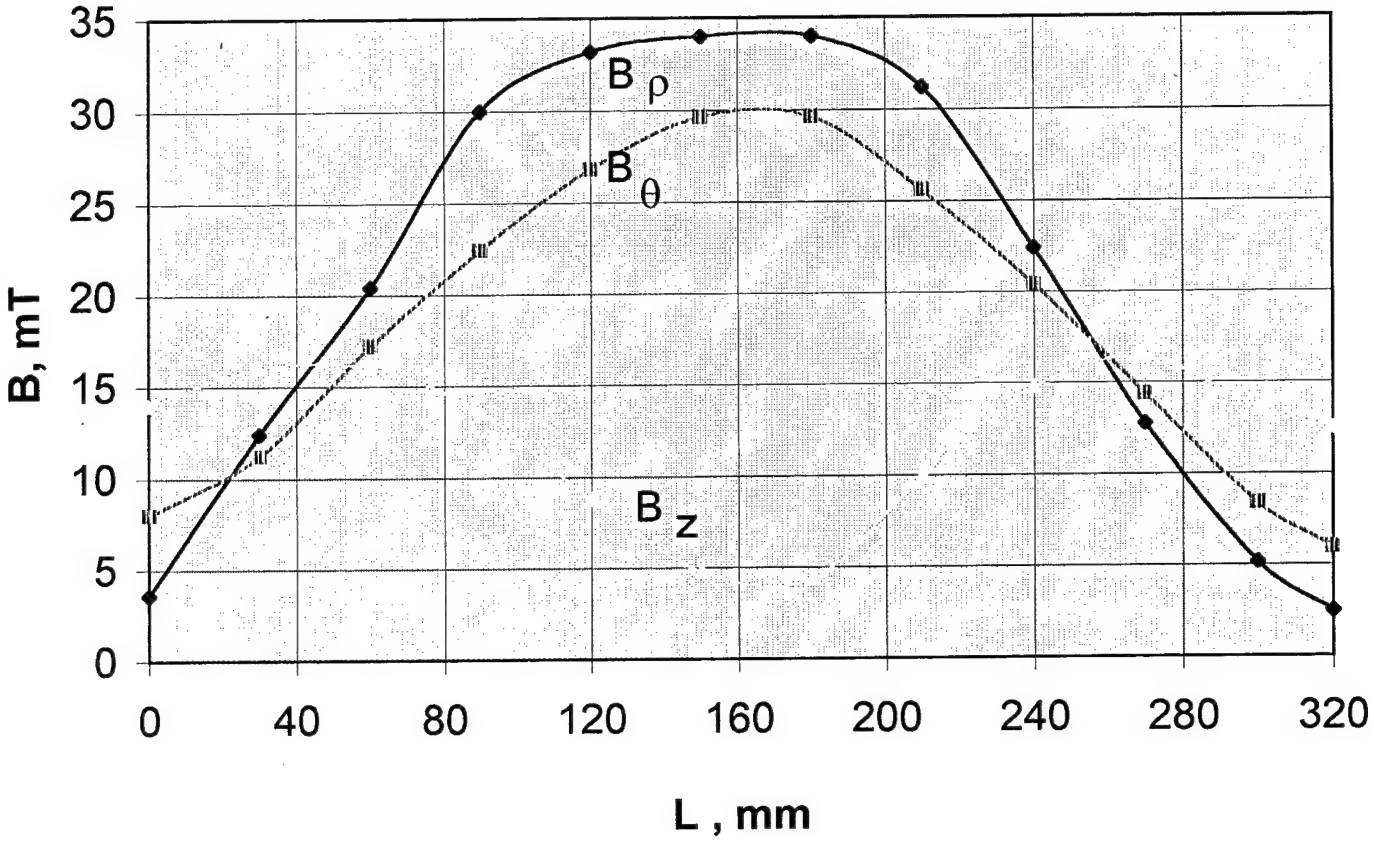

Fig . 4.17. Distribution of magnetic induction along the lenght of the inner surface of suppoting cylinder of helical winding.

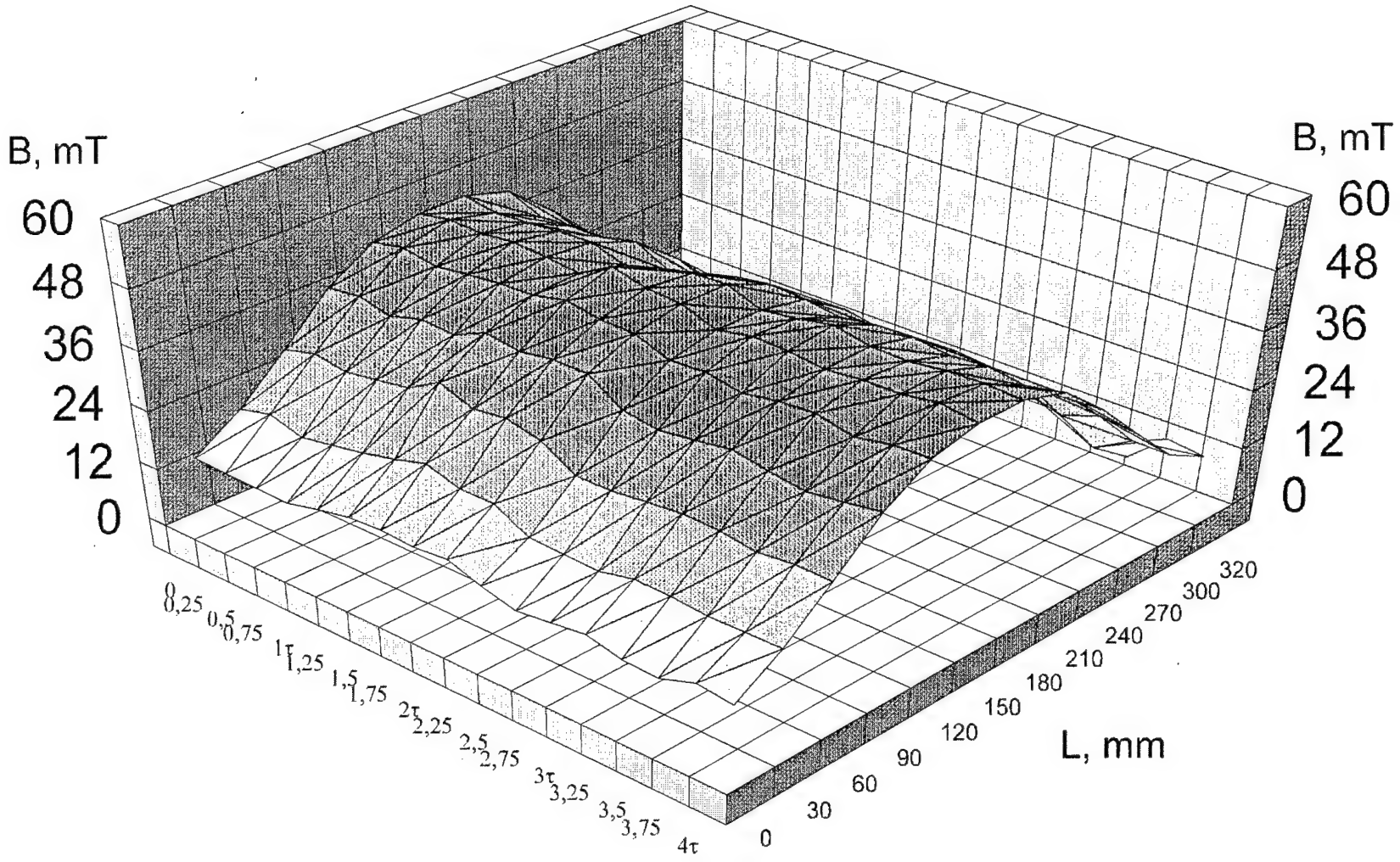

Fig. 4.18. Distribution of 3D magnetic induction on the inner surface of supporting cylinder of helical winding.

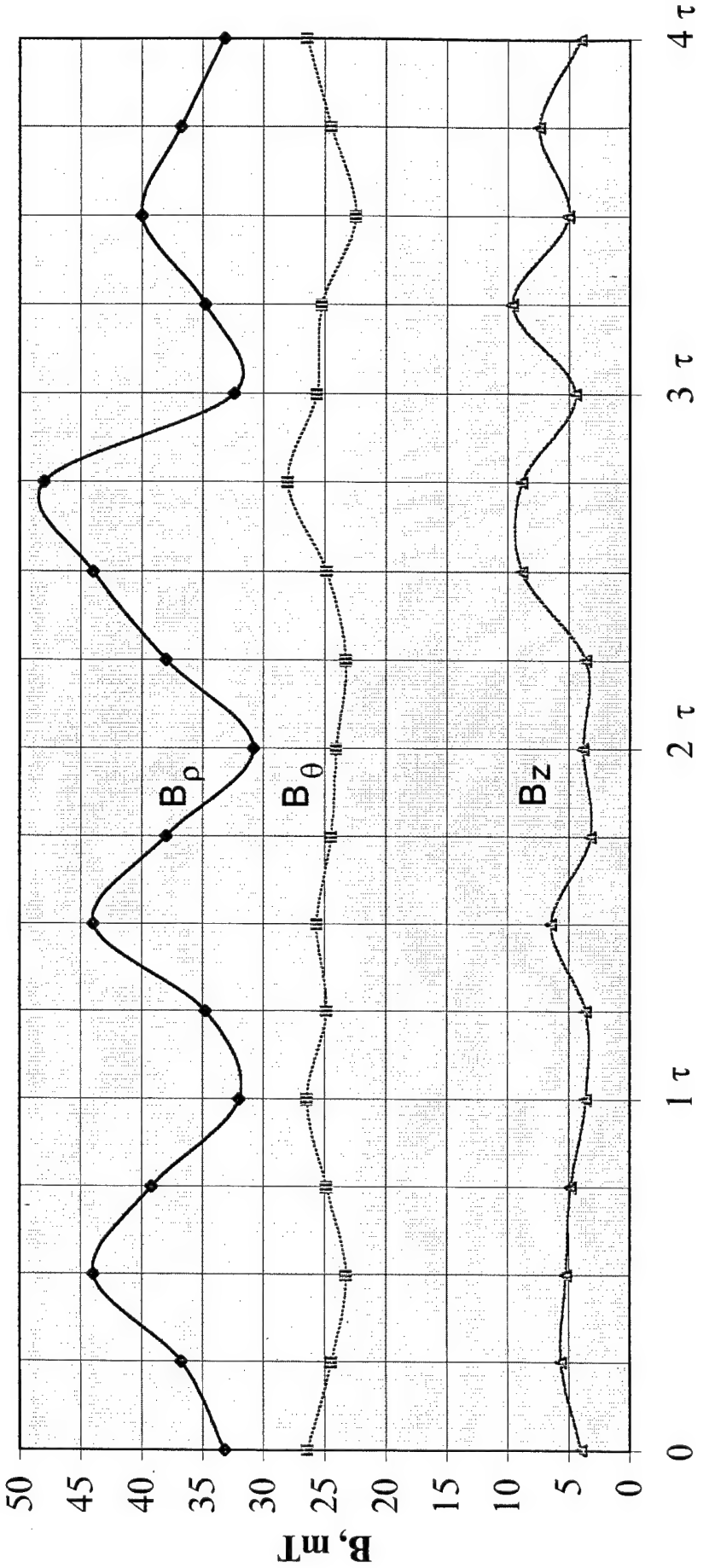

Fig. 4.19. Distribution of magnetic inductuon on the outer surface of helical winding

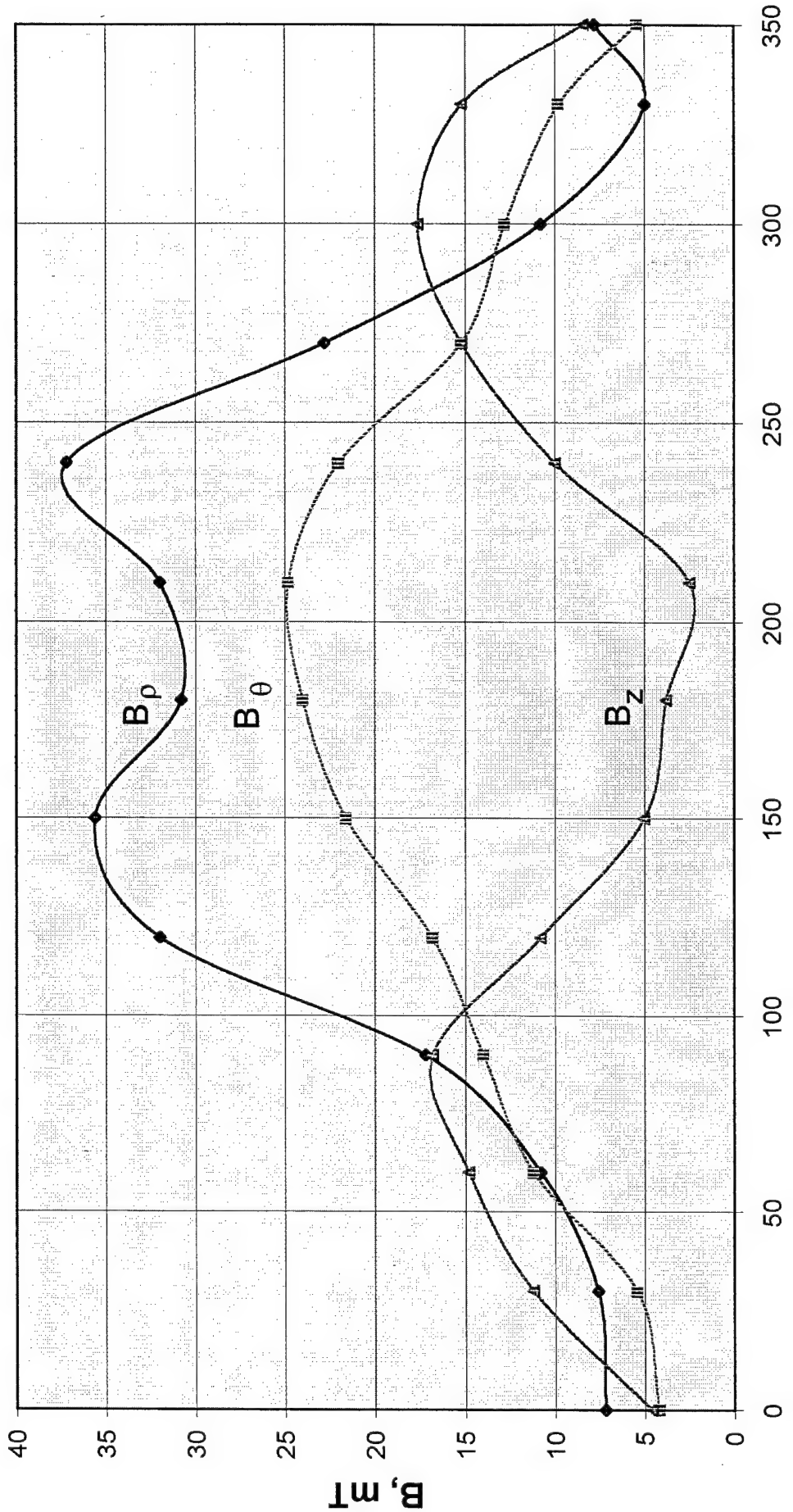

Fig .4.20. Distribution of magnetic induction along the length of outer surface of helical winding.

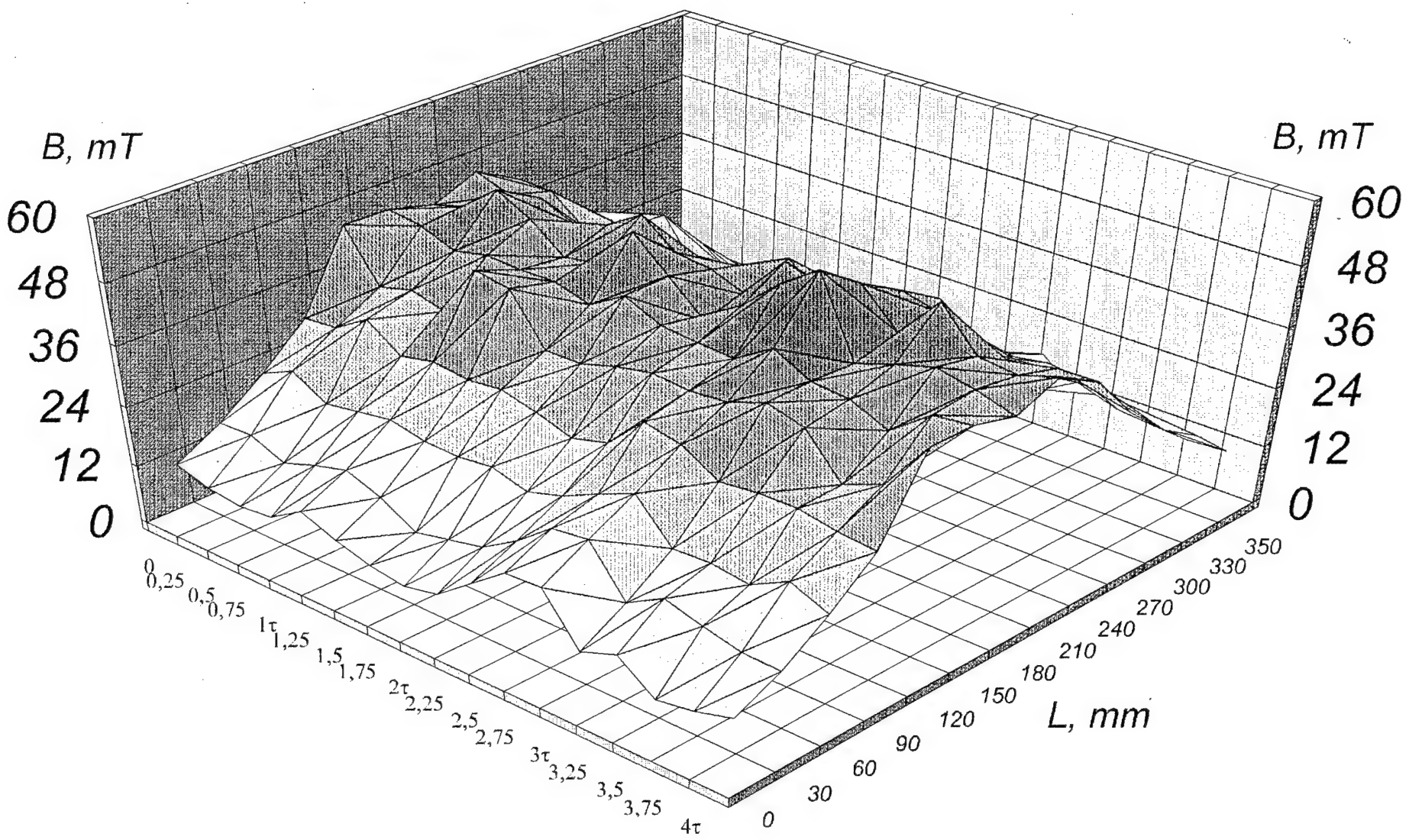

Fig.4.21.Distribution of 3D magnetic induction on outer surface of helical winding

evaluation of the insulation scheme of the winding as the stator bars had no outer insulation to improve the bar cooling.

Thr ready winding was immersed in liquid nitrogen and was tested at DC with the current density 65 A/mm^2, the value of current density was limited by the power supply. Evaluations show the DC current density at 77 K may be increased up to 120 -160 A/mm^2. It means the winding can carry AC up to 200 A. Accounting for 10 kV of the rated voltage the manufactured copper helical winding is suitable for the generator rated at 1-3 MW in case the rotor produced the radial magnetic field of 0.5 T on the average diameter of the armature winding.

CONCLUSION

1. The basic thermal scheme of the developed high power generator of 1-5 MW class is the one with a single cryostat for the rotor and for the armature. Successful results of investigation of special seals for this design prove that the variant of the design is viable.

2. There is no significant difference in the weight of the armature for 1 and 5 MW generators because of relatively high mass of the cryostat with the sealing-bearing unit. (It is worth noting that the rotor in a single cryostat will be simpler and lighter then in the design with two separate cryostats).

3. The ironless type of the generator is about 30 kg less in weight then the one with an iron screen, but the armature winding will be more heavy due to decreased value of the radial component of the main magnetic flux.

4. The iron screen is intended to be manufactured of an amorphous steel. To decrease the mass of the screen it is possible to wind from an amorphous ribbon a multi-shelled construction interlayed by a non-metallic material.

5. The helical winding design is developed in two versions. It is supposed that the winding bars will be positioned either on one or on two sides of a cylindrical support structure.

6. The developed helical armature winding provides 30% gain in weight, about 25 % gain in losses as compared to a most sophisticated conventional one. It also involves much less hand labor and its manufacturing process is several times shorter than that of a lap one.

7. To confirm the developed design and technological process of helical winding a model copper winding for the 1 - 3 MW class generator was manufactured and tested. Its test provided experimental information of the parameters and the 3D magnetic flux distribution.

8. The manufacturing process for the developed helical winding is much more simple than the one for the windings of conventional geometry due to simplified bar geometry and possibility of continuous winding laying out with a decreased quantity of the interphase soldered connections.

9. To simplify the manufacturing process still more the proposed armature bar design is based on an application of a transposed rectangular (square) multifilumentary wire with a multi-stage transposition scheme.

10. The minimal less value in the armature bars is achieved in case the Ohmic losses are equal to the eddy losses. The eddy losses comprise the eddy-

current and circulating current ones. Its possible to shift this balance for higher current density and increased Ohmic losses with lower amount of eddy-current losses, but the total losses in the armature winding will increase.

11. To achieve this balance in the helical armature winding bars operating at high frequencies is necessary to have the elementary high-purity aluminum wire size below 0.1 mm. It means a composite wire technology is to be applied.

12. To have a choice of variants of the armature winding material there were developed and manufactured the helical armature bars with composite aluminum, high purity solid aluminum and conventional copper wires.

13. The native composite wire with high-purity aluminum fibers is intended for AC up to 800 Hz. The matrix is made of aluminum alloy. The wire diameter is 0.3 mm, aluminum fibers have a diameter about 0.03 mm. As it is relatively expensive, a cable of solid high-purity aluminum wires with 0.1 mm diameter was investigated as well.

14. When developing the armature winding insulation scheme it was decided and experimentally verified not to insulate each armature bar, but to insulate the helical winding layers, thus improving the heat removal.

15. As there may exists a two phase hydrogen flow in the armature winding region, the dielectric properties of liquid hydrogen are not being accounted for.

16. Thought the epoxy impregnation of the bars results in poorer current density as compared to a non-impregnated variant, the bars are to be impregnated from the point of view of mechanical properties of the winding.

17. There were manufactured 25 samples of experimental armature bars. They were intended for the two stages of tests: on a disc text fixture and on a cylindrical test fixture.

18. Two types of fixtures were used to have a large variety of experimental data. The tests were carried out at 293. 77 and 4.2 K.

19. The maximum current densities achieved in the experimental bars at DC are :

- bars manufactured of high purity aluminum composite - 275 A/mm^2
- bars manufactured of pure aluminum wires - 250 A/mm^2
- bars manufactured of conventional copper wires - about 200 A/mm^2

20. High-frequency tests at 4.2 K and at decreased current density value showed the resistance increase at 600 Hz for the bars of solid high-purity aluminum wires equals 1.4 and for bars of copper wires - 1.8.

21. The value of resistivity of the composite aluminum wire at 4.2 K and DC equals
$1.8 \cdot 10^{-10}$ Ohm·m and of the solid aluminum wire - about $2.5 \cdot 10^{-10}$ Ohm·m.

22. Evaluation of the experimental investigation of the helical armature bars at frequencies from 20 to 1000 Hz shows they are loaded by the eddy currents. The circulating currents are practically zero, thus confirming the good quality of the transposition scheme developed.

23. Successful high-voltage tests of the model copper helical winding for the 1-3 MW class generator with simplified electrical insulation scheme and improved cooling conditions confirmed it can operate with the voltages up to 10 kV. The winding has no individual bar insulation, but the interlayer insulation only.

REFERENCES

1.1. Cryogenic aluminum armature bar for high power generators (Feasibility study). Preliminary report: Institute of Electrotechnical Problems. Department of Non -Conventional Electrical Machines. November 1994.
1.2. T.Rikitake. Magnetic and electromagnetic shielding. Tokyo: Terra Scientific Publishing Company,1987.228 p.
1.3. V.B.Berezhansky, L.I.Chubraeva et al. Electrical Insulation Degradation Research and Some Practical Applications. Stockholm, Power Tech, June 1995, Int.Symp. on Electric Power Engineering. Rep. SPT HV 01-03-0206, Vol. High Voltage Technology, pp.12-17.
1.4. Reference Book on Electrical Materials. Vol.2, Moscow, Energoisdat, 1987, 464 p. (in Russian).
1.5. G.S.Kuchinsky, V.E.Kisivetter, U.S.Pintal. Insulation of High Voltage Installation. Moscow, Energoisdat, 1987, 368 p. (in Russian)

2.1. Smith J.L., Wilson G.L., Kirtley J.L. MIT-DOE Program to demonstrate an advanced superconducting generator//IEEE Trans. on Mag. 1979. Vol. 15, N 1. P. 727-729.
2.2. Chubraeva L.I. Non-Conventional Electrical Generators. Nauka, St.-Petersburg, 1992. 246 p. (In Russian).
2.3. Rutberg Ph.G., Chubraeva L.I., Tutaev V.A. et.al. 1 MW experimental hyperconducting alternator project. Preliminary evaluation. July 1993, 33 p.
2.4. Rutberg Ph.G., Chubraeva L.I., Tutaev V.A. et.al. Dual-use initiative high power laser assessments study - Prime electric power system. Final report: Institute of Problems of Electrophysics of Russian Academy of Sciences. November 1993.

3.1. Kelly A. Strong solids. Oxford Univ. Press., London and NY, 1966.
3.2. Markovetz M.P. Determination mechanical properties of metal by hardness measurement. Moscow, Mashinostroenie, 1979, 191 p.

SUPPLEMENT

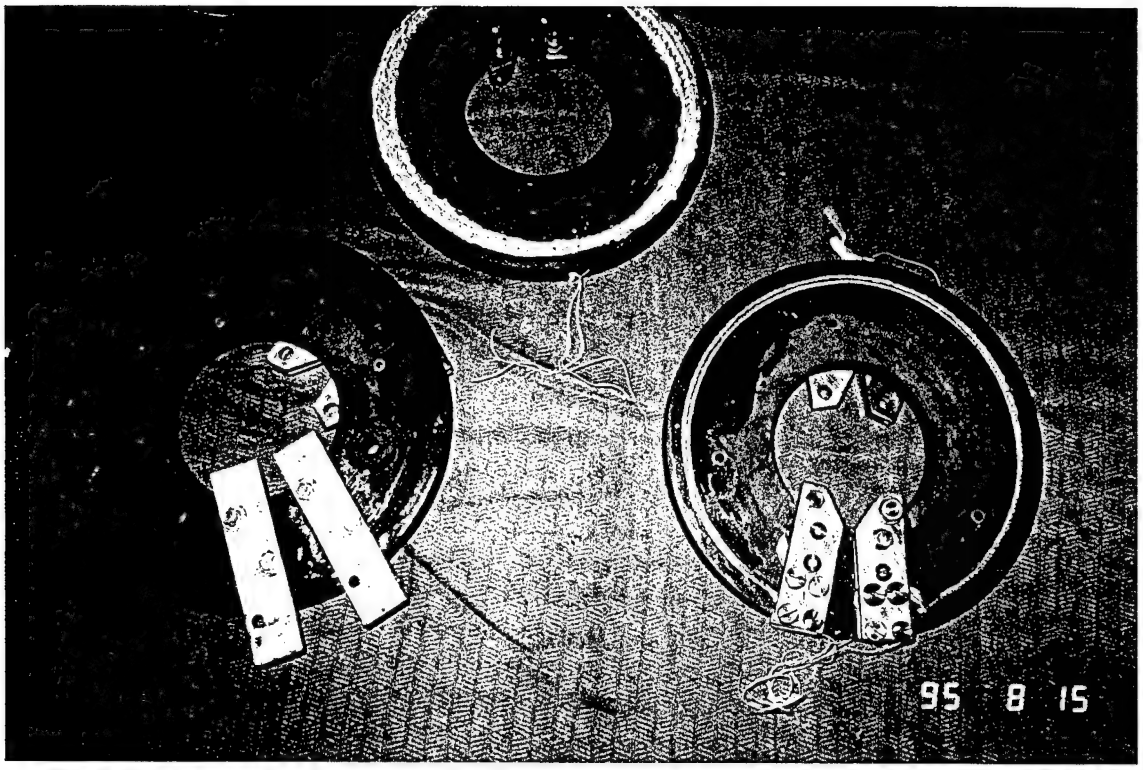

Fig. S.1. Disc test fixture with aluminum and copper bars.

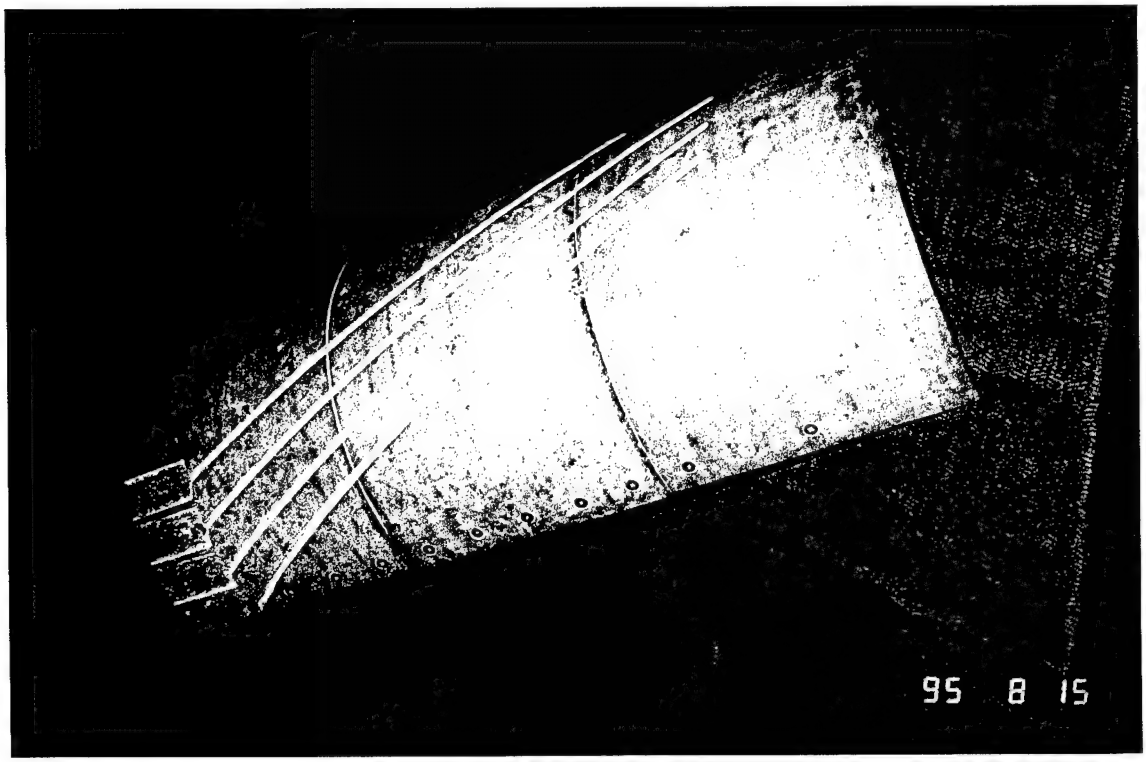

Fig. S.2. Segment with machined helical slots.

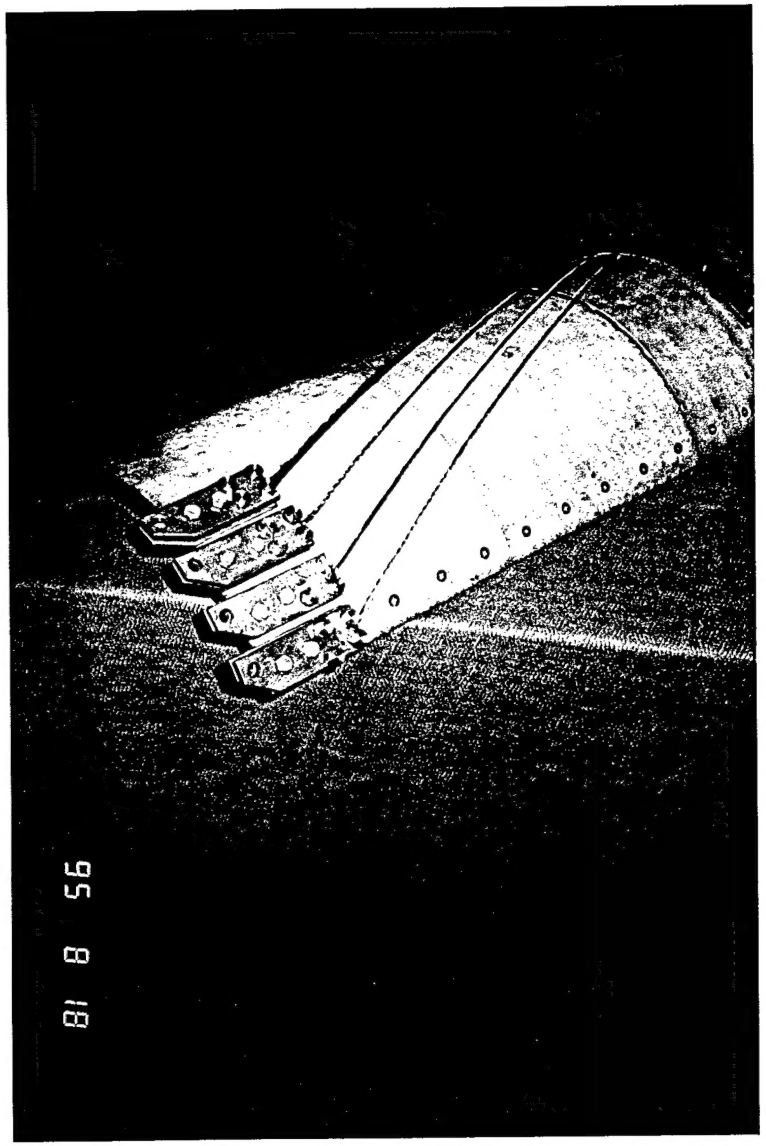

Fig. S.3. Cylindrical test fixture with three aluminum and one copper bars.

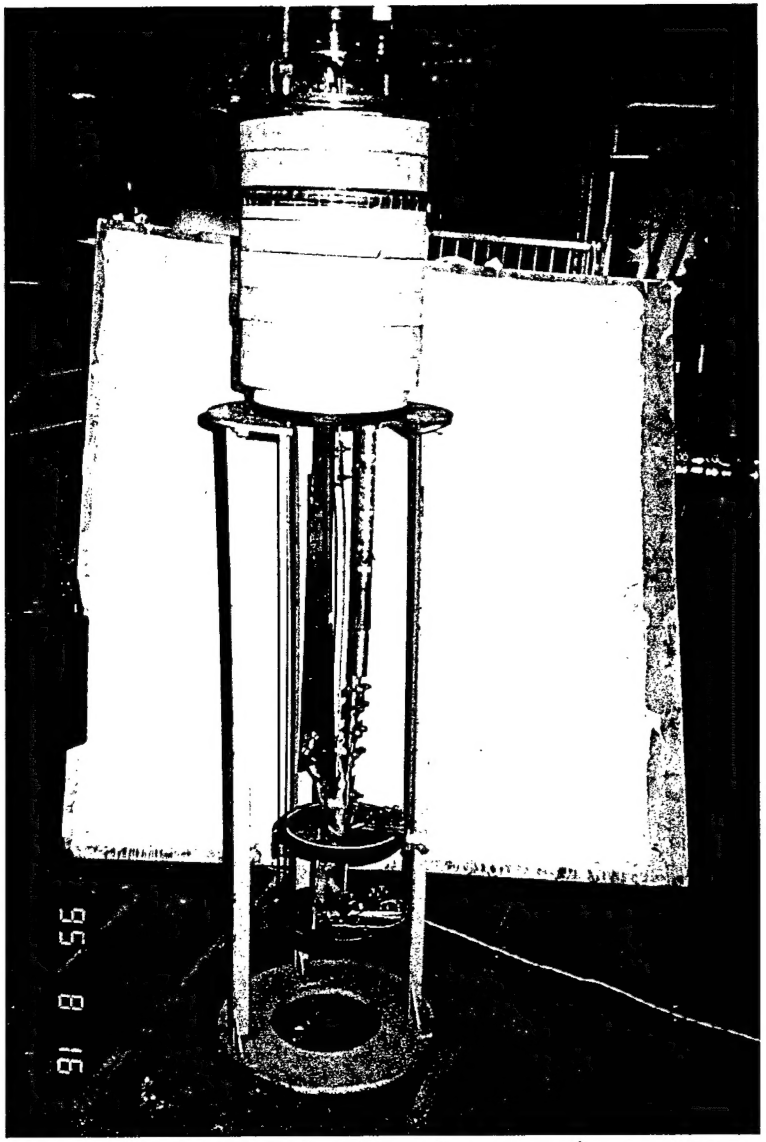

Fig. S.4. Current leads and suspension system for the test fixtures (with disc system mounted).

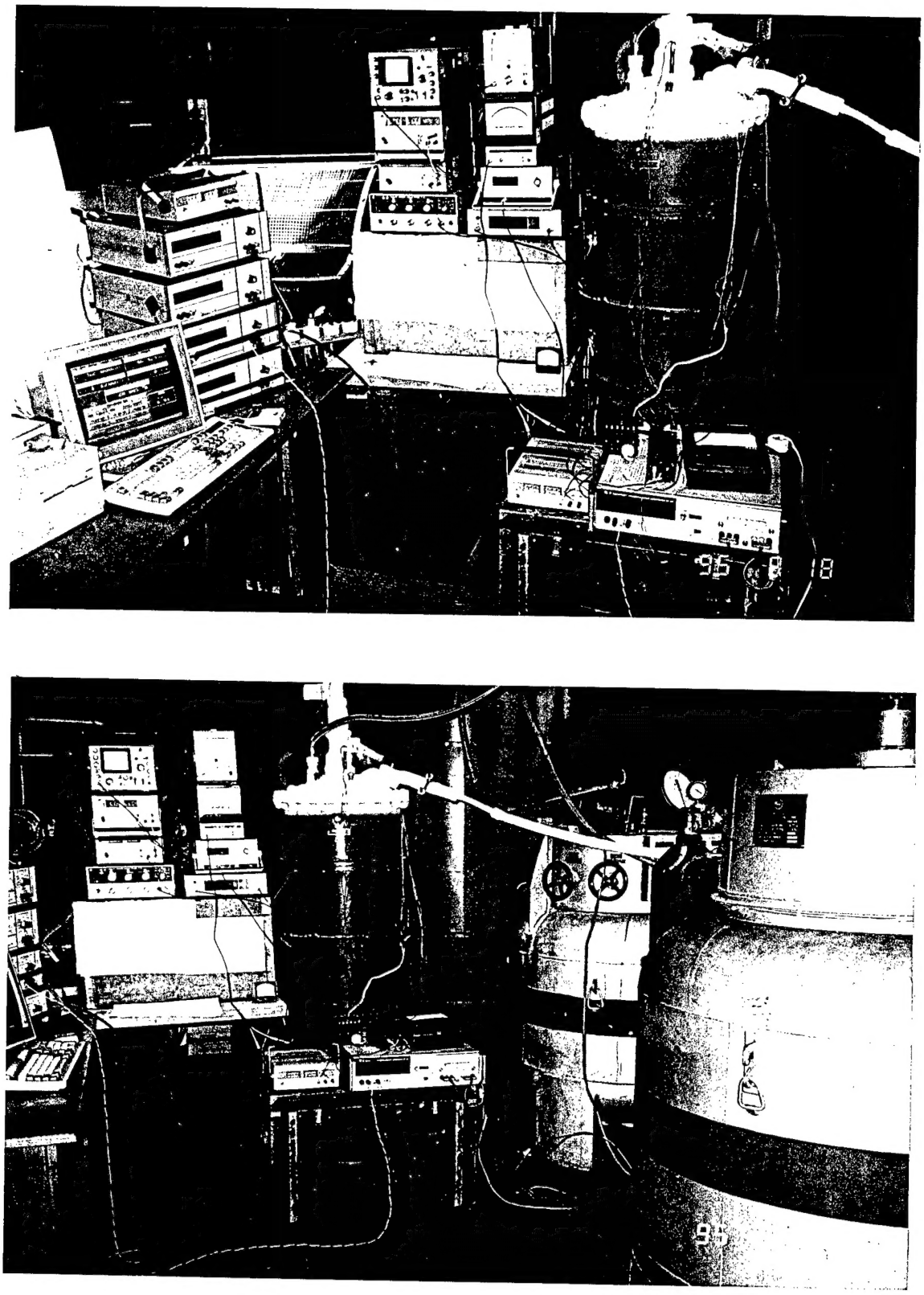

Fig. S.5. Cryogenic test-bed with computer (a) and tanks for liquid helium and liquid nitrogen (b).

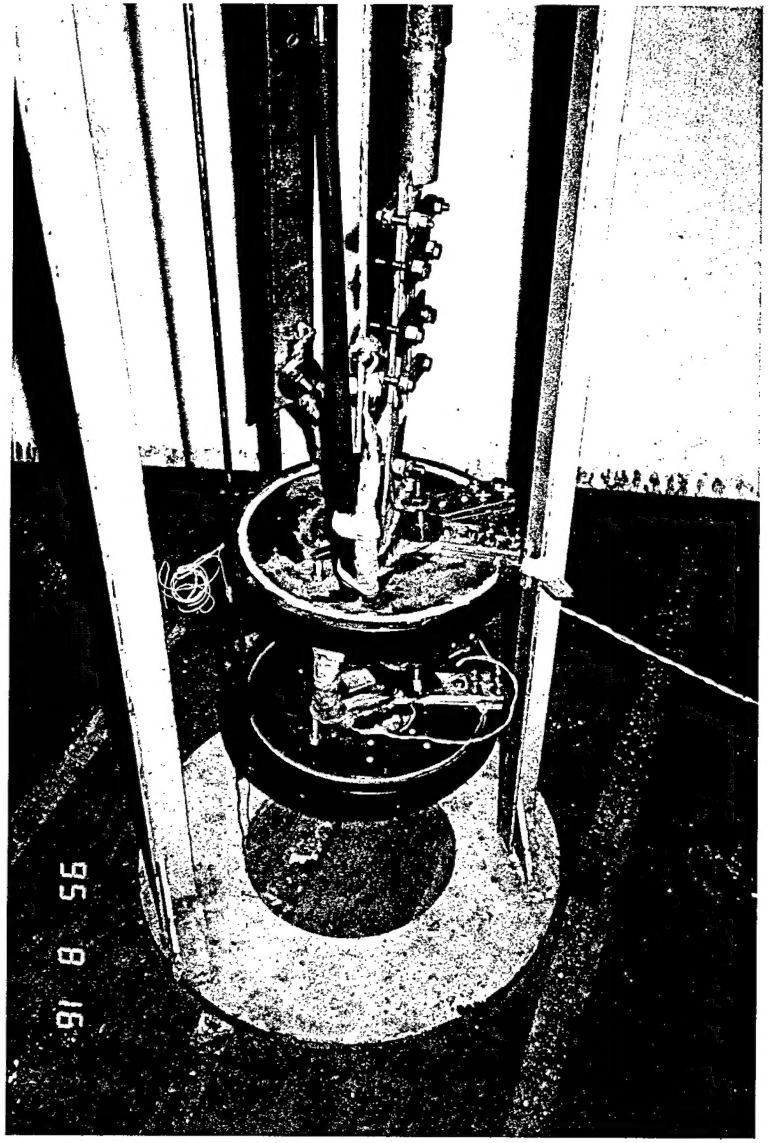

Fig. S.6. Disc test fixture ready for the low temperature tests.

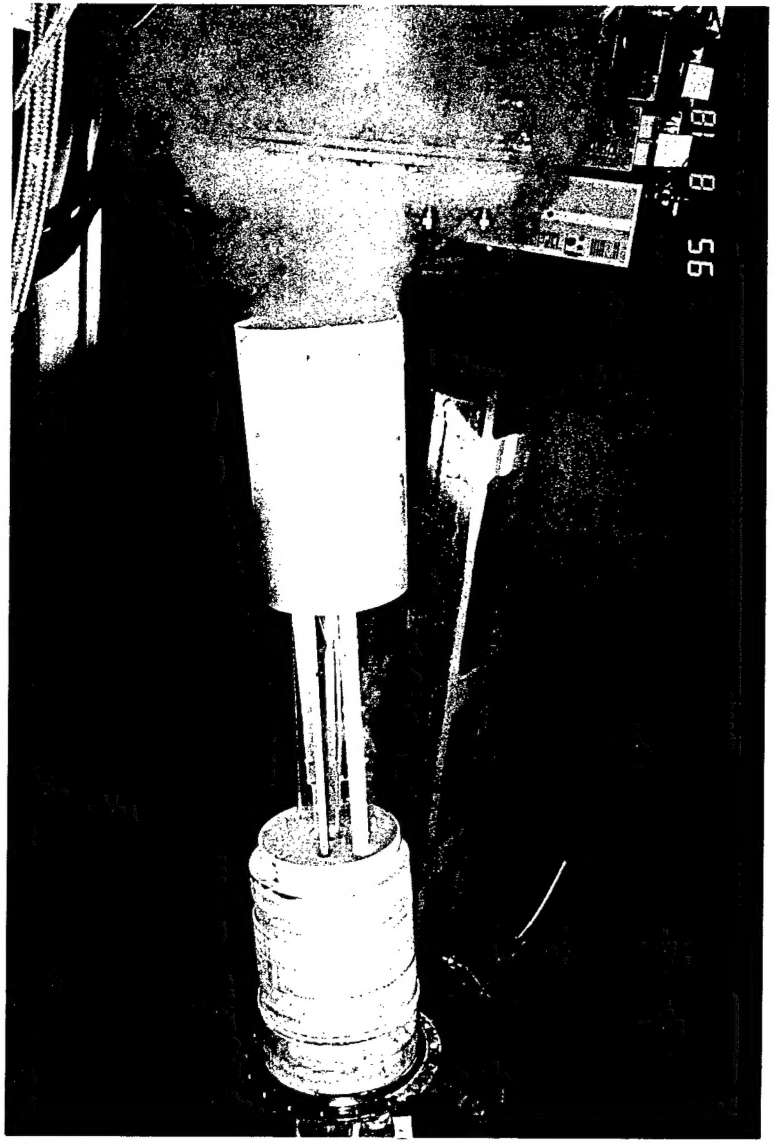

Fig. S.7. Cylindrical test fixture in the process of low temperature experiments (a,b).

b)

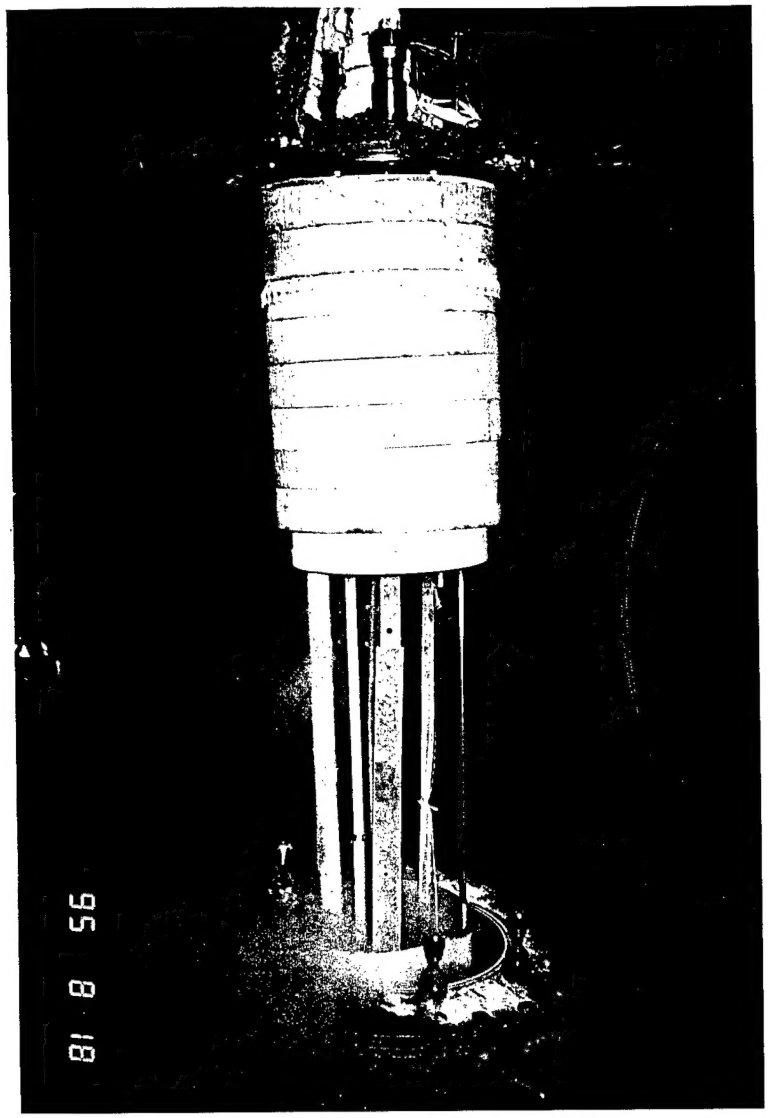

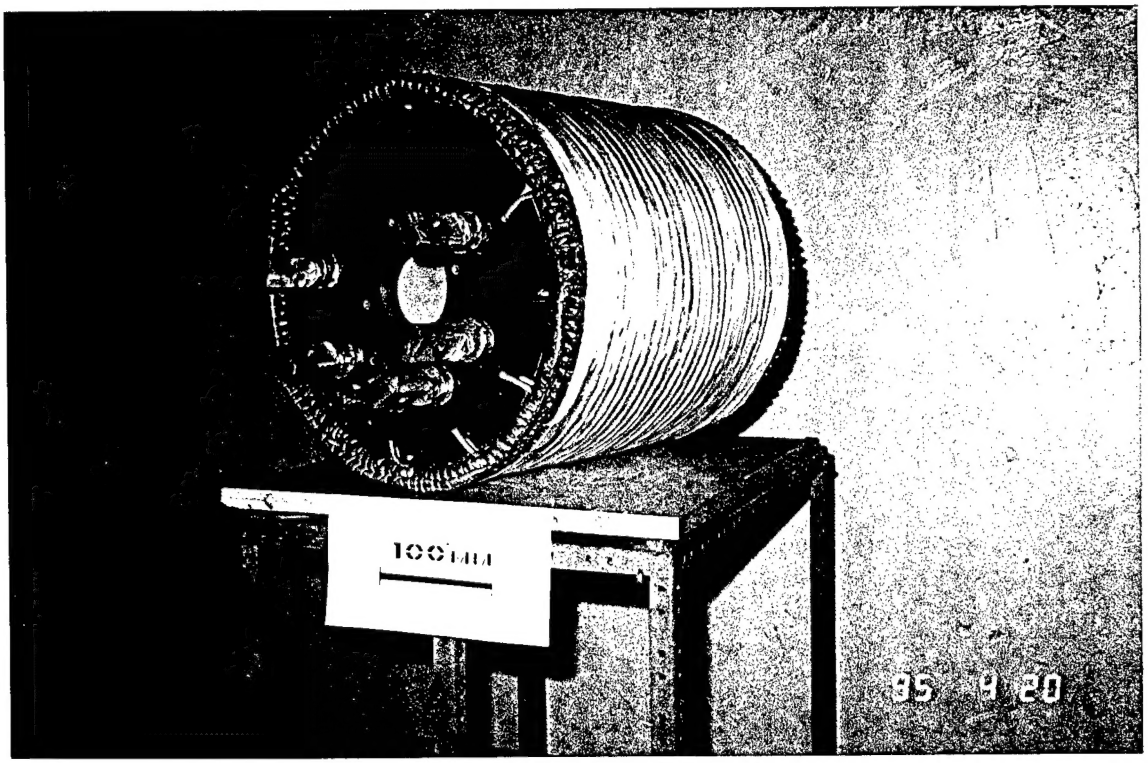

Fig. S.8. Experimental copper helical winding for the alternater of 1-3 MW class.